Influence of geometric imperfections and increasing turbine sizes on validity load transfer functions in bolted ring-flange connections

MSc. Thesis

Ruth Korthals Altes

Influence of geometric imperfections and increasing turbine sizes on validity load transfer functions in bolted ring-flange connections

by

Ruth Korthals Altes

Delft University of Technology

Faculty:	Civil Engineering and Geosciences	
Degree:	MSc. Civil Engineering	
Track:	Structural Engineering	
Student number:	4440242	
Project duration:	October 1st, 2022 – July 6th, 2023	
Thesis committee:	Prof.dr. M. (Milan) Veljkovic,	Delft University of Technology (Chair)
	Ir. H. (Hagar) El Bamby,	Delft University of Technology
	Prof.dr.ir. L.J. (Bert) Sluijs,	Delft University of Technology
	Ir. B. (Bettina) Wesarg,	Ramboll

Preface

This thesis is the final part of my Master of Science in Civil Engineering at the Delft University of Technology, and therefore my final part of being a student. It describes the 'Influence of geometric imperfections and increasing turbine sizes on the validity of load transfer functions in bolted ring-flange connections'. From October 1st 2022 until June 29th 2023, I worked on this research and writing the report.

I am incredibly grateful for everything I have learned over the past 8 years, from starting in Applied Mathematics, which was not the best choice for my academic career, but one of the best choices for my personal life. I started Civil Engineering because I was very interested in the transport and infrastructure side, and developed a great interest for structures and what it takes to make it safe and useful for civilians. Mostly, I am grateful for the past year where I got the opportunity for my internship and master thesis at Ramboll, where I really found my passion in offshore wind.

I would like to thank all teachers and professors for providing the knowledge it takes to call myself a structural engineer (in a week from writing this preface), and making me and all other students enthusiastic about this field. Moreover, I would like to thank everyone at Ramboll for making my time in Hamburg absolutely unforgettable. And ofcourse my family and friends for the incredible support over the past 8 years, motivating me during setbacks and keeping me sane during (most of) my student years. Lastly, I would like to thank my assessment committee for making my thesis possible: Bettina, who has been my supervisor and mentor at Ramboll for both my internship and thesis. Thank you for helping me, especially during times where you were sick at home and started your laptop just to answer my question. Hagar, for helping me with the final phase of my thesis and giving me confidence about my work and some reassurance that 'everything will be fine'. And my professors Milan Veljkovic and Bert Sluijs, for guidance, knowledge and the critical questions that helped me further obtaining this thesis.

Ruth Korthals Altes
Delft, June 2023

Abstract

The global focus on climate change and the transition away from fossil fuels has highlighted the importance of renewable energy sources. Offshore wind turbines are being optimized and are therefore growing in size and power.

This research focuses on bolted ring-flange connections, a connection type that plays a crucial role in the design of offshore wind turbines, as they transfer the external force between parts of a turbine. The objective of this thesis is to analyze how the increasing dimensions from current to future offshore wind turbines and geometric imperfections impact the reliability of analytical approaches for load transfer functions (LTFs) for these connections. Two components of this objective are considered: examining the influence of different dimensions of ring-flange connections and analyzing the impact of various gaps between flanges on LTFs for 'current generation' and 'next generation' turbines. Analytical calculations are compared to results obtained with finite element analyses, which are assumed to represent an actual connection.

Based on the research findings, the following conclusions are made. Firstly, the widely used tri-linear approach by Schmidt/Neuper [18] for obtaining the LTF in bolted ring-flange connections is found to be unreliable for current and future turbine sizes. This method highly underestimates the forces in the bolts when initial gaps are present between the flanges. Calculations performed with this approach could lead to an overestimation of the turbine's lifetime compared to reality by multiple years, possibly causing more maintenance or early failure. Alternative approaches, such as a very new and not yet approved polynomial approach, show reliable results, providing accurate estimations of bolt forces for large connection diameters. Additionally, currently verified tolerances by [4] for gaps between flanges (1 mm over 30° and 2 mm over entire circumference) are outdated, and larger gap heights or smaller gap lengths are expected in practice, especially for future turbines [1]. These gaps lead to a larger bolt force in practice, decreasing the fatigue resistance and lifetime of the structure. Even though very small gaps are expected to occur often, lower bolt forces are obtained compared to larger gaps, both with an expected height to length ratio of $\frac{u_{gap}}{l_{gap}} = 0.53 * 10^{-3}$. In analytical design calculations, it therefore is recommended to consider larger sized gaps with a gap length of approximately 1600 mm with its expected gap height.

Nomenclature

Definition of symbols

d_B	:	Diameter bolt $[mm]$
A_B	:	Cross sectional area of the bolt $[mm^2]$
$A_{B.s}$	:	Stress area in the bolt cross section $[mm^2]$
d_W	:	Diameter of the washer $[mm]$
h_W	:	Height of the washer $[mm]$
a	:	Distance between the center of the bolt and the inside of the flange $[mm]$
b	:	Distance between the center of the bolt and the center of the tower shell $[mm]$
c	:	Width of the flange (at bolts) $[mm]$
c_w	:	Width of the flange (at center of tower wall) $[mm]$
s	:	Thickness tower wall $[mm]$
w_{fl}	:	Total length of the flange $(a + b + \frac{s}{2})$ $[mm]$
t	:	Thickness of flange $[mm]$
E	:	Young's modulus [MPa]
I	:	Moment of inertia $[mm^4]$
EI	:	Bending stiffness $[kNm^2]$
D_O	:	Outer diameter connection $[m]$
D_I	:	Inner diameter tower wall $[m]$
D_r	:	Total diameter of the rotor $[m]$
A_r	:	Total area of the rotor $[mm^2]$
A_{tower}	:	Cross sectional area of the tower shell $[mm^2]$
b'_D	:	Distance between the two hinges in the flange (see Figure 2.2) [mm]
b'_E	:	Distance between the two hinges in the flange (see Figure 2.3) [mm]
ϕ_{imp}	:	Angle of gap height over flange [rad]
ϕ_{en}	:	Initial slope of the circular arch LTF [rad]
C_S	:	Bolt stiffness [kN/mm]
C_D	:	Flange stiffness [kN/mm]
N	:	Axial force $[kN]$
M	:	Bending moment $[kNm]$
σ_N	:	Stress due to axial force$[MPa]$
σ_M	:	Stress due to bending moment $[MPa]$
Z	:	External force on tower $[kN]$
F_V	:	Preload on the bolt $[kN]$
F_S	:	Force in the bolt $[kN]$
$F_{t,Rd}$	:	Tension resistance of the bolt $[kN]$
$f_{u,B}$	:	Characteristic value of ultimate stress of the bolt material [MPa]
$f_{y,B}$	:	Characteristic value of yield stress of the bolt material [MPa]
$f_{y,sh}$	:	Characteristic value of yield stress of the tower/TP shell material [MPa]
$f_{y,fl}$	:	Characteristic value of yield stress of the flange material [MPa]

$M'_{pl,2}$: Plastic moment resistance of the flange at the tower shell [kNm] (see Figure 2.2)
$\Delta M_{pl,2}$: Differential moment from the bolt force
$M_{pl,3}$: Plastic moment resistance of the tower wall, considering M-N interaction [kNm]
$M_{pl,2}$: Plastic moment resistance of the flange at the bolt hole [kNm] (see Figure 2.3)
γ_{M2} : Safety factor (=1.25)

General abbreviations

LTF : Load transfer function
TP : Transition piece
MP : Monopile
ULS : Ultimate limit state
FLS : Fatigue limit state
OWT : Offshore wind turbine
FE : Finite element
FEA : Finite element analysis
FEM : Finite element method
DOF : Degree of freedom
DEL : Damage equivalent load

Abbreviations gaps

u_{gap} : Gap height for one flange
l_{gap} : Gap length for one flange, from contact point of flanges to highest gap height
α_{gap} : Gap angle for one flange, from contact point of flange to highest gap height
TS : Tower sided
FS : Flange sided
PL : Parallel

Abbreviations flange dimensions

BD : Bolt diameter
CD : Connection diameter
BCD : Bolt circle diameter
FT : Flange thickness
TWT : Tower wall thickness
TPWT : Transition piece wall thickness
DI : Distance bolt center to inside flange
DO : Distance bolt center to outside wall

Contents

1 Introduction

1.1. Context

1.1.1. Introduction to offshore wind

Over the last decades, an awareness has grown about climate change, fossil fuels and a need for renewable energy. Wind energy, a so-called second generation renewable energy, has been used for centuries to ground grain, pump water, and since the late 19th century, to generate electricity. For the first 100 years afterwards, many onshore wind farms were built, and since the last few decades, technology has advanced, such that offshore wind is rising in potential and production.

The first offshore wind farm was realized in 1991 in Denmark and with its 11 wind turbines, it could produce almost 5000 kW [23]. Nowadays, offshore wind parks that are being built produce over 9000 kW per wind turbine, with the largest operational offshore wind park generating 1.3 GW [10], enough to produce energy for 1.4 million households. These wind turbines are designed to have an expected operational lifetime of 25-30 years [14]. Many countries worldwide have set goals for adding sources of renewable energy, resulting in an expected 680 GW of wind capacity that will be added globally between 2023 and 2027 [11].

An offshore wind turbine consists of four parts: the foundation, (often) a transition piece, a tower and a turbine, as can be seen in Figure 1.1.

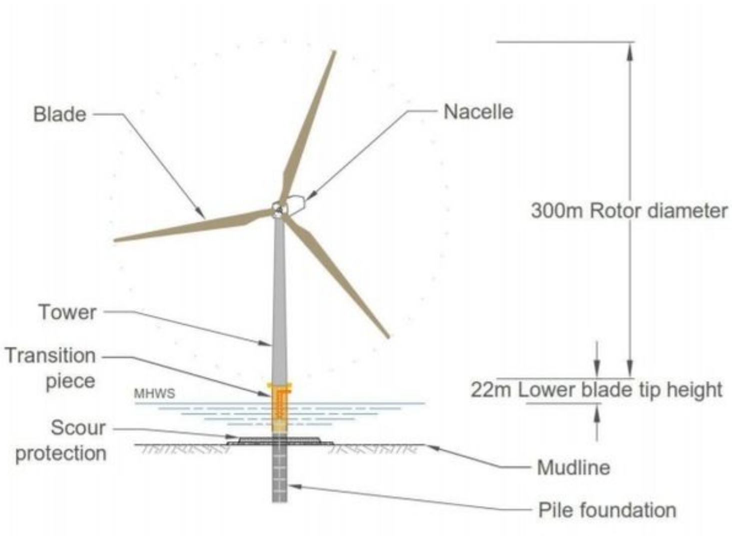

Figure 1.1: Overview parts wind turbine [12]

There are different types of foundations for offshore wind turbines (OWTs). Currently, the most common types of foundations are monopiles and jackets. Monopiles are the most preferred type of wind turbine foundation for water depths up to 40 m [14]. However, monopiles are limited to water depth, therefore jacket structures are applied more often, as they are more cost-effective in deeper waters [14]. In 2018, the percentage of installed monopiles was 81.9% to 6.6% for jacket structures, but due to the increasing water depths the OWTs will be installed, jacket structures are currently increasingly being designed for installation [30].

1.1.2. Bolted ring-flange connection

For offshore wind turbines, different connections between the Transition Piece (TP) and the Monopile (MP) and between the TP and the tower are used. Two often used connection types are grouted connections and bolted ring-flange connections. Bolted ring-flange connections is an often used alternative for grouted connections, because grouted connections caused concerns for increasing turbine sizes [17], where recently numerous offshore wind turbines with large diameters with grouted connections failed for monopiles.

For the connection between the TP and the tower and between tower segments, a bolted ring-flange connection is the most widely used connection type [30]. A representation of a bolted ring-flange connection with possible applied locations can be seen in Figure 1.2. In these connections, two flanges with an L-shape are aligned and are tightened by pretensioning a large number of bolts, such that it can withstand the high (cyclic) loading conditions the wind turbine is subjected to.

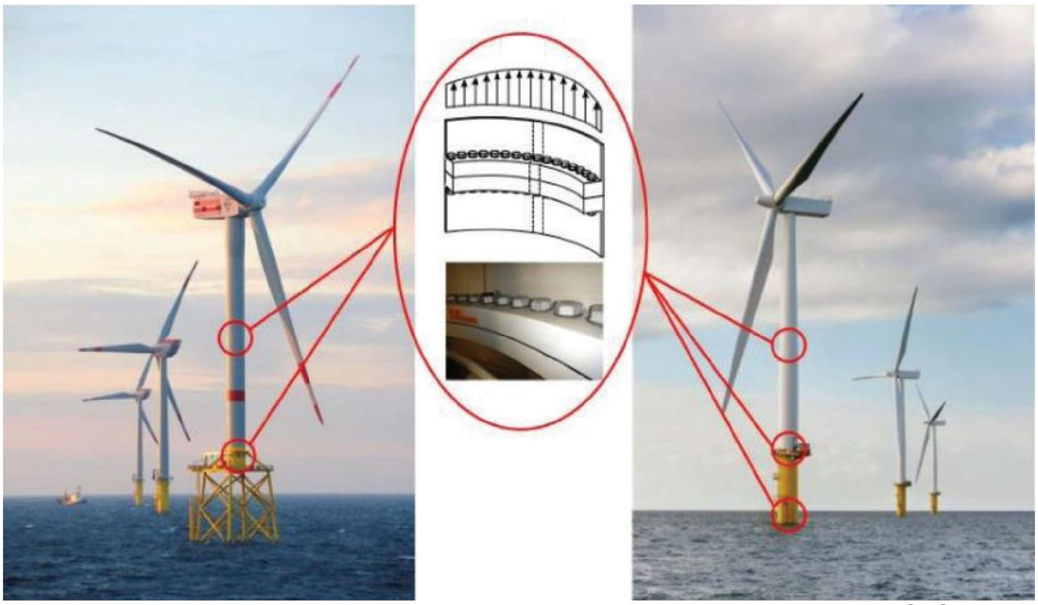

Figure 1.2: Bolted ring-flange connections at offshore wind structures [17]

1.1.3. Load transfer functions

For the design of bolted ring-flange connections in offshore wind turbines, the relation between the external force on the tower wall and the internal bolt force is of importance. This relation is described in load transfer functions (LTFs), which can be analytically and numerically obtained. The curve that represents the LTF is required to verify the design of the connection in fatigue limit state (FLS) and is used to calculate the lifetime of the structure. The external force on a section of the tower shell is denoted by Z and is equal to the tensile force on a segment of the flange that contains one bolt. The bolt force F_S is the force present in that single bolt. A visual representation of this segment with the forces can be seen in Figure 1.3.

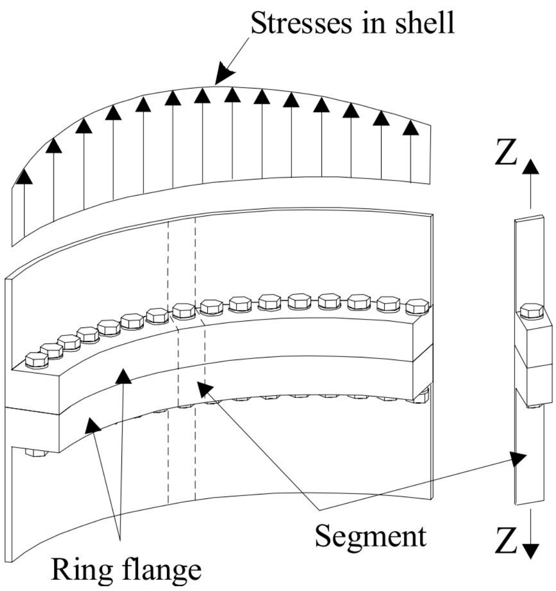

Figure 1.3: Segment model with internal and external force [19]

1.1.4. Geometric imperfections

Ideally, after production, 'perfect' flanges are obtained, that have a completely flat horizontal surface. When installing the connection, with these flanges, no gap forms between the two surfaces, and the connection is completely closed. However, in practice, it is very difficult to obtain these 'perfect' conditions, and manufacturers cannot ensure that no imperfections are formed during production. In these cases, small inclinations of the flanges are obtained, leading to gaps between the two flange before pretensioning of the bolts. These imperfections are characterized as geometric imperfections [22]. Even very small imperfections of one or two millimeters can have a large effect on the fatigue strength of the connection, as part of the preload applied on the bolts is used to close this gap [21].

1.2. Problem description

Current bolted ring-flange connections are mostly designed for 'current generation' wind turbines. These turbines are for example SG 11.0-200 DD and V174-9.5 MW [24, 29]. The nominal power of these turbines ranges from 9.5 MW to 11.0 MW and the rotor diameters range from 164 m to 200 m. With these current turbines, an outer diameter of 6500 mm for the connection between the turbine and TP is common.

The two beforementioned turbine manufacturers (Siemens Gamesa and Vestas) have announced and started developing prototypes for turbines with a larger rotor diameter. These turbines, that henceforth will be called 'next generation' turbines, will presumably be used in future offshore wind farms, as they generate more power per unit of time. The nominal power that is generated by one of these next generation turbines, namely SG 14-236 DD [24], is 14 MW. For these turbines, the diameter of the rotor is 236 m, compared to 164-200 m for 'older' wind turbines, and they will be able to power 18.000 households per operating year. These new turbines with their increasing dimensions come with new challenges for the design of parts of the turbine's substructure.

One of these challenges is the design of the connection between the TP and the tower. As wind turbines become larger, larger forces need to be transferred properly from the tower to the TP, often by a bolted ring-flange connection. For the next generation turbine with a rotor diameter of 236 m, expected is that the outer diameter of the connection will be up to 8000 mm, compared to 6500 mm for 'older' turbines.

Analytical calculations are used to obtain the LTF, often by using approaches that were obtained more than 25 years ago. For a long time, these approaches were valid for the turbine dimensions with the allowed gap tolerances. However, with the growing turbine and connection dimensions, a concern has arisen for the usability of these approaches. It has shown that for certain dimensions, the analytically obtained LTF gives an underestimation of the actual forces in the bolt.

Moreover, with these growing dimensions of the flanges, a challenge arises with respect to geometric imperfections. For these larger turbine diameters, it becomes more difficult for manufacturers to meet the allowed gap limitations, and gaps with different sizes are often obtained in practice.

1.3. Research questions and thesis outline

These problems as described above will be investigated in this thesis. The objective of this thesis is to obtain the influence of increasing the turbine dimensions on the resistance of the connection by analyzing the forces in the bolts. This will be done by answering the following research question:

> "How do the increasing dimensions of next generation offshore wind turbines influence the validity of the current used load transfer functions (LTFs) for bolted ring-flange connections?"

This research question will be answered by dividing the problem into two components. One part focuses on the increase in dimensions of the connection and its influence on the LTF. A parametric study will be done for various dimensions, and this part will be guided by answering the following sub-question:

> "How do different dimensions of ring-flange connections influence the validity of the LTFs?"

The second component of this research focuses on gaps between flanges and its influence on the LTF for both current generation and next generation turbines. Current gap tolerances and expected gap lengths and heights will be considered, where analytically obtained LTFs are analyzed for these gaps. This part will answer the sub-question:

> "Which gap shapes are still covered by the analytically obtained LTFs?"

In this thesis, only gaps that are symmetrical in shape are considered. The shape of the gap modeled is a perfect sinusoidal wave, where the two flanges are in contact every period of the sinus. Moreover, calculations will be performed for ultimate limit state and fatigue limit state, as these are the relevant resistances for wind turbines. Within the fatigue limit state, the calculations are performed to obtain the load transfer functions. Calculations to obtain the actual fatigue life by using S-N curves are not performed.

The objective of this thesis will be obtained by performing analytical calculations of existing approaches to obtain the LTF and comparing them to numerical calculations using the finite element method. The outline of this thesis is therefore as follows: Firstly, in Chapter 2, background information will be given obtained by literature study about geometric imperfections and relevant calculations and analytical approaches. The case study which contains the approach to achieve the objective is described in Chapter 3. In Chapter 4, the finite element model is elaborated that will be used for the numerical calculations. Chapter 5 contains the analytical calculations performed on the considered connections in ULS and the approaches chosen for the LTF. Following the analytical calculations, the numerical calculations are performed and analyzed in Chapter 6. In this chapter, the results of the analytical calculations are compared to the finite element results and partial conclusions are obtained. Finally, the most important findings of this thesis are summarized in the conclusion in Chapter 7, together with recommendations for further research.

2
Design methods for bolted ring-flange connections

In this chapter, the procedure and relevant calculations for the design of a bolted ring-flange connection for offshore wind turbines is described. The two type of calculations that are carried out in this thesis are for the resistance in ultimate limit state and fatigue limit state. Two other limit states, namely serviceability and accidental [4], are not considered, as those limit states are not relevant for this research. First, the calculation in ultimate limit state will be elaborated, followed by the fatigue limit state, where the approaches to obtain the load transfer function are described. Finally, the types of geometric imperfections and their relevance for the design of such a connection are elaborated.

2.1. Ultimate limit state

The ultimate limit state (ULS) is the state of the connection in which the maximum load-carrying capacity is reached, resulting in failure of the connection when exceeded. To ensure a safe structure, the connection therefore must be checked if it is resistant against possible failure mechanisms. According to Petersen [16], there are three failure mechanisms that can occur in L-flange connections (A, B and C). Seidel [20] proposed D and E as sub-mechanisms for C, as the location of yielding can be at the location of the bolt hole that is next to the bolt hole center or that is closest to the tower shell (see Figure 2.1). These possible failure mechanisms are listed below:

- A: Bolt failure only
- B: Bolt failure with plastic hinge in flange-to-shell junction
- C: Plastic hinge in flange and flange-to-shell junction. Two sub-mechanisms:
  - D: Plastic hinge in flange at bolt hole center and flange-to-shell junction
  - E: Plastic hinge in flange next to bolt hole center and flange-to-shell junction

In ULS, the L-flange is idealized as a beam, with the bolt included as a point load [25]. In Figure 2.1, the mechanical models of the failure modes A, B, D and E are shown, where the locations of the plastic hinges are shown.

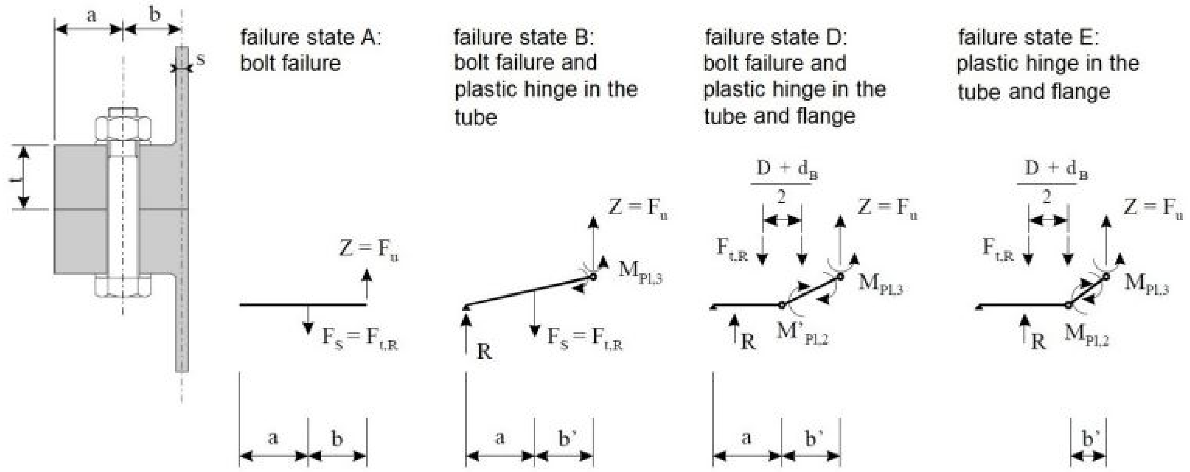

Figure 2.1: Failure modes of an L-flange connection [16] and [20]

In the following sections, each failure mode is further elaborated. Failure mode C is divided into its sub-mechanisms D and E, and will therefore not be elaborated separately.

2.1.1. Failure mode A

The first failure mode describes the bolt failure. This failure mode occurs when the internal bolt force is higher than the tension resistance of the bolt. When this situation occurs, a fracture emerges in the thread of the bolt, leading to bolt rupture and therefore ultimate failure. This failure mode is obtained by first calculating the design tensile resistance of the bolt $F_{t.Rd}$ [6] obtained by:

$$F_{t,Rd} = \frac{0.9 * f_{u,B} * A_{B.s}}{\gamma_{M2}} \tag{2.1}$$

The ultimate resistance of the connection for this failure mechanism is, therefore:

$$F_{u,A} = F_{t,Rd} \tag{2.2}$$

The bending moment at the location of the tower shell is the ultimate bolt force multiplied with the distance to the center of the shell. The condition of the resistance against this failure mode is therefore that the bending moment resistance at the location of the shell is higher than this bending moment:

$$M_{pl,3} \geq F_{t,Rd} * b \tag{2.3}$$

2.1.2. Failure mode B

In plastic failure mode B of the connection, bolt failure occurs and a plastic hinge forms in the flange-to-shell junction. The ultimate resistance of the connection for this failure mechanism is:

$$F_{u,B} = \frac{M_{pl,3} + a * F_{t,Rd}}{a + b} \tag{2.4}$$

A visual representation of distances a and b can be seen in Figure 2.1. The plastic bending moment in the shell $M_{pl,3}$ considers the M/N or M/V interaction [25] and is calculated with equations 2.5 and 2.6.

$$M_{pl,3} = min(M_{pl,N,sh}; M_{pl,V,fl}) \tag{2.5}$$

where

$$M_{pl,N,sh} = \left[1 - \left(\frac{N}{N_{pl,sh}}\right)^2\right] * M_{pl,sh} = \left[1 - \left(\frac{F_u}{c_w * s * f_{y,sh}}\right)^2\right] * \frac{c_w * s^2}{4} * f_{y,sh}$$

$$M_{pl,V,fl} = \left[\sqrt{1 - \left(\frac{V}{V_{pl,fl}}\right)^2}\right] * M_{pl,fl} = \left[\sqrt{1 - \left(\frac{F_u}{c * t * f_{y,fl}/\sqrt{3}}\right)^2}\right] * \frac{c * t^2}{4} * f_{y,fl} \tag{2.6}$$

In this failure mode, a prying force R is present at the tip of the flange. This prying force creates a bending moment at the location of the bolt, namely $R * a$. For this failure mode, this bending moment must be smaller than the bending moment resistance at the location of the bolt $M'_{pl,2}$. The condition for resistance against this failure mode, therefore, is:

$$M'_{pl,2} \geq R * a \tag{2.7}$$

2.1.3. Failure mode D

Failure mode D by [20] is a sub-mechanism for failure mode C determined by [16]. In this failure mode, a plastic hinge forms in the flange at the bolt hole center and flange-to-shell junction. With the following formula, the resistance against failure mode D can be calculated.

$$F_{u,D} = \frac{M'_{pl,2} + \Delta M_{pl,2} + M_{pl,3}}{b'_D} \tag{2.8}$$

where:

$$\Delta M_{pl,2} = \frac{F_{t,Rd}}{2} * \frac{d_W + d_B}{4} \tag{2.9}$$

This failure mode with certain characteristics is shown in Figure 2.2

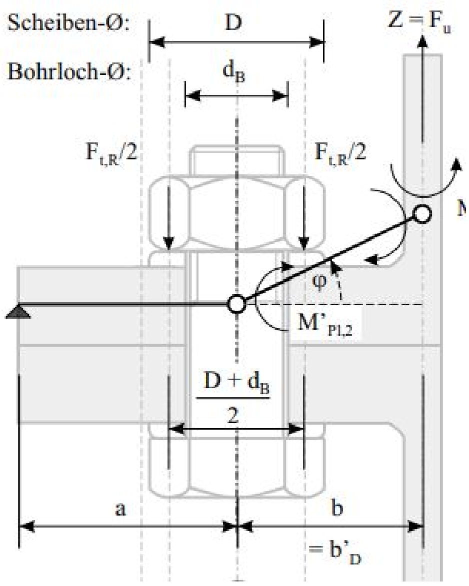

Figure 2.2: Failure mode D [20]

Condition:

$$\left(\frac{F_{t,Rd}}{2} - F_{u,D}\right) * \left(\frac{d_W + d_B}{4}\right) \leq M_{pl,2} - M'_{pl,2}$$
$$and \tag{2.10}$$
$$r = \frac{M'_{pl,2} + \Delta M_{pl,2}}{F_{t,Rd} - F_u} \leq a$$

2.1.4. Failure mode E

Failure mode E by [20] is the second sub-mechanism for failure mode C. In this failure mode, a plastic hinge forms in the flange next to the bolt hole center at the flange-to-shell junction (see Figure 2.3). The following formula calculates the resistance against this failure mode:

$$F_{u,E} = \frac{M_{pl,2} + M_{pl,3}}{b'_E} \tag{2.11}$$

where

$$M_{pl,2} = \frac{c * t^2}{4} * f_y \tag{2.12}$$

This failure mode with certain characteristics is shown in Figure 2.3

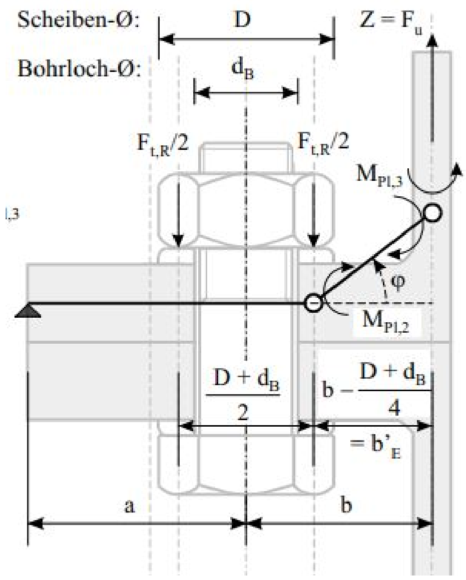

Figure 2.3: Failure mode E [20]

Condition:

$$\left(\frac{F_{t,Rd}}{2} - F_{u,E}\right) * \left(\frac{d_W + d_B}{4}\right) \geq M_{pl,2} - M'_{pl,2}$$
$$and \tag{2.13}$$
$$r = \frac{M'_{pl,2} + 2 * \Delta M_{pl,2}}{F_{t,Rd} - F_u} - \frac{d_W + d_B}{4} \leq a$$

2.1.5. Overview

In Table 2.1, an overview is given with the ultimate resistances and conditions for each failure mode.

Table 2.1: Overview failure modes with corresponding ultimate resistances and conditions

Failure mode	Ultimate resistance	Condition
A	$F_{u,A} = F_{t,Rd} = \frac{0.9 * f_{u,B} * A_{B.s}}{\gamma_{M2}}$	$M_{pl,3} \geq F_{t,Rd} * b$
B	$F_{u,B} = \frac{M_{pl,3} + a * F_{t,Rd}}{a+b}$	$M'_{pl,2} \geq R * a$
D	$F_{u,D} = \frac{M'_{pl,2} + \Delta M_{pl,2} + M_{pl,3}}{b'_D}$	$\left(\frac{F_{t,Rd}}{2} - F_{u,D}\right) * \frac{d_W + d_B}{4} \leq (M_{pl,2} - M'_{pl,2})$ $r = \frac{M'_{pl,2} + \Delta M_{pl,2}}{F_{t,Rd} - F_u} \leq a$
E	$F_{u,E} = \frac{M_{pl,2} + M_{pl,3}}{b'_E}$	$\left(\frac{F_{t,Rd}}{2} - F_{u,E}\right) * \frac{d_W + d_B}{4} \geq M_{pl,2} - M'_{pl,2}$ $r = \frac{M'_{pl,2} + 2 * \Delta M_{pl,2}}{F_{t,Rd} - F_u} - \frac{d_W + d_B}{4} \leq a$

2.2. Fatigue limit state

As offshore wind turbines are subjected to high dynamic loads, it is essential that a fatigue assessment is done for the connection of the structure. One part of the calculation of the resistance against fatigue is determining the forces in the bolt at certain external loads. The relation between this axial tensile force on the tower and the force in the bolt is described in the load transfer function (LTF).
In the following sections, the initial preload applied on the bolts and the characteristics of the LTF are elaborated and approaches to analytically calculate this LTF are explained.

2.2.1. Pretension

When installing the connection of an offshore wind turbine, pretension is applied to the bolts to tighten the connection, and, in case of gaps present between the flanges, to close the gap. The pretension applied on each bolt F_V is calculated with Equation 2.14. The pretension is reduced with a factor of 0.9 because of losses in pretension due to the large number of load cycles [3].

$$F_V = 0.9 * (0.7 * f_{u.B} * A_{B.s}) \tag{2.14}$$

2.2.2. Load transfer functions

This subsection will contain an overview of different approaches for the load transfer function of a bolted ring-flange connection. Previously, many studies were performed to obtain approaches for the LTF. A few well known and most used load transfer functions are elaborated in this subsection and finally, an overview will be given of these LTFs and a comparison will be made. With this comparison, analytical approaches are determined that will be used for the calculation of the LTF and the validity check with numerical results. In LTFs, the external force Z in the LTF is obtained by integrating the axial stresses over the cross-sectional area of the tower shell for a segment of one bolt. In FLS calculations, the 'worst' segment should be considered, meaning the largest load applied on the tower and the largest force in the bolts.

The LTF of a geometrically perfect bolted ring-flange connection, so without any gaps present, is non-linear due to the eccentric load and presence of the preload F_V of the bolts [22] and it can be divided into four regions. The first region is an almost linear function where the connection is closed. The variation in bolt force in this region is small [30]. In the second region, the stresses between the flanges increase and the curve of the LTF increases rapidly. This region of the LTF describes the opening of the flange. In the the third region, the stresses between the flanges are high and the curve describes an opened flange. The slope of the curve in this region depends on the loads and geometry of the flange [30]. In the fourth and final region, the high stresses lead to plastic deformation in the bolts and/or flanges, until ultimate failure of the connection. For fatigue calculations, the first two regions are most relevant, because the most relevant loads for fatigue resistance are in these regions [22]. A visual representation of a non-linear curve of external load versus the internal bolt force with these four regions is shown in Figure 2.4.

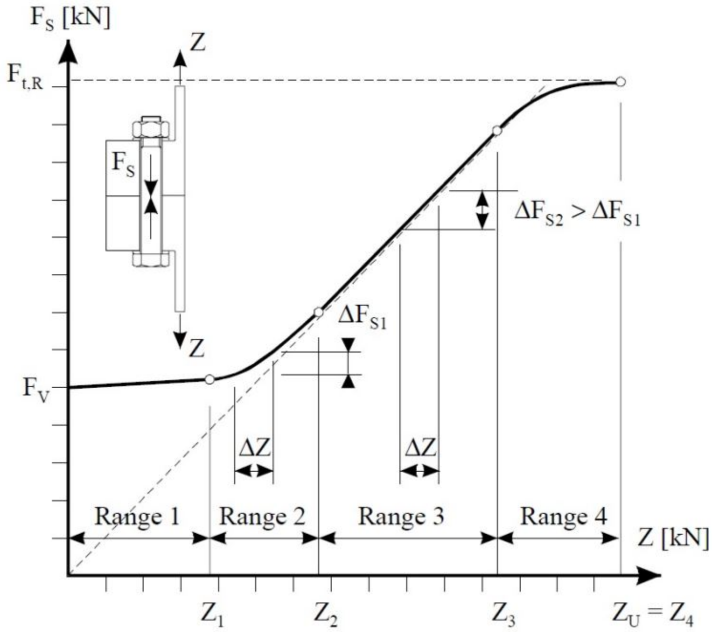

Figure 2.4: Load transfer function [19]

The first region of the LTF is mainly influenced by the preloading of the connection and a possible gap between the flanges. The pretension on the bolts results in a lower variation in bolt force at this region, which results in a higher resistance of the connection to fatigue loads in the bolts [17].

Each load transfer function that will be elaborated in this subsection uses as input parameters two stiffnesses C_S and C_D. These stiffnesses are respectively the stiffness of the bolt and the stiffness of the flange. Petersen [16] suggested a set of formulas to calculate these stiffnesses, see Equation 2.15.

$$\begin{aligned} C_{S.Pet} &= \frac{1}{\delta_S} = \frac{E * A_B}{2 * t + 2 * h_W} \\ C_{D.Pet} &= \frac{1}{\delta_D} = \frac{E * \pi}{4 * 2 * t} * \left(\left(d_W + \frac{2 * t}{10}\right)^2 - d_B^2\right) \end{aligned} \tag{2.15}$$

A more accurate method to calculate the stiffness of the bolt was obtained by [27], where different parts of the bolt were taken into account, see Equation 2.16. For the calculation of the LTFs for each method, the stiffness of the bolts from this approach is used.

$$C_{S.VDI} = \frac{1}{\delta_S}$$
$$\delta_{S.VDI} = \delta_{SK} + \delta_l + \delta_{Gew} + \delta_G + \delta_M$$
$$\text{where}$$
$$\delta_{Gew} = 0 \tag{2.16}$$
$$\delta_{SK} = \frac{0.5 * d_B}{E * A_B} \qquad \delta_l = \frac{2 * t}{E * A_B}$$
$$\delta_G = \frac{0.5 * d_B}{E * A_B} \qquad \delta_M = \frac{0.4 * d_B}{E * A_B}$$

The spring values p and q are obtained using these stiffnesses:

$$p = \frac{C_S}{C_S + C_D}, \quad q = \frac{C_D}{C_S + C_D} \tag{2.17}$$

Bi-linear (Petersen)

The bi-linear LTF by Petersen [16], determined in 1988, is a simplified approach of the relation between the external load and internal bolt force. As the name states, it is a function with two linear parts, connected by a critical external load Z_{crit}. The LTF according to the bi-linear approach is shown in Figure 2.5 and is determined with equations 2.18. For this approach, no limits were given.

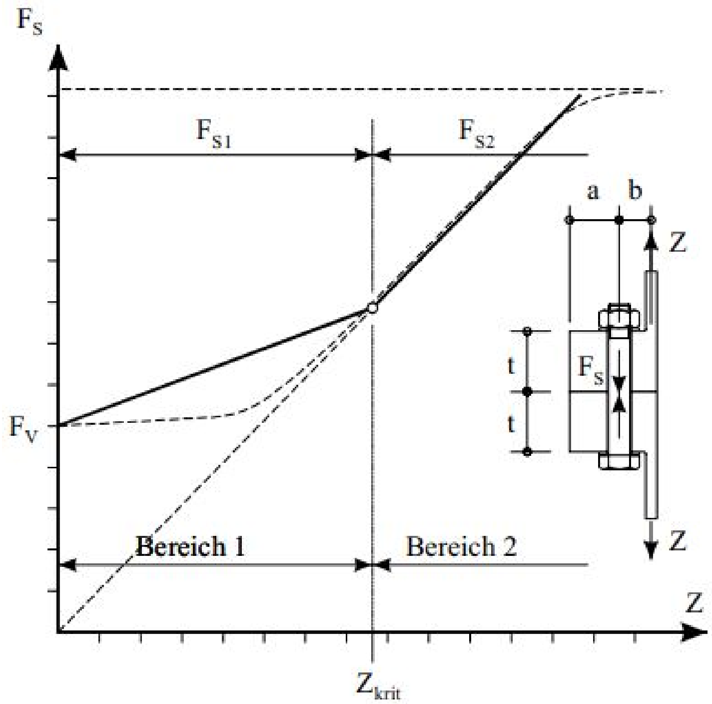

Figure 2.5: Bi-linear LTF by Petersen [20]

$$F_{S,1} = F_V + p * \lambda * Z_I$$
$$F_{S,2} = \lambda * Z \tag{2.18}$$

where

$$Z_{crit} = \frac{F_V}{\lambda * q}$$
$$\lambda = \frac{a+b}{a} \tag{2.19}$$

Compared to the LTF of an actual model, the bi-linear approach is conservative. As can be seen in Figure 2.5, the first region of the LTF shows an overestimation compared to an actual curve, and is therefore a safe approximation. The second region, however, is an unsafe approximation when the connection is not a perfect flange and contains imperfections. Moreover, the bi-linear approach does not consider stresses due to bending of the bolt. [28]

Circular arch (Faulhaber/Thomala)

The circular arch approach from Faulhaber/Thomala [9], determined in 1987, describes a curve of the LTF with two linear functions connected by a circular arch. This approach is a close estimation of the LTF of a perfect flange, as can be seen in Figure 2.6.
The limit of this approach is:
$a + b \leq D_{washer} + t$

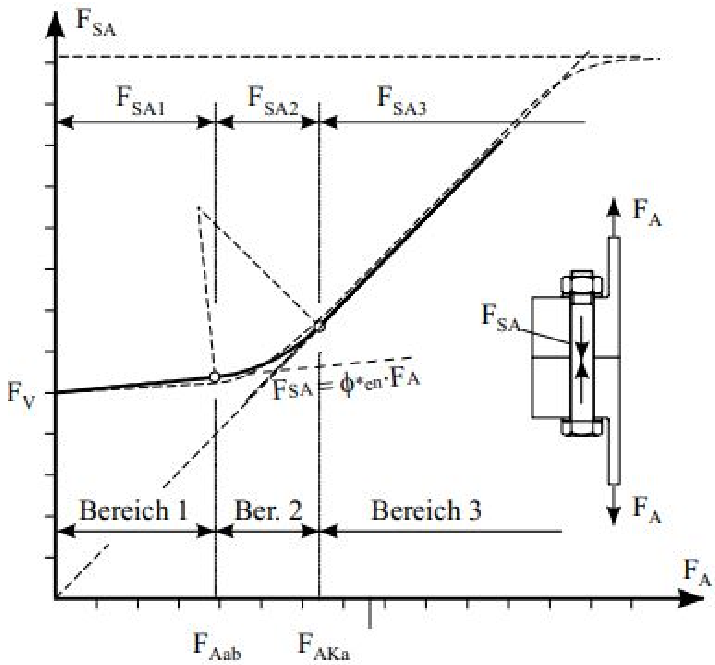

Figure 2.6: Circular arch LTF by Faulhaber/Thomala [20]

$$F_{S,1} = \phi_{en} * Z + F_V$$
$$F_{S,2} = F_V + n_k - \sqrt{r_k^2 - (Z - m_k)^2} \tag{2.20}$$
$$F_{S,3} = \frac{v + a}{v + s_{sym}} * Z$$

The slope of the third region of the function is very close to the LTF of a geometrically perfect flange. At this third region, so at high forces in the tower shell, this approach can lead to an underestimation of the internal bolt force and therefore unsafe results.

Polynomial (Petersen)

The polynomial approach determined by Petersen in 1998 [16] is a calculation method that describes the LTF with one equation.

$$F_S = F_V + \alpha * p * \lambda * Z + c * Z^2 + d * Z^3 \tag{2.21}$$

where

$$c = [3 * p - (\beta + 2 * \alpha * p) * \gamma] * \frac{\lambda}{\gamma^2 * Z_{crit}}$$
$$d = -[2 * p - (\beta + \alpha * p) * \gamma] * \frac{\lambda}{\gamma^3 * Z_{crit}^2}\lambda \quad = \frac{a + b}{a} \tag{2.22}$$
$$Z_{crit} = \frac{F_V}{\lambda} * q$$

and

$$\alpha = 0.3, \quad \beta = 0.5, \quad \gamma = 0.8 \tag{2.23}$$

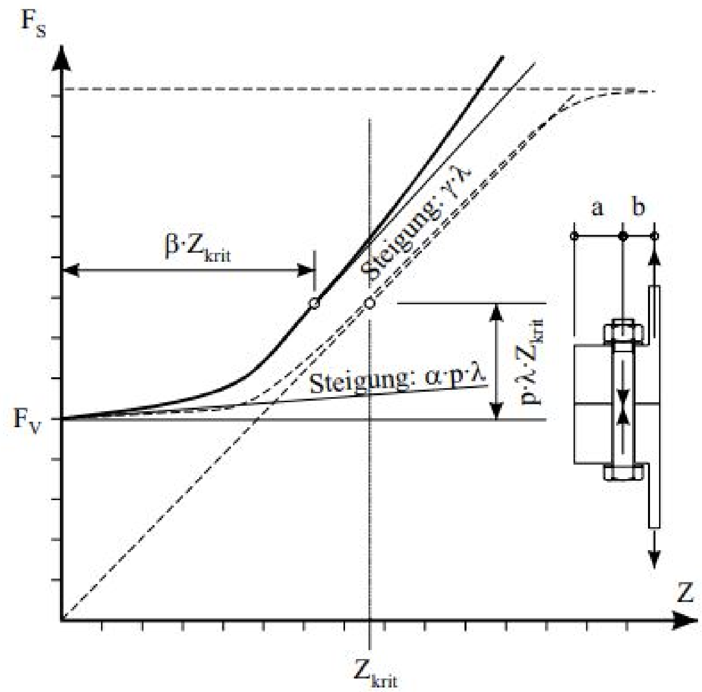

Figure 2.7: Polynomial approach by Petersen [16]

Tri-linear (Schmidt/Neuper)

The LTF by Schmidt/Neuper is a tri-linear approach developed in 1997 in [18] and is currently the most widely used method in practice and recommended to use by DNV [4]. For the tri-linear approach, the flange is idealized as a beam. As it is a tri-linear function, it contains three linear segments that are obtained by equations 2.24 and 2.25.
The limitation of the function is:

$\frac{a+b}{t} \leq 3$

As the curve describes a the LTF of a symmetrical flange, t the thickness of both of the flanges (see Figure 2.8).

$$\begin{aligned} F_{S,1} &= F_V + p * Z \\ F_{S,2} &= F_V + p * Z_I + [\lambda * Z_{II} - (F_V + p * Z_I)] * \frac{Z - Z_I}{Z_{II} - Z_I} \\ F_{S,3} &= \lambda * Z \end{aligned} \tag{2.24}$$

where

$$\begin{aligned} Z_I &= \frac{a - 0.5 * b}{a + b} F_V \\ Z_{II} &= \frac{1}{\lambda * q} F_V \end{aligned} \tag{2.25}$$

The three linear functions that describe the LTF are $F_{S,1}$, $F_{S,2}$ and $F_{S,3}$ and they are connected by the external loads Z_I and Z_{II}. The first region of the tri-linear LTF represents a closed connection, the second region describes the successive opening of the flange and the third region describes an open connection. The tri-linear LTF with these resions is shown in Figure 2.8.

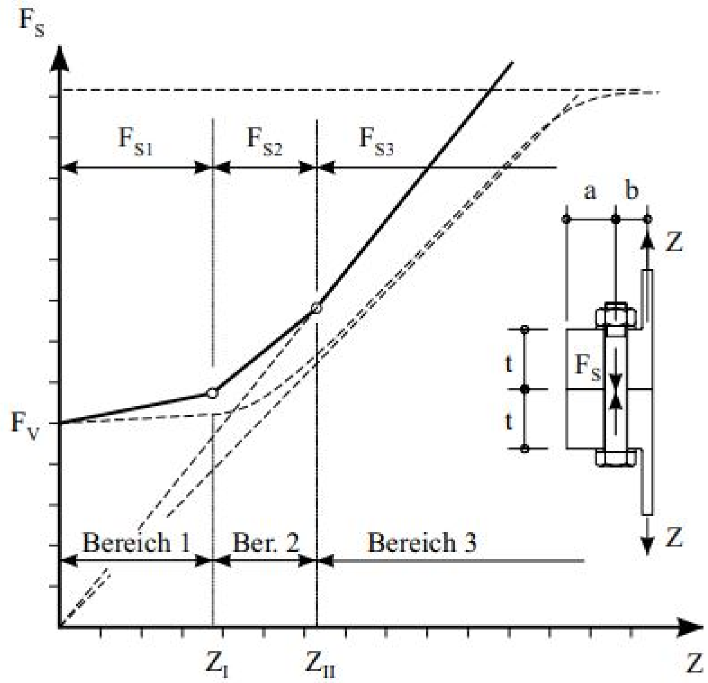

Figure 2.8: Tri-linear LTF by Schmidt/Neuper [20]

Even though the tri-linear approach by Schmidt/Neuper is the most widely used method, the approach is known to be conservative, as it does not take gaps explicitly into account. As can be seen in Figure 2.8 and comparing that to 2.5, the slope of the first region is low compared to the bi-linear approach by Petersen. For low external forces Z, this function is therefore less conservative than the bi-linear approach. The third region of the LTF by Schmidt/Neuper, looks overestimated compared to a perfect flange. This region of the LTF, however, is determined taking small imperfections into account. The LTF by Schmidt/Neuper covers, therefore, certain gap shapes and sizes, but the range of these imperfections is unknown [22].

With the increasing dimensions of OWTs, the dimensions of the connections consequently grow in size as well. Concerns about the use of this LTF have arisen for connections with these larger dimensions, and the applicability of this LTF is therefore questioned [30].

Non-linear (Seidel)

The non-linear approach by Seidel [19] is an iterative calculation where the flange is idealized as a cantilever beam that is fixed at the intersection of the flanges [28]. The cantilever bends due to the tension force in the tower shell and creates a rotation ϕ, as can be seen in Figure 2.9. This rotation results in an elongation of the bolt Δl_S, which can be calculated by obtaining the stress in the bolts. The internal bolt force results from a centric and eccentric part, see Equation 2.26.

$$
\begin{aligned}
F_S &= F_V + \Delta F_S \\
\Delta F_S &= \Delta F_{S,centric} + \Delta F_{S,eccentric}
\end{aligned}
\tag{2.26}
$$

In these formulas, the centric bolt force is calculated using the VDI 2230 guidelines [27] and the eccentric bolt force by including a bending moment and geometric imperfections. The calculation of this bolt force F_S is done iteratively and calculates the force resulting from the bending moment and the axial force. The iterative calculation of the centric and eccentric part result in a non-linear curve that is obtained with Equation 2.27. The complete approach is worked out in Chapter 5.

$$F_S = \frac{t * s_{sym} * C_S * Z * (b + s_{sym}) + EI * (\Phi * Z + F_V + s_{sym} * C_S * \phi_{imp})}{s_{sym}^2 * t * C_S + EI} \tag{2.27}$$

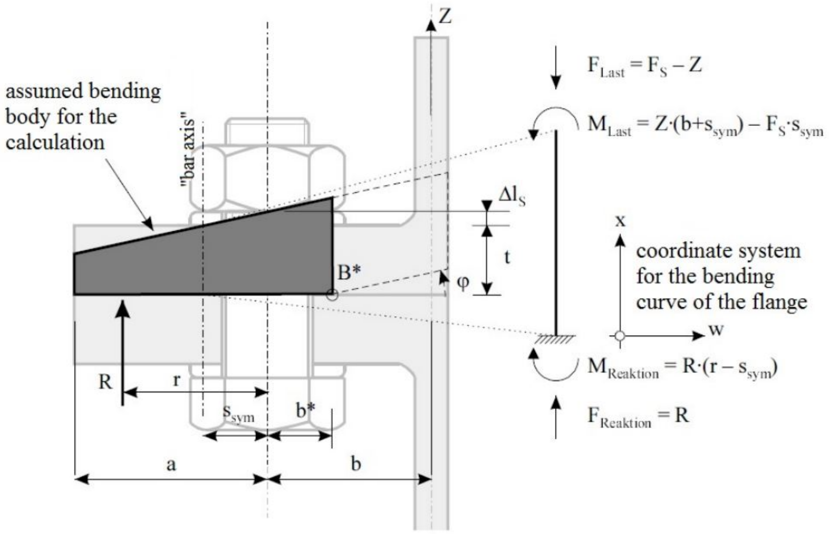

Figure 2.9: Model of flange according to approach Seidel [20]

The non-linear approach is a less conservative approach compared to earlier determined methods, as it takes into account the bending moment stresses in the bolt. For earlier approaches, only the axial force in the bolt was considered [17]. Moreover, this approach explicitly considers geometric imperfections, implemented by an angle ϕ_{imp} that is calculated from the gap height. For this approach, the limit of application is obtained from [20]:

$$t \leq \sqrt{\frac{8 * a^2 * b^2 * A_B}{c * (a + b)}} \tag{2.28}$$

Polynomial (Seidel)

During the writing of this thesis, a new approach was developed to analytically obtain the LTF. This LTF is represented by a polynomial that fits through three constructed points. An improvement of this approach compared to the abovementioned approaches, is that both gap height and gap length are input variables. This approach is, at the moment of writing, still under review and has not been approved yet to be used in practice. The document containing the calculation steps has therefore not been published yet.

Comparison of models

A number of analytical approaches for the LTF were analyzed in [20] and a comparison was done between the approaches and an FE model. A figure with the LTF of a.o. the approaches mentioned in previous subsections and the results using FEA are shown in 2.10 for external load regions up to 360 kN. From this comparison, a few conclusions are obtained. Firstly, some LTF are more conservative than others. The bi-linear approach from Petersen is the most conservative approach and leads to much higher damage values than the values obtained by FEM. The tri-linear approach from Schmidt/Neuper and the polynomial approach from Petersen are conservative as well. However, they are less conservative compared to the bi-linear approach from Petersen. The non-linear approach by Seidel is close to the results obtained by FEM. The circular arch approach by Faulhaber/Thomala is also close to the results obtained by FEM. However, this curve results for some flanges in lower bolt forces than the results obtained by FEM, resulting in an unreliable and unsafe approach.

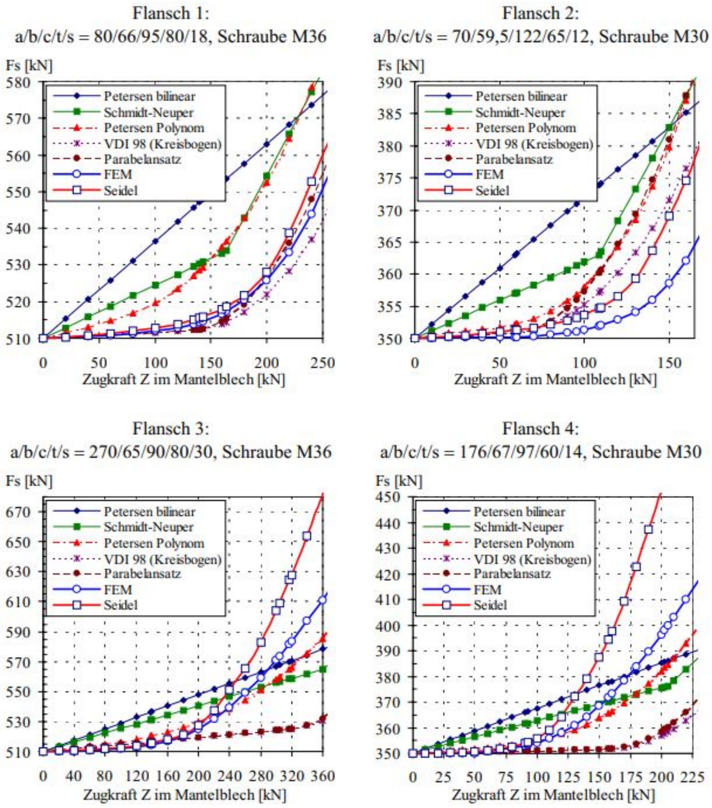

Figure 2.10: Comparison of FE results and different LTF approaches [20]

For the calculations in this report, three approaches are chosen to calculate the load transfer function. The tri-linear LTF by Schmidt/Neuper [18] is chosen, because it is the most used approach in current practice. Moreover, the non-linear approach by Seidel [20] is chosen, because this approach takes bending moments and geometric imperfections explicitly into account. A third approach that is considered in this thesis, is the recently created polynomial approach by Seidel. This approach is investigated, as it explicitly takes into account both the gap height and the gap length.Other approaches will not be used for the calculations, because they are either too conservative or known to lead to unsafe results at either low or high external forces.

2.3. Geometric imperfections

Flanges with geometric imperfections can be classified in flanges with three types of gaps: flange sided gaps, tower sided gaps and parallel gaps. These types of geometric imperfections can occur over part of the circumference of the connection or over the entire circumference. An overview of different types of gaps in a bolted ring-flange connection is shown in Figure 2.11.

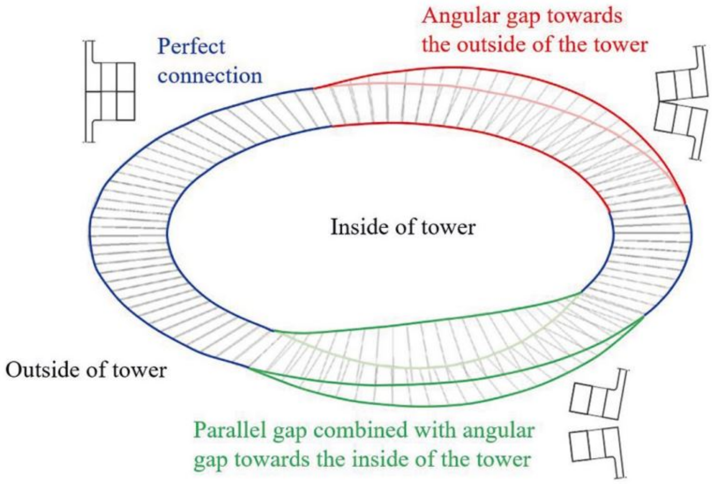

Figure 2.11: Schematic illustration of different types of gaps in a ring-flange [1]

Geometric imperfections in bolted ring-flange connections have been studied in many researches, including [13], where it was obtained that for the fatigue calculation, flange sided gaps have a positive influence on the LTF. In [30], it was obtained that flange sided gaps indeed result in a more shallow tri-linear LTF than a geometric perfect flange in load region one and two. Moreover, it was obtained that tower sided and parallel gaps are more difficult to close and the closing of these gaps result in bolt bending and a clamp solid that is at an unfavourable location, namely toward the inside of the flange.

The effect of parallel gaps on the ring-flange connection is shown in Figure 2.12. Ideally, the preload force is transferred by the contact between the flanges. However, when parallel gaps are formed between flanges, the preload force is partially transferred into the tower wall [13]. Tensile membrane stresses occur in the middle of the gap and compressive membrane stresses adjacent to the gap. This causes an increase in fatigue loading for the center bolts. Initial parallel gaps between bolted ring-flange connections can significantly increase the fatigue load of the connecting fasteners.

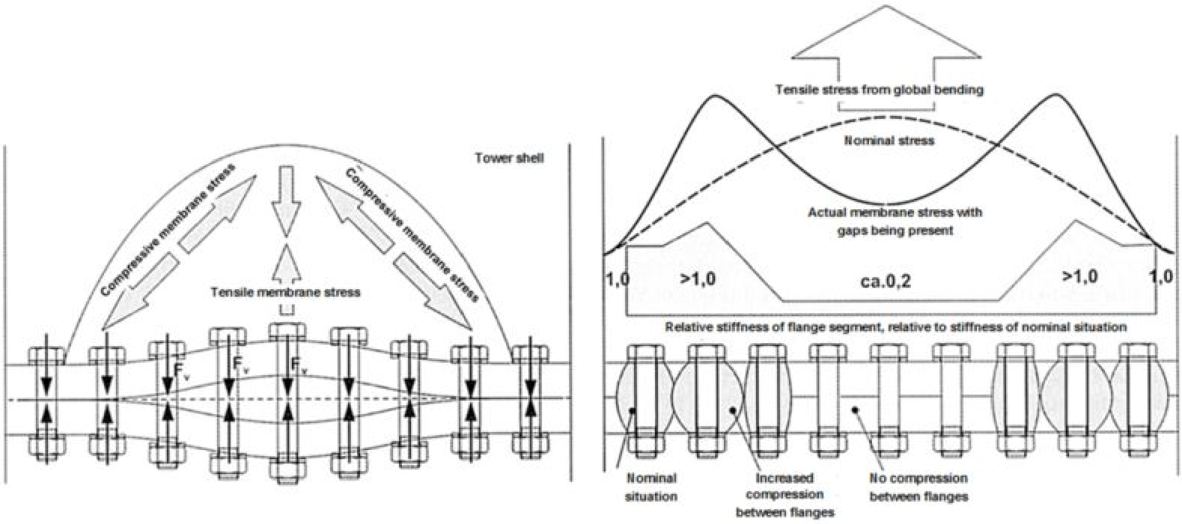

Figure 2.12: Force behaviour for bolted flanges with gap [13]

Due to the preloading of the bolted connection, a pressure body develops around the location of contact between the flanges. For a geometrically perfect ring-flange, the so-called 'clamp solid' develops centrically around the bolt, see Figure 2.13 (left). If the external loads on the connection do not lead to gapping, the additional bolt forces due to the formed pressure body are significantly reduced [22].

For geometrically imperfect flanges, this clamp solid can develop eccentrically at the location where the flanges are in contact. A figure of the different types geometrical imperfections with its pressure bodies is shown in Figure 2.13. For flange sided gaps, the clamp solid develops at the outer side of the tower (see Figure 2.13), which is favourable because this is close to the resulting axis of external forces.

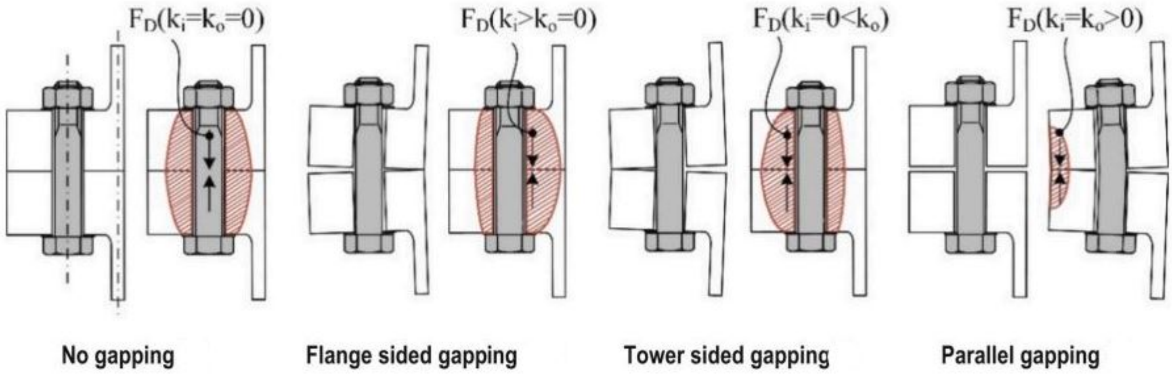

Figure 2.13: Schematic illustration of different gap types with their pressure bodies [22]

An illustration of a LTF for a perfect flange with in the same graph a LTF for a flange with geometric imperfections is shown in Figure 2.14. In this figure, it can be seen that the forces in the bolt increase from the first load region.

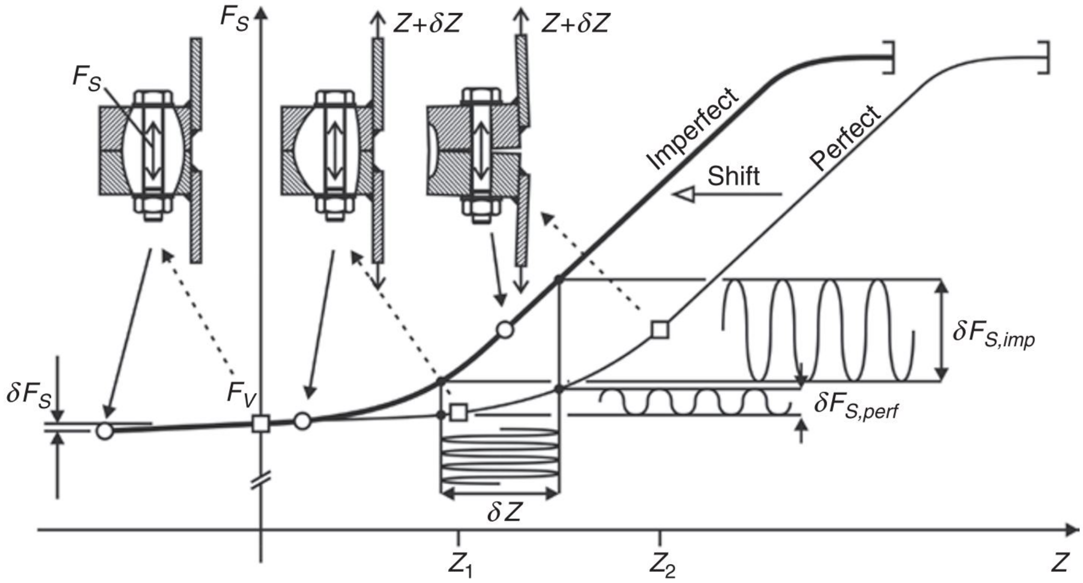

Figure 2.14: Difference between a perfect flange and the shift to an imperfect flange [28]

2.3.1. Limitations

Due to a number of wind turbine failures at the bolted connection during operation, inspection showed that these failures were caused by bolt rupture. In the failure reports, it was concluded that this bolt rupture was caused by gaps that originated during production [21]. To prevent this type of failure from happening, a maximum tolerance was determined on the flatness deviation of these flanges In current rules and guidelines by DNV [4], requirements and limitations are stated for the design of support structures for wind turbines, including these geometric imperfections. Two limitations are given for the flatness tolerance of the flanges, so that the LTF can be approximated with the tri-linear approach by Schmidt/Neuper [30]:

Flatness deviation	u_{gap}	$\leq 1mm$	over	segment of $30°$
Flatness deviation	u_{gap}	$\leq 2mm$	over	entire circumference

In Figure 2.15, an illustration of gaps between flanges is shown. The flatness deviation, henceforth called 'gap height', u_{gap}, of X mm is defined as the distance between the surface of a 'perfect' flange and the largest deviation (in Figure 2.15 equal to $k/2$). A length of the gap of Y mm and a gap angle of Z° are correspondingly the distance between one contact point of the flange and the largest height of the gap (in Figure 2.15 equal to $l_k/2$).

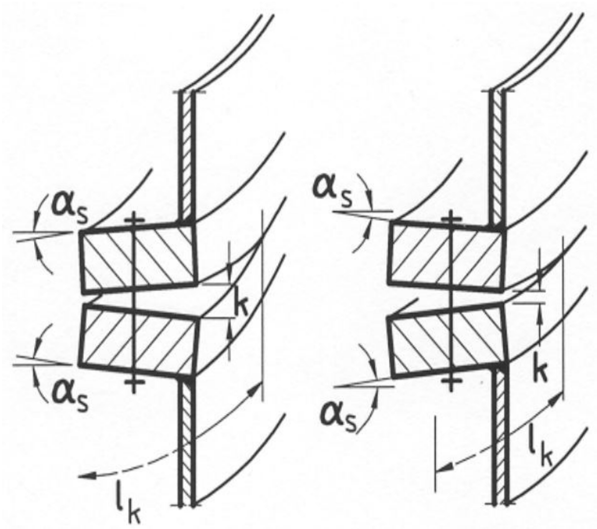

Figure 2.15: Flatness deviation flanges [4]

These abovementioned tolerances are valid for flanges before the connection is preloaded. In the DIBt-Guideline for wind turbines [3], another limitation was given, namely a maximum inclination after preloading:

$$\alpha_s \leq 2\%$$

In [21], another gap height limitation was proposed, which takes into account the available gap closing stress of the flanges. The preload that is applied on the bolts is used to close the initial gap between the flanges. To ensure that this gap can actually be closed, the tower flange and shell stiffnesses are calculated and limitations for either the gap height and length or tower wall thickness and segment width are determined. The gap height limitations are defined with the following equations:

$$\begin{gathered}
\alpha_{gap} * 2 \leq 90^\circ : l_{gap} = \frac{\alpha_{gap} * 2}{360^\circ} * \pi * D_O \\
\alpha_{gap} * 2 \geq 90^\circ : l_{gap} = \frac{\pi}{4} * D_O \\
\\
u_0 = 1mm * \frac{l_{gap}}{1000mm} \\
u = u_0 * \frac{\frac{F_V}{c*s}}{325MPa}
\end{gathered} \tag{2.29}$$

In the new document by Seidel that includes the new polynomial approach, an updated limitation has been proposed, where a gap closing force is, using the stiffness of the shell and flanges, is defined, which cannot exceed 50% of the design preload.

2.3.2. Cyclic loading

Another aspect that is of importance for the calculation of the resistance of the connection against fatigue is the load variation range. A wind turbine is subjected to an extremely large number of load cycles with lower external forces than the load determined for the ultimate limit state. Therefore, it is of importance to know what the forces in the bolts are at these lower external forces. This is measures by calculating the load variation range, which is defined as the variation in bolt force ΔF_S at a range in external force ΔZ. As can be seen in Figure 2.14, when observing the LTF for perfect flanges and imperfect flanges, the variation in bolt force at a certain external load range increases significantly for imperfect flanges.

2.4. Finite element analysis

Most problems are too complicated to be solved analytically. When complexity of for example geometry, non-linearity or certain loads are added to a problem, it gets very complicated or even impossible to solve it analytically. In bolted ring-flanges, it is therefore necessary to perform tests to ensure safety of the connection. However, it is not feasible to do full-scale laboratory tests on large bolted ring-flange connections. For these problems, the use of the finite element method (FEM) is used. The basic idea of modelling with FEM is that a structure is divided into a number of small elements. For each element, when solving the problem using the software, equilibrium equations are formed and solved numerically. In [22], a study has been performed on the effect of imperfections and a comparison was made between numerical results and an actual wind turbine. This paper showed that the effect of imperfections can be predicted very well with finite element analyses (FEA). Therefore, in this thesis, analytical calculations are made and these analytical results are checked numerically by doing finite element analyses.

2.5. Guidelines

For the calculations and assumptions in this thesis, a few rules and standards are used. The following guidelines that are used in this thesis is listed below:

- DNV-ST-0126 - Support structures for wind turbines [4]
- DNV-RP-C203 - Fatigue design of offshore steel structures [5]
- Eurocode 3: Design of steel structures - Part 1-8: Design of joints [6]
- Eurocode 3: Design of steel structures - Part 1-9: Fatigue [7]
- VDI Richtinien - Systematic calculation of highly stressed bolted joints [27, 26]
- DASt - Richtlinie für Schraubenverbindungen [2]
- DIBt - Richtlinie für Windenergieanlagen [3]

3
Case study

In this chapter, the method of approach to answer the research question will be described. The research question stated for this thesis is:

> "How do the increasing dimensions of next generation offshore wind turbines influence the validity of the current used load transfer functions (LTFs) for bolted ring-flange connections?"

The following section describes the approach how the objective of this thesis will be obtained.

3.1. Approach

To answer the research question stated above, several general steps need to be made. Firstly, a model of a bolted ring-flange connection needs to be determined as a base for all calculations. The dimensions of this model and how they are obtained is described in Section 3.2. This model will hereafter be called 'reference model'. The reference model will firstly be made without geometric imperfections. The results of the analytical approaches, as described in Chapter 2, will be compared to results obtained with finite element (FE) calculations. The properties assigned to this model are described in Chapter 4.

After the load transfer functions are obtained numerically and analytically for this reference model, geometric imperfections are applied to the flange. The applied geometric imperfections and how they are determined is discussed in Section 3.5. This section focuses mainly on what range of gap shapes are covered by analytical approaches that obtain the LTF. The second sub-question will be answered by parameterizing the dimensions of certain parts of the ring-flange connection. A number of dimensions is chosen and elaborated in Section 3.4 that will be altered to obtain what the influence is on the LTF, both numerically and analytically.

An objective of this thesis is to obtain the validity of these analytical approaches of the LTF for wind turbines that will be used in future projects. Therefore, dimensions are approximated that are likely to represent a future wind turbine A hereafter called 'next generation model' is made with these dimensions. This next generation model is described in Section 3.3 and is used for the parameterization of the geometric imperfections and flange dimensions. By answering the two sub-questions that focus on two aspects of the increasing dimensions of ring-flange connections, an answer will be able to be given to the main research question.

As decided in Chapter 2, the three analytical approaches that are considered in this research are the approaches listed below.

- Tri-linear approach by Schmidt/Neuper (1997)
- Non-linear approach by Seidel (2001)
- Polynomial approach by Seidel (2023, not published yet)

For convenience, these approaches will be referred to as its LTF shape. Therefore, when referring to the polynomial approach, the approach by Seidel (2023) is referred to, not the polynomial approach by Petersen [16].

3.2. Reference model

In this section, the dimensions of the reference model are obtained and elaborated. To ensure that the dimension of this reference model are valid, it will be based on realistic dimensions. These dimensions are obtained by a combination of projects from Ramboll with verified designs of a ring-flange connection with a diameter of 6.5 m. As these projects are made for clients and are therefore confidential, the dimensions are not shown (when publishing on repository). The dimensions of this reference model and other material characteristics are given in the following section.

3.2.1. Dimensions

The reference model is based on projects with similar dimensions for turbines of 9.5MW and 10MW, with an outer diameter of the connection of 6500 mm. The dimensions of the projects that the reference model is based on is listed in Table 3.1. In the bottom line of the table, the dimensions that are chosen for the reference model are listed. In the first row, the abbreviations of the connection dimensions are given. The full list of abbreviations, including these, can be found at the beginning of this report.

Table 3.1: Dimensions of reference model and connections based on, all dimensions in [mm]

	BD	Power	CD	BCD	FT	TWT	TPWT	DI	DO
[redacted]	[redacted]	[redacted]	[redacted]	[redacted]	[redacted]	[redacted]	[redacted]	[redacted]	[redacted]
[redacted]	[redacted]	[redacted]	[redacted]	[redacted]	[redacted]	[redacted]	[redacted]	[redacted]	[redacted]
[redacted]	[redacted]	[redacted]	[redacted]	[redacted]	[redacted]	[redacted]	[redacted]	[redacted]	[redacted]
Reference model	M64		6500	6220	135	35	60	175	140

A figure with these and other relevant dimensions of the flange is shown in Figure 3.1(a). In Figure 3.1(b), the dimensions of the bolts and the washers are shown. In the reference model, 156 bolts are used with a bolt size M64. A full list of these dimensions is added in Appendix A.

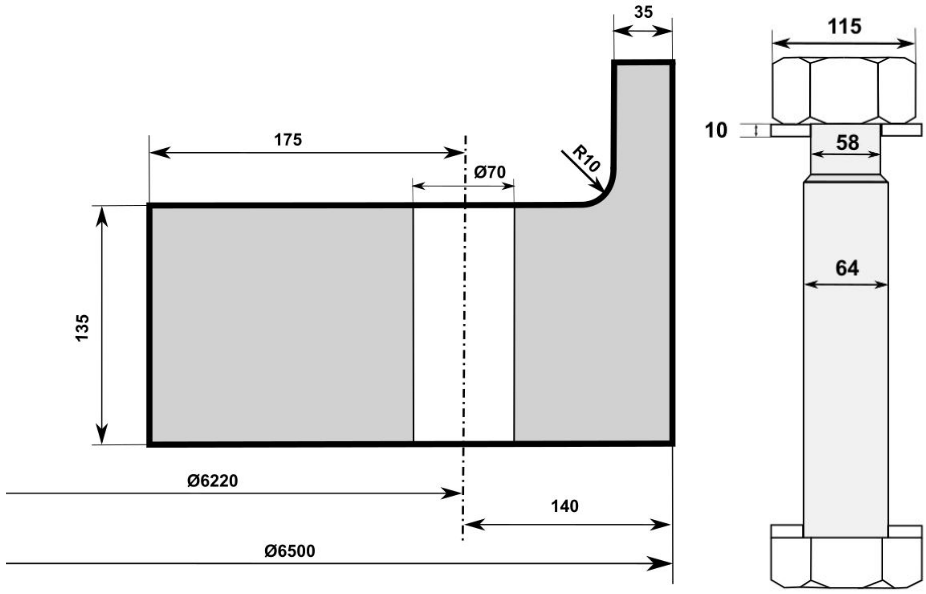

(a) (b)

Figure 3.1: Dimensions reference model (a) flange (b) bolts

3.3. Next generation model

In this section, the dimensions for the next generation model are approximated. Turbines that are considered to be next generation turbines, are turbines that have a nominal power of 14MW to 15MW [24, 29], which are turbines with a rotor diameter of 236 m.

For these next generation turbines, exact dimensions and loading conditions will be approximated. As stated in Chapter 1, expected is that the outer diameter of the connection for these turbines will be 8000 mm. For the other dimensions of the connection, an assumption will be made by using this diameter and other dimensions from the reference model. Assumed is that the dimensions of the flanges increase proportionally to the diameter of the connection. That means, the dimensions will be increased with a factor $8000/6500 = 1.23$ in relation to the reference model. The dimensions of the next generation model will therefore be:

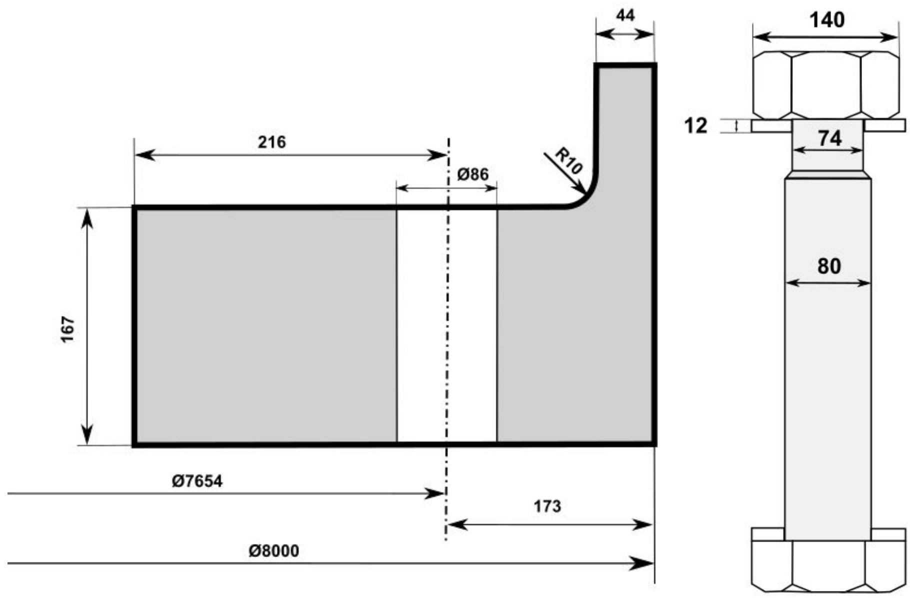

(a) (b)

Figure 3.2: Dimensions next generation model (a) flange (b) bolts

The calculation of the number of bolts used for this connection, the diameter of the bolts and the width of the flange is calculated in Chapter 5. As can be seen in Figure 3.2, M80 bolts are used for this connection, with 162 of these bolts distributed evenly over the circumference.

3.4. Parametrization dimensions

One aspect of the analysis on the validity of the LTF for these next generation turbines is the increase in dimensions. In this study, various dimensions of a ring-flange connection are analyzed to obtain the effect of that dimension on the forces in the bolts. Firstly, analytical calculations are made to approximate which dimensions are likely to have an influence on the LTF. The factor with which each dimension is multiplied is the growth factor for the connection from the reference model to the 'next generation' model, namely 1.23. For these same dimensions, numerical calculations are performed on a segment without geometric imperfections. The following dimensions are chosen for this parameterization:

- Bolt circle diameter (BCD)
- Tower wall thickness (TWT)
- Distance center of bolt to outside wall (DO)
- Distance center of bolt to inside flange (DI)
- Flange thickness (FT)

The dimensions as listed above are shown in Figure 3.3 with the abbreviations.

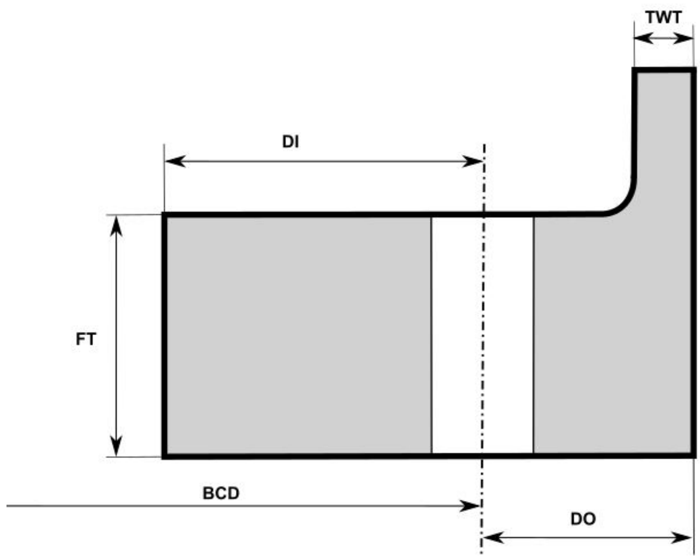

Figure 3.3: Flange with abbreviations of dimensions

After these analytical and FE calculations are done, the differences in LTFs are compared for each dimension. With the result of this comparison, an approximation is made which of the abovementioned parameters are relevant to be analyzed for the next generation connection.

3.5. Parametrization gapping

As offshore wind turbines are growing in size from a connection diameter of 6500 mm to 8000 mm in the next years (and after that presumably even higher to 10.000 mm), naturally, the circumference of the connection becomes larger too. Currently, the DNV verified limitations of geometric imperfections in bolted ring-flange connections. As stated before, it is becoming more difficult for manufacturers to ensure these tolerances for a maximum gap height or minimum gap length. Therefore, it is important to obtain information on the impact on the bolt force for connections with larger dimensions, and consequently, which gap sizes and shapes are covered by the analytical approaches for the LTF.

In this thesis, this influence will be investigated by doing a parametric study. In this parametric study, analytical and numerical results of bolted ring-flanges are compared for various geometric imperfections. In the first study, the reference model with an outer diameter of 6500 mm, as described in Section 3.2, is taken. For these dimensions, the influence of different types of gaps on the bolt force is obtained by increasing the gap height or the decreasing the gap length. The 'base' geometric imperfections are taken as the DNV verified gaps, as elaborated in Section 2.3. Firstly, analytical calculations are performed, where the three approaches are compared for a connection without geometric imperfections. Afterwards, the approaches are compared for gaps, where the influence of a change in gap height and gap length is investigated. The length and the height of the gap are changed with the same factor to obtain which characteristic has the largest influence on the LTF. This is relevant to investigate, because as the circumference increases with the larger turbines, an angle of 30° of an 8000 mm connection is larger than for an 6500 mm connection.

Therefore, numerical and analytical calculations are done for the same connection, but with a gap height increase and a gap length decrease of a factor of 1.2. For each type of geometric imperfections, namely tower sided and parallel gaps, as previously determined, the first parameterization that is done analytically and numerically is:

- 1 mm over 30° (DNV verified)
- 1.2 mm over 30°
- 1 mm over 25°
- 2 mm over 360° (DNV verified)
- 2.4 mm over 360°

An illustration of these tower sided and parallel gaps can be found in Figure 2.13. After the analyses of the abovementioned gaps are performed for the reference model, the influence of these various gap shapes is analyzed. Firstly, the difference between tower sided and parallel gaps is obtained, and the type of gap with the highest bolt forces when closing the gap is chosen for further analyses. Moreover, an approximation will be made which gaps are relevant to be calculated for the next generation turbine connections. In [21] a suggestion was made to focus on the length of the gap instead of the angle of the gap. In this paper, it was proposed to use a minimum gap length of $l_{gap} = 1000mm$, with a tolerance of $u_{gap} = 1mm$ per flange. Therefore, after obtaining the results of the first analyses, this gap shape is applied to the connection and will be analyzed.

- 1 mm over 1000 mm (≈ 17.63° for D_o= 6500mm)

During the making of this thesis, a paper was published [1], where almost 2000 measurements in flange flatness were collected from various offshore wind turbines with different dimensions. These measurements showed a distribution of gaps occurring in practice, where it was found that an almost linear relation exists between the measured gap lengths and gap heights. One of the findings in this paper, was that gaps with a length much smaller than an angle of 30° occurred often in practice. A distribution that shows the measured gaps and its frequency is shown in Figure 3.5. In this frequency distribution, it can be seen that either very long gaps or very short gaps occur. It is therefore logical to focus on smaller gap lengths than a length of 30°, in case shorter lengths result in 'worse results' for the bolt force. Moreover, what this study showed, was that a gap height of 1 mm per flange for a gap length of 1000 mm is much larger than is expected to occur in practice. In Figure 3.4, an overview is shown of design gap heights that are proposed for certain gap lengths. In this figure, it is shown that for a gap length of 1000 mm, a 95% fractile design gap height is 0.5 mm. This gap shape will therefore be analyzed as well in Chapter 6.

With these proposed design gap heights and the results for the abovementioned gaps, geometric imperfections are chosen to be calculated for the connection with next generation dimensions.

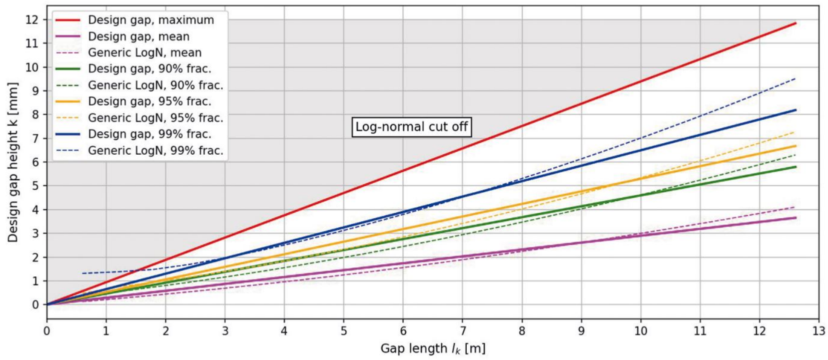

Figure 3.4: Proposed design gap heights at lengths [1]

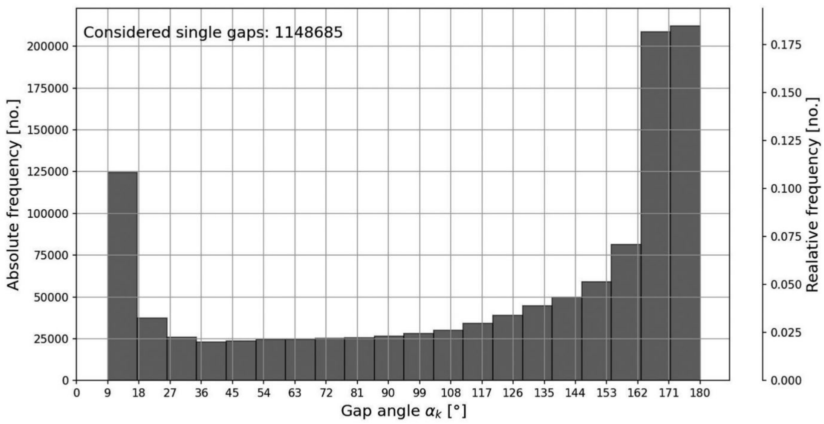

Figure 3.5: Frequency gaps of 1900 analyses of turbines [1]

What should be noted is that a different formulation of gap heights and gap lengths is used in this thesis than in certain literature. In [4], the same notation is used as in this thesis. However, in the paper that contains the large number of measurements Buchholz & Seidel [1], the gap length is defined as the total length between two contact points of the flange, so twice as large as the gap length defined in this thesis, and the gap height is the total height between the flanges. An illustration of the gap notation used in this thesis is shown in Figure 3.6. Similarly, the gap height in this paper mentioned is the largest distance between the two flanges, so twice as high as the height defined in the abovementioned gaps. The shape of a gap of 1 mm over 1000 mm is:

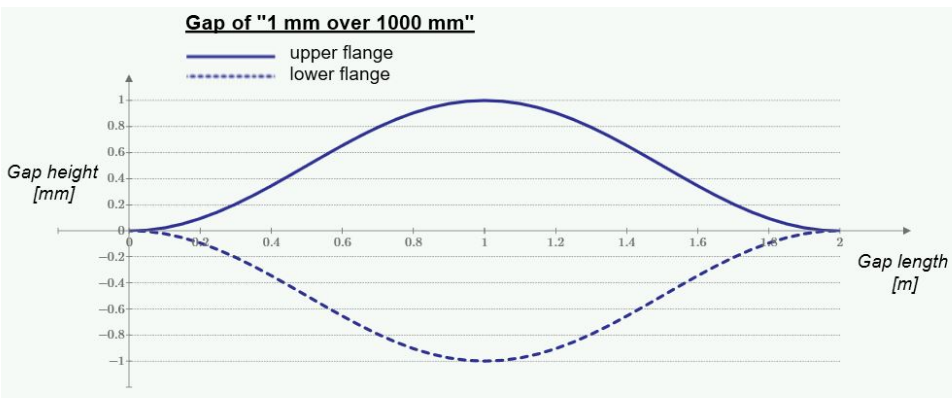

Figure 3.6: Gap notation

3.5.1. Cyclic loading

As stated in Chapter 2, the load variation range is of importance for the resistance of a bolted ring-flange connection. Because the load variation range can increase significantly when imperfections are present in the connection, this range is inspected as well for the geometric imperfections. In Chapter 6, in addition to the absolute force in the bolts, a comparison is made between the analytical approaches and the numerical results for the load variation range at a certain external force where most damages are expected to occur. The load variation range is expressed in $\Delta F_S/\Delta Z$, and is therefore the slope of the LTF at an external load value. This high-frequency external load value is equal to the damage equivalent load (DEL) [15], which is mostly used for the verification of the resistance against fatigue damage in OWTs. For the reference model, the value for this external force is [redacted], and for the next generation model, this value is [redacted]

With this load variation range, damages can be obtained using the Palmgren-Miner rule [5, 7].

$$\begin{aligned}
\Delta\sigma_C &= \Delta\sigma_{C0} * \left(\frac{30mm}{d_B}\right)^{0.25} \\
\Delta\sigma_S &= \frac{\Delta F_S}{A_{B.S}} \\
N_c &= \begin{cases} N_1 * \left(\frac{\Delta\sigma_D}{\Delta\sigma_S}\right)^{m_1} & \text{for} \frac{\Delta\sigma_D}{\Delta\sigma_S} < 1 \\ N_2 * \left(\frac{\Delta\sigma_D}{\Delta\sigma_S}\right)^{m_2} & \text{for} \frac{\Delta\sigma_D}{\Delta\sigma_S} \geq 1 \end{cases} \\
D &= \sum \frac{n_c}{N_c}
\end{aligned} \tag{3.1}$$

With these damages and the damage fatigue factor, the design lifetime of a structure can be calculated. When the calculated stress range in the bolts are high, the number of cycles the structure can withstand these loads are low. For the bolted ring-flange connections considered in this thesis, the values for the number of cycles N_1 and N_2 are respectively $2 * 10^6$ and $1 * 10^7$ corresponding to $m_1 = 3$ and $m_2 = 5$.

3.6. Outline

In the next few chapters, the abovementioned steps are worked out to give an answer to the research question. All calculations are firstly performed analytically in Chapter 5, using the three approaches as mentioned in Chapter 2. In Chapter 6, the numerical results of the external force to the bolt force are obtained and compared to the analytical results.

4 Numerical model

In this chapter, the model that is used for the numerical calculation is described. The software that is used including its underlying theory is elaborated, followed by the characteristics and the construction of the model itself.

4.1. ANSYS

The modelling and numerical calculation of the designed connection will be done in the finite element software ANSYS (version ANSYS 2022 R1). In the DesignModeler of ANSYS Workbench, the geometry is constructed, and in ANSYS Mechanical, the mesh is made, boundary conditions are applied and the model is solved which gives the results used for the analyses.

4.2. Segment model

A range of models is made for the calculation in this thesis. As stated in Section 3.2, first, a model is made of a connection with an outer diameter of 6.5 m. This reference model is made over various angles over the circumference: a full model, smaller segments (for geometric imperfections) and a segment of one bolt: the 'segment model' as a base model and to parameterize dimensions.

When designing a 'perfect' flange, so a flange without gaps, the segment approach is often applied. In this approach, the focus lies on only a segment of the bolted ring-flange, where the most heavily loaded segment of the flange is modelled [22]. Often, the segment that is modelled only contains one bolt with a width of the center-to-center distance between two bolts. It therefore cannot be used for connections where gaps are present, except for gaps that are uniform over the entire circumference. What will be analyzed in Chapter 6, is if a smaller segment than the entire circumference can be used for the FE calculation for geometric imperfections. The benefit of using a segment of only one bolt or multiple bolts compared to an entire flange is that the computational time and effort can be significantly reduced.

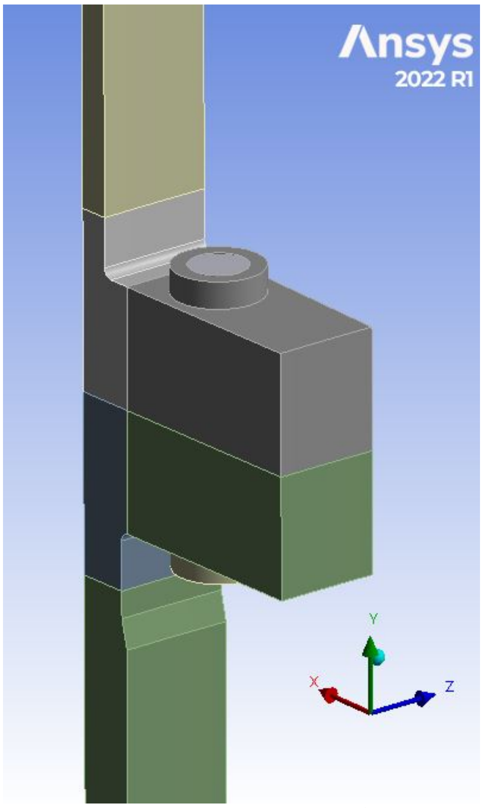

Figure 4.1: Segment FE model (unmeshed)

The FE modelling of the reference model including its parametrization of the dimensions, as explained in Section 3.4, is done using the segment approach. The models that are used for these analyses have either no gap or a uniform gap over the entire length. By making use of symmetry boundary conditions, the segment acts as a part of a model over the entire circumference. The segment that is used for these analyses is shown in Figure 4.1.

The finite element analysis is performed with a linear material model, as plastic strain is not expected to occur with the cyclic loading conditions these offshore wind turbines are subjected to.

4.2.1. Elements

When performing a structural finite element analyses, various element types can be used that have different properties. The entire model of the ring-flange connection, so both parts of the flanges and the bolts, is made using solid elements. Solid elements are chosen, as they are more suitable for structures with a varying geometry. Parts of the structure, such as the flanges, are very difficult to model with shell elements and solid elements give more accurate results. Shell elements could be used for the canned section to reduce computational effort. However, for uniformity, those parts are modeled with solid elements as well, with a coarser mesh to reduce computational effort. Within ANSYS, multi-point constraints (MPCs) could be used to make shell elements and solid elements compatible.

Some properties of finite elements are the amount of degrees of freedom (DOFs) per node, the geometry and the number of nodes. Solid elements have a 3D topological dimension, and the amount of degrees of freedom in each node is three, namely only translational: u_x, u_y, u_z. A solid brick element with its degrees of freedom is shown in Figure 4.2(a).

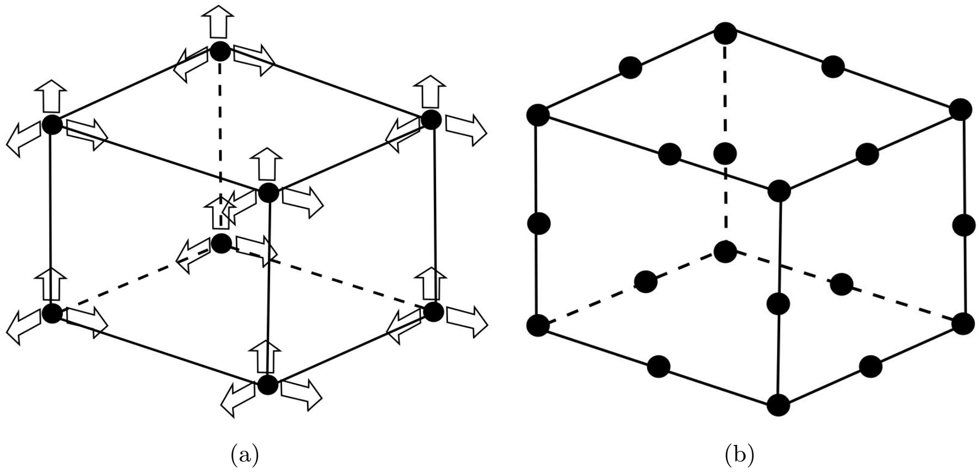

Figure 4.2: Finite element (a) solid element with DOFs (b) quadratic element

4.2.2. Mesh

The model of the ring-flange connection mostly consists of brick elements, as can be seen in Figure 4.3(a). The mesh is made with quadratic elements, meaning each element edge contains three nodes, shown in Figure 4.2(b). Quadratic elements are chosen, as they are better suited for complex geometries. In the ring-flange connection, many curved edges are present, and therefore preferred to be modeled with quadratic elements. When linear elements are used with 3D elements, shear locking can occur, as linear elements cannot capture bending, making the brick elements too stiff. When using linear elements, many more elements are needed to obtain a similarly accurate stress distribution as quadratic elements.

Quadratic brick elements have a high computational effort, as these elements have a larger number of nodes and a high amount of DOFs per node. When making numerical FE calculations, it is desired to have a low computational effort. Therefore, the computational time of the analyses will be reduced by removing elements that are unnecessary for the calculation. The FE model will, therefore, be a simplified version of an actual turbine. Secondary components of the connection, such as a boat landing platform, ladders, and railings are removed to reduce the complexity of the FE model. Moreover, the shank and nuts of the bolts will be modeled as cylindrical parts, so without the thread of the bolt or other irregularities. Furthermore, to reduce computational time and effort, analyses will be performed to see if the size of the model can be reduced. This is further elaborated in Chapter 6.

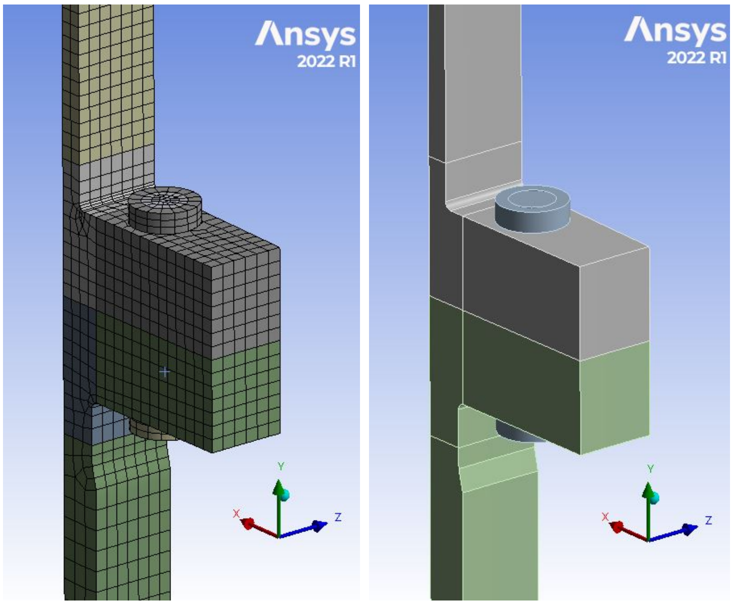

(a) (b)

Figure 4.3: Segment model (a) meshed (b) different parts

Another method to reduce the computational time and effort of the FE model, is by efficiently meshing the model in ANSYS. Parts of the structure that are expected to have a lower variation of stresses will be made with large elements, so will have a coarse mesh. When sections that are expected to have a higher variation of stresses are modeled with a coarse mesh, singularities can occur. To prevent singularities from forming, and obtaining a more accurate representation of the stress distribution over the elements, these sections are meshed with smaller elements. In Figure 4.3(a), edges such as the rounding of the welds have a finer mesh than the upper part of the tower, which has a very coarse mesh.

4.2.3. Connectivity

Within ANSYS, various types of contacts between parts are possible. The two types of contacts that are used in the FE models are frictional and bonded contacts. For bodies that are formed into the same part in the DesignModeler of ANSYS Workbench, a bonded contact is automatically generated. The geometries of the FE models are divided in three parts:

- Bolts
- Transition Piece
- Tower

In Figure 4.3(b), the parts are shown in different colours. Between these parts, manual contacts are created in ANSYS Mechanical. At the contact between the TP and tower flanges, a frictional contact is made, as the bodies are not bonded together and sliding might occur. The connection is a mainly axially loaded connection, so the effect of sliding is assumed to be negligible for the analysis. A coefficient of friction μ of 0.46 is obtained due to the contact between the two steel surfaces of the flanges [8].

Between the surface of the bolt nuts that is in contact with the flanges, a bonded contact is made manually. This was done to reduce computational time, as with an early analysis, it was obtained that the force in the bolts almost didn't change from going to frictional to bonded, namely 0.02%. The results of this small test are shown in Figure 4.4 The computational time, however, was reduced by around 10%. For segmented models, this difference is in absolute computational time not very significant. However, for large models with many bolts (such as a fully modelled ring-flange connection with 156 bolts) the total computational time can be significantly reduced when using bonded contacts.

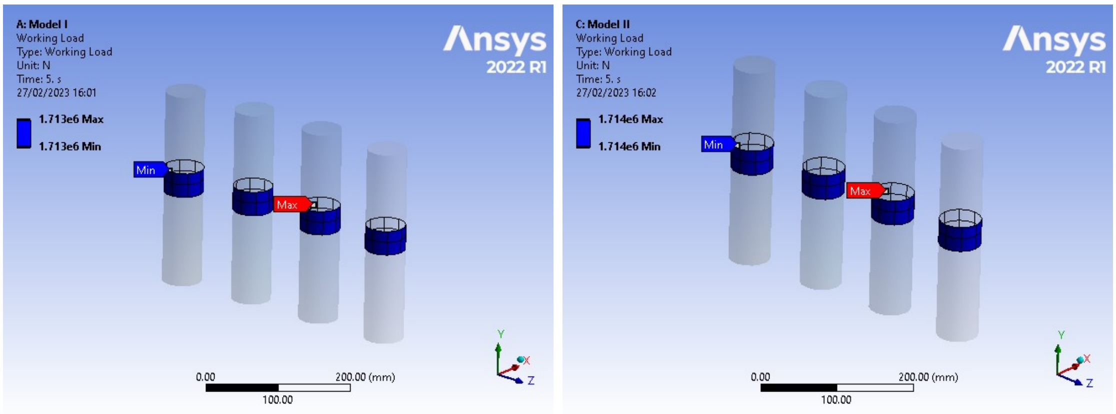

(a) (b)

Figure 4.4: Forces in bolts with (a) bonded contacts (b) frictional contacts

The contacts of the bolted ring-flange connection as made in ANSYS Mechanical are shown in figures 4.5.

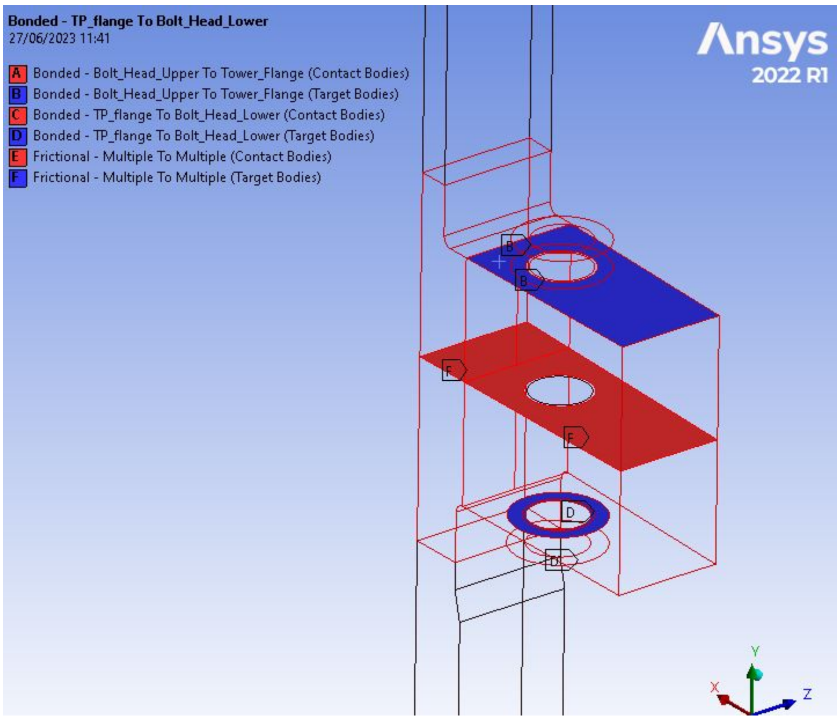

Figure 4.5: Contacts between parts of structure (ANSYS)

4.2.4. Constraints

As the model in ANSYS needs to represent a part of a bottom-fixed offshore wind turbine, boundary conditions should be applied so that it is properly constrained and cannot move freely. A fixed support is applied on the bottom of the shell to constrain the model, and an external load, as elaborated in Section 4.4, is applied on the top surface of the structure. Moreover, symmetry conditions are applied such that the structure is constrained against free translation and rotation in the X- and Z- direction.

As bending moments cannot be applied in ANSYS in combination with 'regular' symmetry functions, such as a cyclic axis of symmetry, a frictionless support was made at the symmetry faces. When the face on which the frictionless support is applied is geometrically flat, a frictionless support applied on a curved section is equivalent to symmetrical conditions.

Even though the top flange is connected to the bottom-fixed lower flange by the connections described in previous section, an additional constraint is applied to this top flange. A very small initial displacement is inserted on the top flange which results in better convergence, with still the same results. The initial displacement of 0.001 mm is applied in the first load step only, and deactivated in the successive load steps. It therefore does not influence the behaviour of the structure in the relevant load steps.

4.3. Parameterized model

In this section, the models that are used for the parameterization are elaborated. First, the method of parameterizing is explained, and afterwards the models that are used are explained.

4.3.1. Parameterization

For the parametrization of the FE model, a Microsoft Excel file containing dimensions of the ring-flange connection was imported into ANSYS Workbench. Certain dimensions listed in this Excel file are linked to the geometry in ANSYS. Instead of changing the dimensions in the DesignModeler, the linked dimensions can be altered by changing values in this Excel file for multiple projects at the same time.

4.3.2. Model with imperfections

For the model that is made to make the numerical calculation for geometric imperfections, it is not always possible to use a segment model of 1 bolt. For gaps that are homogeneous over the circumference, a segment model could be used because each segment of the ring-flange is equal. For gaps with irregular shape, it is not possible to use a segment model of one bolt, as the geometry of the segments are not identical. Therefore, a few analyses will be done to obtain what section of the ring-flange connection can be used for each type of geometric imperfection. These analyses are elaborated and performed in Section 6.2. As a first assumption, numerical analyses with geometric imperfections are performed with flanges of a segment of 360°, and afterwards reduced to 180°, see Figure 4.6, or smaller. By using a segment of 180° or smaller, the computational time is reduced compared to an entire flange. The geometric imperfections and all models that are analyzed are described in Chapter 3. In previous section is described, how the geometric imperfections are implemented in the FE model.

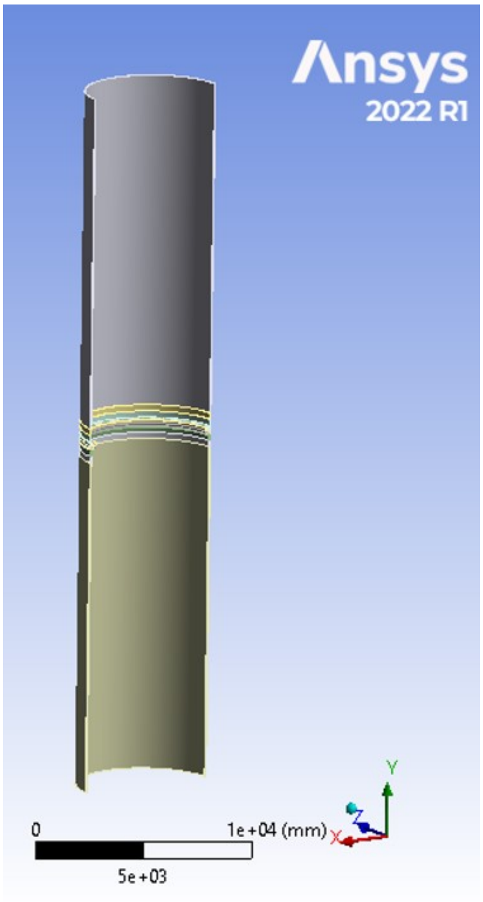

Figure 4.6: Finite element model of 180°

As can be seen in Figure 4.6, the FE model has a large height of the canned section. Due to a long region of influence in this shell from preloading of the bolts, it is recommended to use a height of the shell of at least 2 times the diameter of the connection, to achieve proper load distribution [22]. In Figure 4.7 the model over half of the circumference is shown with its generated mesh and with the different parts that are connected with the same contacts as in Section 4.2.

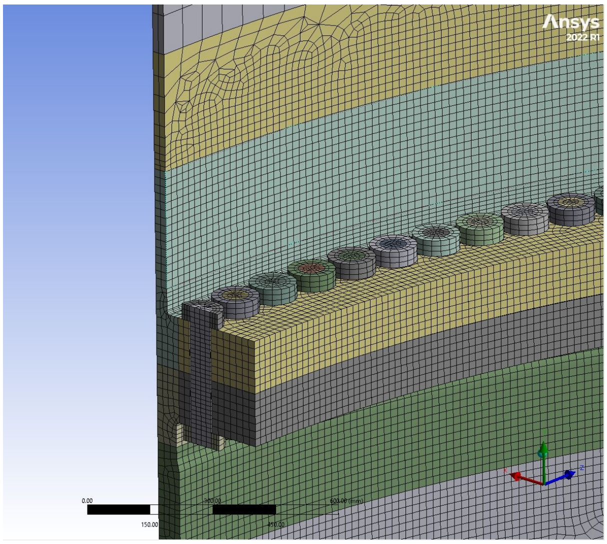

(a)

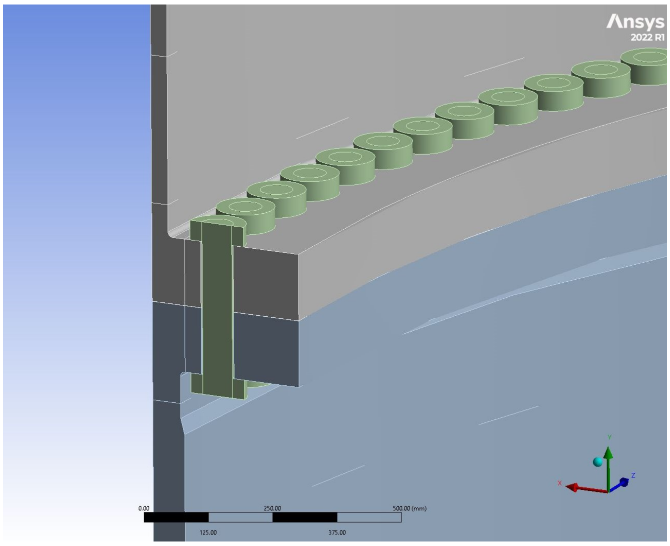

(b)

Figure 4.7: Half model (a) meshed (b) different parts

4.3.3. Modelling of geometric imperfections

The geometric imperfections are modelled in the DesignModeler of ANSYS Workbench. A line was made with a coordinate file as input. The coordinate file that is used for the input values is a .txt file that is obtained by the output of a macro. A macro is an action, implemented by a function or a written code, that stores output values, in this case coordinates of the gap, in the .txt file. The X- Y- and Z- coordinates form a sinusoidal wave with a certain gap length and height (Equation 4.1). In this formulation, l_{gap} and u_{gap} are the gap length and height with the notations as defined in Section 3.5.

$$y = \frac{u_{gap}}{2} * \sin\left(\left(x - \frac{l_{gap}}{2}\right) * \frac{\pi}{l_{gap}}\right) + \frac{u_{gap}}{2} \tag{4.1}$$

In ANSYS DesignModeler, lines are generated from these coordinates and a surface is generated between these lines. The surfaces that represent these gaps are shown in Figure 4.8, where the orange lines are the gap coordinates scaled in y-direction (i.e. upwards) with a factor 50 for better visualization. The flange is sliced by the surfaces and the solid body that should correspond as a gap is deleted. This way, a gap is formed between the flanges.

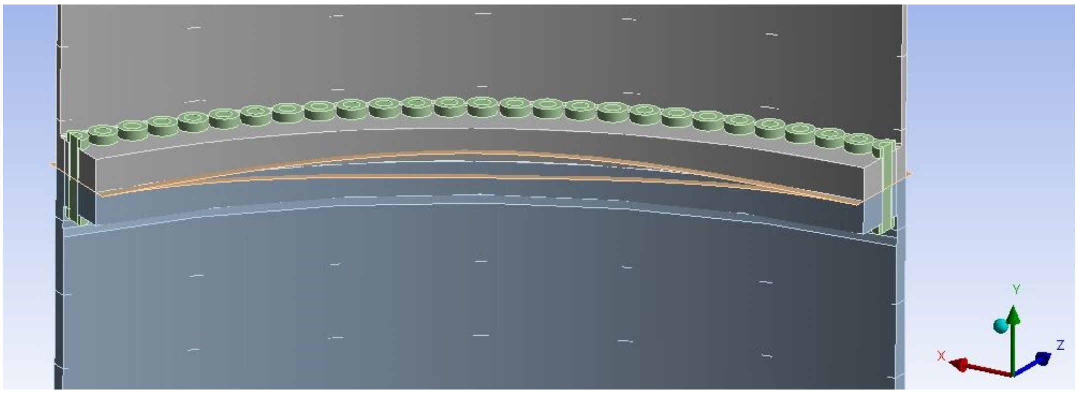

(a)

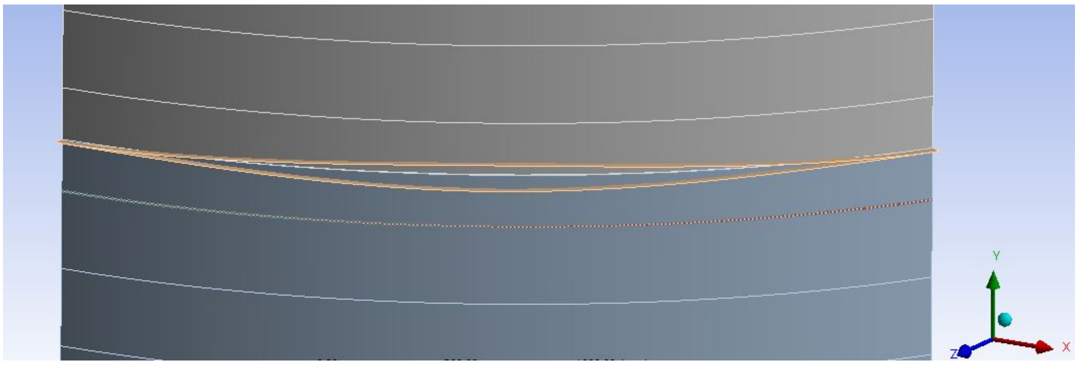

(b)

Figure 4.8: Gap surface slicing flange (a) inside flange (b) outside flange

What should be noted is that this is not an actual representation of how the flange will be fabricated. In this model, I assumed that the surface of the flange that is connected to the bolts remains flat. The surface where the flange is connected to the other flange is not perfectly flat and has imperfections. This results in that the thickness of the flange is not homogeneous over the entire circumference, but at some locations 1 or 2 mm thinner than the designed thickness. This difference, is, however, negligible compared to the total thickness of 135 mm for the reference model, so this method is assumed to be acceptable.

4.4. Loads

In this section, the loads applied on the structure are elaborated. Two types of loads are present in the FE model: pretension loads and external loads.

4.4.1. Pretension loads

To increase the fatigue resistance of the connection, pretension is applied on the shank of the bolts before applying external tension force. In Table 4.1, the number and size of the bolts with its desired pretension is shown in an overview for the reference model and the next generation model. The equations used to calculate the pretension can be found in Section 2.2. In ANSYS, the preload force that is applied on the bolts is as shown in Figure 4.9.

Table 4.1: Overview bolts considered connections

Model	Amount bolts	Bolt type	Pretension applied
Reference	156	M64	1686 kN
Next generation	162	M80	2737 kN

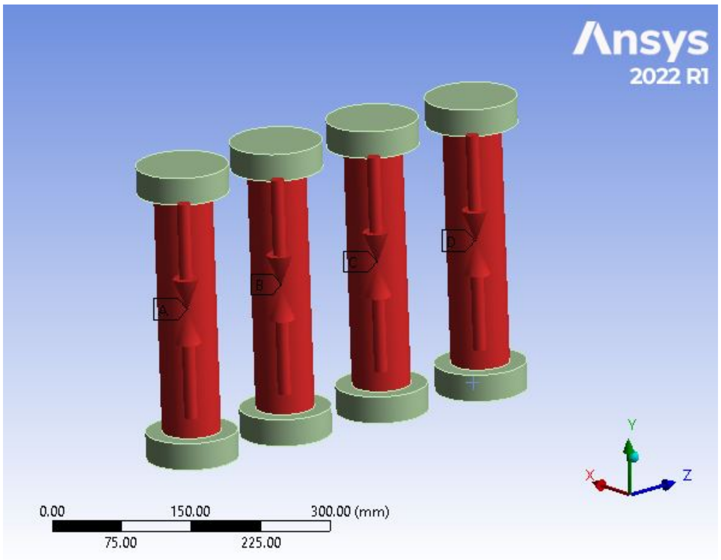

Figure 4.9: Pretension on bolt shanks (ANSYS)

For better convergence when solving the model, the pretension on the bolts is applied in load steps. At the first load step, a small part of the pretension is applied on the bolts, and at the second load step, divided in multiple sub-steps, the full pretension is applied on all bolts and remains on the bolt during the rest of the analysis.

4.4.2. External loads

As the FE model represents a part of a wind turbine, external loads, such as loads due to wind and waves act on the structure. Moreover, the load due to the self-weight of the structure is present. Loads due to self-weight are easily calculated, as the material type and the amount of material is known for most of the structure. Loads due to wind and waves are, however, more difficult to calculate, as it depends on the site conditions and the loads are highly dynamic. Large calculations must be done to obtain the values for the loads and moments that should be applied on the structure. With advanced software used by Ramboll, these loads are calculated for previous projects that were used to obtain the reference model, see Section 3.2. As this software is too advanced to understand and to be used to calculate these loads for the time frame of this thesis, the loads from these projects are used for the calculation of the reference model.

The design axial load that was obtained for the projects used to determine the reference model was [redacted], and the design bending moment applied on the structure for ULS is [redacted].

For a fully modelled structure in ANSYS or a model with only half of the flange, this external load can be applied as a bending moment. For a segment of one bolt or a larger segment, a bending moment cannot be applied on the tower wall. For these models, the external loads are applied to the structure as a uniformly distributed pressure. Therefore, both the axial load and the external moment should be converted to a pressure that represents the section that takes the highest loading by the bending moment. This is done by doing the following calculation:

$$\begin{aligned} A_{tower} &= \frac{1}{4} * \pi * (D_O^2 - D_I^2) \\ I_w &= \frac{1}{64} * \pi * (D_O^4 - D_I^4) \\ \sigma_N &= \frac{N_{ax.ULS}}{A_{tower}} \\ \sigma_M &= \frac{M_{b.ULS}}{I_w} * \frac{D_O}{2} \\ \sigma_{tot} &= \sigma_N + \sigma_M \end{aligned} \tag{4.2}$$

A PDF of the analytical LTF calculation in Mathcad for the reference model is added in Appendix B, where this calculation can be found. Similar to the load due to pretension, the external loads on the structure are applied in load steps. The pressure that represents the external moment is applied on the upper open surface of the tower.

Next generation loads

For the connection with next generation dimensions, as described in Section 3.3, an approximation is made for the external loads the structure is subjected to. For connections with next generation dimensions, an assumption is made that a linear relation exists between the external bending moment and the sweeping area of the blades. As the diameter of the rotor for is known for both the reference model and the next generation model, the moment acting on the structure can be calculated with the following formulas:

$$\begin{aligned} A_{r.ref} &= \frac{1}{4} * \pi * D_{r.ref}^2 \\ A_{r.next} &= \frac{1}{4} * \pi * D_{r.next}^2 \\ M_{next} &= M_{ref} * \frac{A_{r.next}}{A_{r.ref}} \end{aligned} \tag{4.3}$$

with [redacted], $D_{r.ref} = 200m$ and $D_{r.next} = 236m$, the bending moment applied on the next generation model M_{next} is equal to [redacted]. This bending moment is applied in ten load steps, with each load step equal in size. What should be noted is that the actual ULS load conditions might be higher than this approximated value due to site-related factors.

5
Analytical calculation

In this chapter, analytical calculations are elaborated and results are obtained for the resistance of the connection. Firstly, the connection is checked for its resistance in ultimate limit state (ULS) with the loads as defined in Section 4.4. After that, the load transfer functions are obtained with the approaches as discussed in Chapter 2: the tri-linear approach by Schmidt/Neuper [18], the non-linear approach by Seidel [20] and the polynomial approach by Seidel (not published yet). All analytical calculations are made using the software Mathcad Prime version 8.0.0.0. A list of the definition of symbols used in this thesis is added at the beginning of this report.

5.1. Reference model

In this section, the analytical calculations for the reference model are carried out. The dimensions of the reference model can be found in Section 3.2.

5.1.1. Number of bolts

The maximum number of bolts is determined by looking at the bolt circle diameter and the minimum spacing between the bolts. Characteristic values for a number of large bolt types (M64, M72 and M80) are obtained from [2] and can be found in Table 5.1. The minimum spacing s_{min} between these large bolt types is determined by a tightening tool, obtained from confidential information provided to Ramboll. With the minimum required spacing, the maximum number of bolts is determined by:

$$n_{bolt.max} = \frac{\pi * D_{B.axis}}{s_{min}}$$

The calculation of this value for the reference model is added in Appendix B, where the maximum amount of M64 bolts for a bolt circle diameter of 6220 mm is 162. The number of bolts for the reference model, namely 156, is therefore sufficient with the minimum required spacing.

Table 5.1: Characteristic dimensions bolts

Bolt type	Bolt diameter [mm]	Diameter washer [mm]	Bolt hole tolerance [mm]
M64	64	115	6
M72	72	125	6
M80	80	140	6

5.1.2. Limitation gap closing stress

In this section, the allowable flatness deviation according to the available gap closing stress [21] is calculated, as described in Section 2.3. For a gap length of 30°, 1000 mm and the entire circumference, allowable gap height per flange is:

$$\begin{aligned}
\alpha_{gap} &= 30^\circ * 2 && \leq 90^\circ : u && = 1.7mm \\
\alpha_{gap} &= \frac{2 * 1000mm}{\pi * D_O} * 360^\circ = 35.3^\circ && \leq 90^\circ : u && = 1.0mm \\
\alpha_{gap} &= 360^\circ && \geq 90^\circ : u && = 2.6mm
\end{aligned} \tag{5.1}$$

With this calculation, the gap heights as chosen for the parameterization (see Section 3.5) are obtained to be allowed according to the maximum gap closing stress. A condition for this allowable flatness deviation is that the gap has a minimum length of $l_{gap} = 1000mm$.

5.1.3. Analytical check: ULS

In this section, the calculations of the connection of the reference model in ULS are made. A printout of the calculation in Mathcad Prime is added in Appendix C. In Table 5.2, an overview is given with the limit of the load carrying capacity and the utilization ratios for each failure mode. In the next sections, the calculation for each failure mode is performed.

Failure mode A

The calculation of this failure mode describes the resistance of the connection against bolt failure.

$$F_{u,A} = F_{t,Rd} = \frac{0.9 * f_{u,B} * A_{B.s}}{\gamma_{M2}} = 1926.7kN \tag{5.2}$$

Failure mode B

This failure mode is obtained by calculating the resistance against bolt failure with the forming of a plastic hinge in the flange-to-shell junction.

$$F_{u,B} = \frac{M_{pl,3} + a * F_{t,Rd}}{a + b} = 1048.8kN \tag{5.3}$$

where

$$M_{pl,3} = min(M_{pl,N,sh}; M_{pl,V,fl}) = 6.32kNm$$

$$M_{pl,N,sh} = \left[1 - \left(\frac{N}{N_{pl,sh}}\right)^2\right] * M_{pl,sh} = \left[1 - \left(\frac{F_u}{c_w * s * f_{y,sh}}\right)^2\right] * \frac{c_w * s^2}{4} * f_{y,sh} = 6.32kNm$$

$$M_{pl,V,fl} = \left[\sqrt{1 - \left(\frac{V}{V_{pl,fl}}\right)^2}\right] * M_{pl,fl} = \left[\sqrt{1 - \left(\frac{F_u}{c * t * f_{y,fl}/\sqrt{3}}\right)^2}\right] * \frac{c * t^2}{4} * f_{y,fl} = 12.16kNm \tag{5.4}$$

Failure mode D

This failure mode is a sub-mechanism for failure mode C and is the failure of the connection by the forming of a plastic hinge at the center of the bolt hole.

$$F_{u,D} = \frac{M'_{pl,2} + \Delta M_{pl,2} + M_{pl,3}}{b'_D} = 1078.7kN \tag{5.5}$$

where

$$\begin{aligned} \Delta M_{pl,2} &= \frac{F_{t,Rd}}{2} * \frac{d_W + d_B}{4} = 44.55kNm \\ M'_{pl,2} &= \frac{c_m * t^2}{4} * f_y = 81.26kNm \end{aligned} \tag{5.6}$$

Failure mode E

This failure mode is the second sub-mechanism for failure mode C and calculates the resistance against failure of the connection by forming a plastic hinge next to the bolt hole.

$$F_{u,E} = \frac{M_{pl,2} + M_{pl,3}}{b'_E} = 2498.5kN \tag{5.7}$$

where

$$M_{pl,2} = \frac{c * t^2}{4} * f_y = 184.19kNm \tag{5.8}$$

Overview

In the table below, the failure modes are summarized with its corresponding ultimate resistance and the utilization ratio. As can be seen in this table, failure mode B is governing for the reference model, with an utilization ratio of 83.9%. The reference model, therefore, is proven to have sufficient resistance in ULS.

Table 5.2: Overview failure modes ULS (reference model)

Failure mode	Ultimate resistance	Utilization ratio
A	1927 kN	45.7 %
B	1049 kN	**83.9%**
D	1079 kN	81.6 %
E	2499 kN	35.2 %

5.1.4. Analytical check: LTF

As written in Section 2.2, for the analytical calculations of the load transfer function, three approaches are chosen to be calculated: the tri-linear approach by Schmidt/Neuper, the non-linear approach by Seidel (2001) and the polynomial approach by Seidel (2023). In this section, the calculations for these approaches are made and calculation steps are elaborated. In Chapter 2, a general explanation of these calculations with its limitations is given. A printout of the calculation in Mathcad is added in Appendix B.

The first step of the calculation for the LTFs is obtaining the stiffnesses. The stiffnesses of the flange and of the bolts are calculated in the following formulas:

$$
\begin{aligned}
C_D &= C_{D.Pet} = \frac{E * \pi}{4 * 2 * t} * \left(\left(d_W + \frac{2 * t}{10} \right)^2 - d_B^2 \right) && = 9815 \frac{kN}{mm} \\
\delta_S &= \delta_{S.VDI} = \delta_{SK} + \delta_l + \delta_{Gew} + \delta_G + \delta_M && = 0.53 \frac{mm}{MN} \\
C_S &= C_{S.VDI} = \frac{1}{\delta_S} && = 1879 \frac{kN}{mm}
\end{aligned}
\tag{5.9}
$$

These values result in spring values p and q:

$$
p = \frac{C_S}{C_S + C_D} = 0.16, \quad q = \frac{C_D}{C_S + C_D} = 0.84
\tag{5.10}
$$

Tri-linear LTF (Schmidt/Neuper)

As explained in Chapter 2, the LTF by Schmidt/Neuper [18] is an approach, determined by three linear functions, connected by two critical loads. This approach is, compared to the other two approaches, conservative as its calculation method is simple and does not have geometric imperfections as variable. In this section, the limitation of the function and the loads that define the regions are calculated (in Equations 5.11 and 5.12).

$$
\begin{aligned}
Z_I &= \frac{a - 0.5 * b}{a + b} * F_V && = 645kN \\
Z_{II} &= \frac{1}{\lambda * q} * F_V && = 1004kN \\
&\text{where} \\
\lambda &= \frac{0.7 * a + b}{0.7 * a} && = 2
\end{aligned}
\tag{5.11}
$$

With these forces, the corresponding internal bolt forces are calculated:

$$
\begin{aligned}
F_V &= 0.9 * (0.7 * f_{u.B} * A_{B.s}) && = 1686kN \\
F_{S,1} &= F_V + p * Z_I && = 1789kN \\
F_{S,2} &= F_V + p * Z_I + [\lambda * Z_{II} - (F_V + p * Z_I)] * \frac{Z - Z_I}{Z_{II} - Z_I} && = 2009kN \\
F_{S,3} &= \lambda * Z_{ult} && = 2400kN
\end{aligned}
\tag{5.12}
$$

In the calculations, the ultimate load should be taken as the load Z applied on the segment converted from the ultimate external loads, see Section 4.4. As this ultimate load does not succeed $F_{S,2}$, the value for Z_{ult} is taken as a larger value to show all three parts of the LTF, namely $1200kN$. The tri-linear LTF that is obtained for the reference model is shown in Figure 5.1.

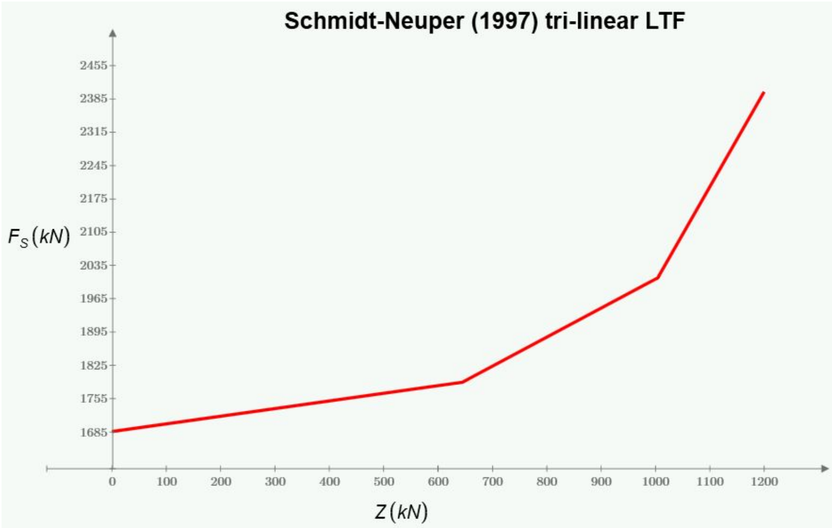

Figure 5.1: Tri-linear LTF for reference model

Non-linear LTF (Seidel, (2001))

In this section, the calculation for the non-linear approach by [20] is shown and worked out. Important parts are explained and eventually the obtained LTF is shown in Figure 5.2. This approach is not explicitly stated to be used exclusively for certain gap types (i.e. parallel, tower sided or flange sided gaps). The force in the bolt for the non-linear approach is calculated with Equation 5.13. It consists of the preload force F_V and an additional bolt force ΔF_S, which consist of a centric and an eccentric part.

$$\begin{aligned} F_S &= F_V + \Delta F_S \\ &\text{where} \\ \Delta F_S &= \Delta F_{S.centr} + \Delta F_{S.ecc} \end{aligned} \tag{5.13}$$

A bending moment M_S in the bolt only occurs as a result of the eccentric tension force, which causes the flange to rotate, see Figure 2.9. By idealizing the flange as a rigid body, the bending angle ϕ can eventually be determined from the bending moment. The calculation for the centric part was developed by VDI 2230 [27]. For this centric part, the additional bolt force $\Delta F_{S.centr}$ is calculated by combining the load induction factor n with the elastic resilience of the bolts δ_S and the flanges δ_D (Equation 5.9)

The load induction factor n that is used to calculate Φ always lies between 0 and 1. For relatively thick flanges, as used in wind turbines, the value often lies between 0.1 and 0.3. Using the formulas from VDI 2230 [27], the calculation of the load induction factor n is shown in Equation 5.14.

$$
\begin{aligned}
n &= n_{2D} * k_{ar} * k_{dh} * k_{dw} = 0.15 \\
&\text{where} \\
n_{2D} &= 0.52 - 0.703 * \frac{a_k}{t} \\
a_k &= b - \frac{d_W}{2} \\
a_r &= \frac{c - d_W}{2} \\
k_{ar} &= 1 - 1.74 * \left(\frac{a_r}{t}\right) + 1.24 * \left(\frac{a_r}{t}\right)^2 = 0.94 \\
k_{dh} &= 0.85 \\
k_{dw} &= 1
\end{aligned} \tag{5.14}
$$

With this information, the force ratio and therefore the centric part of the additional bolt force is obtained:

$$
\begin{aligned}
\Phi &= n * \frac{\delta_D}{\delta_D + \delta_S} \quad = 0.02 \\
\Delta F_{S.centr} &= \Phi * Z
\end{aligned} \tag{5.15}
$$

The value for Z in this centric part of the bolt force ranges from $0kN - Z_{ult}$, where the value for Z_{ult} is taken as the same value as in the calculation for the tri-linear LTF by Schmidt/Neuper (see previous section). The value for $\Delta F_{S.centr}$, therefore ranges from $0kN - 27.8kN$, and is the same for flanges with and without geometric imperfections.

The eccentric part of the additional bolt force is a more complicated calculation, where the force in the bolts is calculated iteratively and it changes when different gap heights are used. The calculation time and complexity of this approach is therefore higher than the tri-linear approach. This calculation includes additional bending stresses in the bolt due to eccentricity of the external load on the tower.
The first step in this calculation is to reduce the dimension a to a^* and to obtain the bending stiffness EI with this reduced value. Afterwards, the stress in the bolt is obtained, see equations 5.17 and 5.18.

$$
a^* = \min \begin{cases} a \\ 0.9 * t \\ b + (a - b) * \frac{t}{3*b}, \text{ if } a > b \end{cases} = 121.5mm \tag{5.16}
$$

$$
\begin{aligned}
EI &= E * c * \frac{a^* + b^*}{12} \\
b^* &= \left(b + \frac{s}{2}\right) \quad = 140mm \\
b_R &= \frac{d_W}{2} + 0.4 * t \quad = 116.1mm
\end{aligned} \tag{5.17}
$$

$$\sigma_N = 2 * \frac{R * (b^* - b_R)}{c * (a * b^* + b^{*2} - 2 * a * b_R - 2 * b^* * b_R)}$$
$$\sigma = \sigma_N - \frac{M}{I} * (a^* + b^*)/2$$

where

$$s_{sym} = \frac{a^* + b^*}{2} \tag{5.18}$$
$$R = \frac{t * s_{sym} * C_S * Z * b + EI * (\Phi * Z + F_V - Z + s_{sym} * C_S * \phi_{imp})}{s_{sym}^2 * t * C_S + EI}$$
$$M = \frac{EI * (s_{sym} * Z + Z * b - F_V * s_{sym} - \Phi * Z * s_{sym} - s_{sym}^2 * C_S * \phi_{imp})}{s_{sym}^2 * t * C_S + EI}$$

As stated in Chapter 2, a benefit of using this approach is that the height of the gap is included explicitly in the calculation. This is done by calculating the angle ϕ_{imp} of the gap over the width of the flange (Equation 5.19). In calculations where no gap is present, this value for ϕ_{imp} is equal to zero, which results in the last part of the equation falling away.

$$\phi_{imp} = \arctan\left(\frac{u_{gap}}{w_{fl}}\right) \tag{5.19}$$

With the abovementioned obtained values, the eccentric part of the additional bolt force $\Delta F_{S.ecc}$ is calculated with Equation 5.20. For a range of Z from $0kN - Z_{ult}$, the value for $\Delta F_{S.ecc}$ ranges from $(-0.1)kN - 889.8kN$, and is therefore more important for the LTF than $\Delta F_{S.centr}$, which has a much smaller range.

$$\Delta F_{S.ecc} = \left(\frac{t}{EI} * M + \phi_{imp}\right) * s_{sym} * C_S \tag{5.20}$$

The value for b^*, and therefore the other quantities in equations 5.17 and 5.18, are calculated iteratively. In this approach, as a start value, b^* is set to its maximum value $b + \frac{s}{2}$, which is the distance between the center of the bolt and the outer edge of the wall. The value for σ must be larger than 0 for each load step. Therefore, b^* is iteratively reduced by 0.1 mm with every iteration step, until the value for $\sigma > 0$. The sheet in Mathcad that is used to obtain these values, including the code that represents the iterative calculation, is added in Appendix B. In the figure below, the LTF by Seidel is shown for both a perfect flange and a gap of 1 mm.

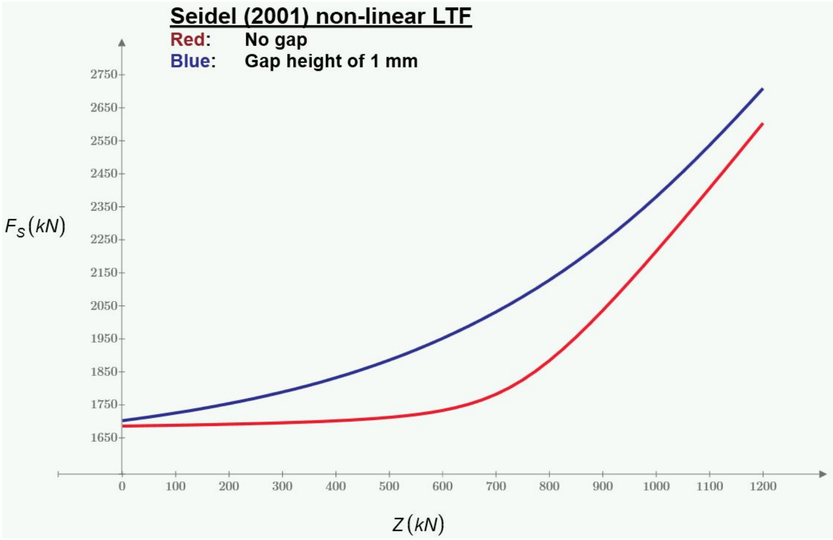

Figure 5.2: Non-linear LTF with no gap and a gap of 1 mm for reference model

Polynomial LTF (Seidel, (2023))

As stated before, during the making of this thesis, a new approach was created to analytically obtain the LTF. This approach is still under review and the document containing this approach has not been published yet. As this approach has not been verified yet, calculation steps might be adjusted between the making of this thesis and the approval of the approach. The calculation steps for this approach will not be shown, but certain aspects that are taken into account in this approach will be described and the LTF will be shown in this section.

An aspect of the polynomial approach that can be an improvement compared to other approaches, is that both gap height and gap length are explicitly taken into account as input variables. Moreover, unlike the non-linear approach, its calculation is doesn't require to be calculated iteratively, and is therefore reduced in calculation time and effort. In this approach, three points are constructed: one that only considers the dead weight of the structure, a second point that represents the ultimate force, taking into account the force needed to close the gap, and the third point is chosen so that the LTF has an accurate initial slope.

In Figure 5.3, the LTF obtained with the polynomial approach is shown for a connection without a gap present, and where a 1 mm gap is present over 30°. In the LTF for a connection without a gap, the initial slope of the function is close to zero, as there is no gap that needs to be closed. With a gap present, the slope of the LTF is higher than without a gap present, increasing the forces in the bolt.

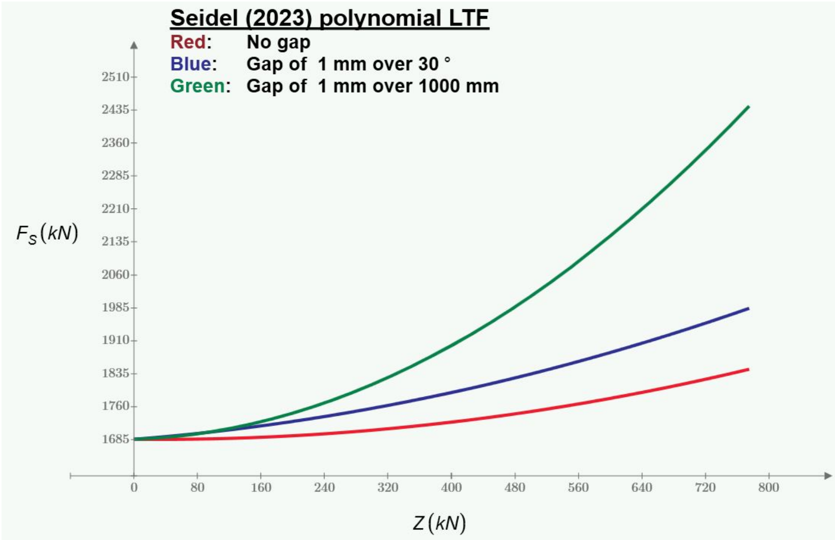

Figure 5.3: Polynomial LTF with no gap and a gap of 1 mm over 30° and 1000 mm for reference model

Overview

In the figures below, the three approaches are shown for the dimensions of the reference model. In Figure 5.4(a), the approaches are shown for connections without gaps, and in Figure 5.4(b), for a gap of 1 mm (for the polynomial approach over two different lengths). The non-linear approach from Seidel (2001) is shown for both no gap and a gap of 1 mm. In Table 5.3, once more an overview is shown which approach takes into account what gap parameter.

Table 5.3: Overview failure modes ULS (next generation model)

Approach	u_{gap} variable	l_{gap} variable
Tri-linear (Schmidt/Neuper)	No	No
Non-linear (Seidel)	Yes	No
Polynomial (Seidel)	Yes	Yes

As can be seen in Figures 5.4, the three approaches for a connection where no initial gap is present show a slightly similar range in bolt forces until $Z \approx 850kN$. Afterwards, the polynomial approach shows the lowest bolt forces, followed by the tri-linear approach and the non-linear approach, that gives the largest bolt forces.

The LTFs that include a geometric imperfection show a much larger difference between the approaches. The tri-linear LTF gives the lowest bolt forces until $Z \approx 1100kN$, which is larger than the external force in ULS, and therefore does this approach give the lowest bolt forces during the operational lifetime of a turbine. A difference can be seen as well for the two approaches that take gaps into account. The non-linear approach for a gap height of 1 mm is located between the polynomial LTFs for two different gap lengths (30° $\approx 1700mm$ and 1000 mm). In Section 5.3, different gap shapes are analyzed for different approaches, and in Chapter 6, a comparison is made between these analytical approaches and LTFs obtained by modelling the connection and performing finite element analyses.

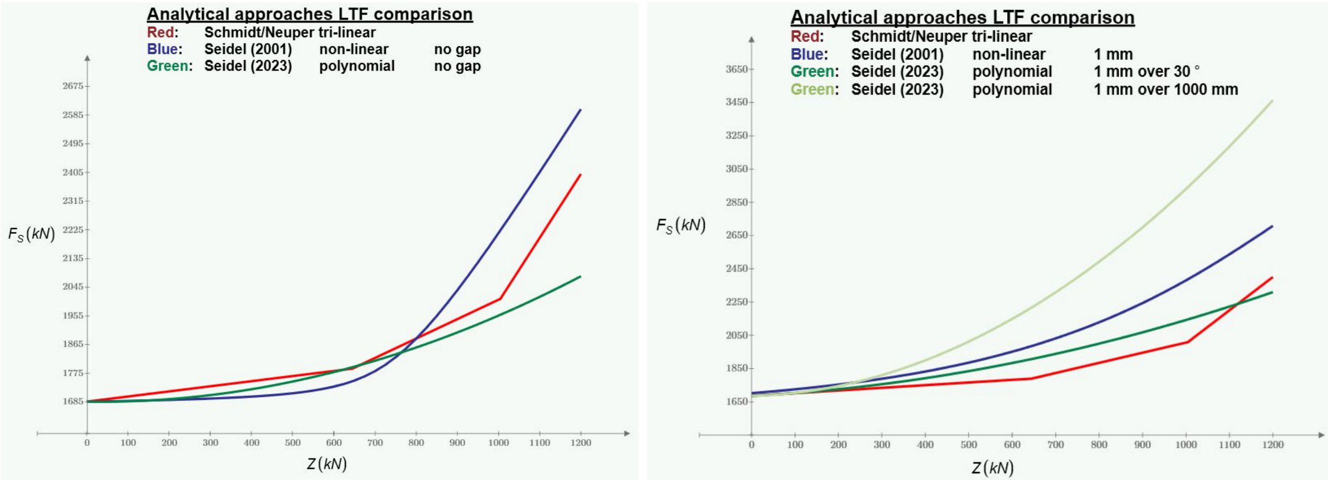

(a) (b)

Figure 5.4: LTF comparison reference model for (a) no gap (b) gap of 1 mm over 30° and 1000 mm

5.2. Next generation model

In this section, the next generation model is calculated in ULS, where the number of bolts and the bolt type is determined. Moreover, the LTF for different approaches and gap shapes are analyzed and compared to the reference model.

5.2.1. Analytical check: ULS

Firstly, the number and type of bolts are determined using ULS and LTF calculations. The aim for this model is to have a sufficient resistance of the connection in ULS, with acceptable spacing between the bolt nuts. The same calculations are performed as for the reference model, so the calculation steps are not worked out in this section. The ULS calculation for the reference model is added in Appendix C and the dimensions for the next generation model are added in Appendix A. With the design external force on the wind turbine, the connection would suffice with smaller bolts than M80. However, the stresses and therefore forces in the bolt would be too high. Therefore M80 bolts are chosen for this connection, so ensure sufficient resistance.

For M80 bolts, a minimum washer diameter of 140 mm is used. With this washer diameter and a minimum spacing between the bolt nuts, the maximum number of bolts that can be used can be determined with $n_{bolt.max} = \frac{\pi * D_{B.axis}}{s_{min}} = 165$. The amount of bolts that will be used for this connection is 162. A bolt diameter of 80 mm requires a minimum bolt hole diameter of 86 mm. Moreover, the same bolt grade will be used as for the reference model, namely 10.9, and the same steel grade, namely S355. The characteristic values for these materials and dimensions result in a desired pretension and design tension resistance per bolt of:

$$\begin{aligned} F_V &= 2737kN \\ F_{t.Rd} &= 3128kN \end{aligned} \tag{5.21}$$

By performing the same calculations as described in Section 5.1, the following ultimate resistances for each failure mode and the corresponding utilization ratios are found:

Table 5.4: Overview failure modes ULS (next generation model)

Failure mode	Ultimate resistance	Utilization ratio
A	3128 kN	30.6 %
B	1591 kN	**60.1%**
D	1591 kN	**60.1%**
E	3655 kN	26.2 %

Similar to the reference model, failure mode B is governing in ULS. Moreover, failure mode D is nearly equally governing, with a negligibly lower utilization ratio of 0.01%. Both failure modes have an utilization ratio of 60.1%.

5.2.2. Analytical check: LTF

The next generation model is calculated as well with the chosen analytical approaches, and the calculation steps are identical to the calculation steps showed in Section 5.1.4. They will therefore not be worked out once more, and only the LTFs for each approach are shown.

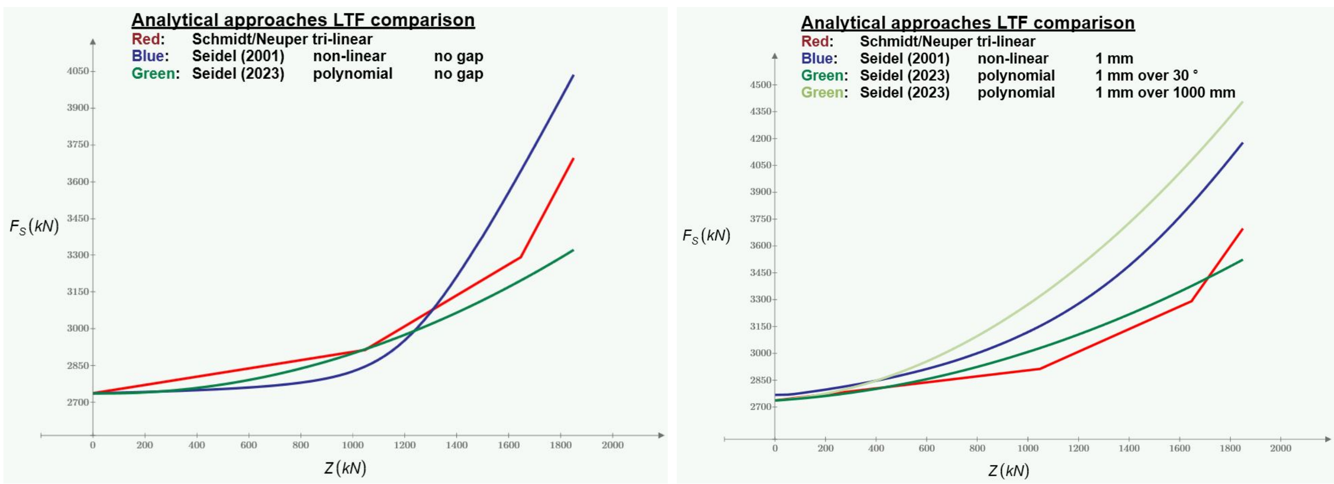

(a) (b)

Figure 5.5: LTF comparison next generation model for (a) no gap (b) gap of 1 mm over 30° and 1000 mm

The LTFs for the approaches without explicitly considering geometric imperfections show a very similar curve to the LTFs for the reference model. As the bolt size changes, the preload applied on each bolt increases to $3128kN$, which results in the LTFs shift to a higher bolt force and external force, as can be seen in Figure 5.5. Comparing the figure that include geometric imperfections (Figure 5.5(b)) to the LTFs of the reference model, the shapes of the LTFs are again similar, except for the polynomial approach. The LTF of the 1 mm gap over 30° (Figure 5.5(b)) for the next generation model is similarly close to the other two approaches compared to the reference model (see Figure 5.4(b)).
For the gap of 1 mm over 1000 mm (Figure 5.5(b)), the LTF of the polynomial approach is closer to the other two approaches compared to the reference model. A possible explanation for this relation is that both the tri-linear and non-linear approaches are designed for the DNV verified design gap shape of 1 mm over 30°. Another explanation for this behaviour is

that either the polynomial approach expects too high bolt forces for very small gap lengths in connections with smaller diameters, or the other two approaches underestimate the bolt force for large dimensions. In Chapter 6, FEA will be done to obtain which approach for the next generation connection is closer to these numerical results.

5.3. Parametrization gaps

In this section, the influences of different gap lengths and heights are analyzed with the analytical approaches. As stated before, the tri-linear approach by Schmidt/Neuper takes geometric imperfections into account implicitly, not explicitly. Therefore, this LTF cannot be parameterized for different gap lengths or heights, and will not be further elaborated in this section.

Non-linear LTF (Seidel, (2001))

As stated before, in the non-linear approach by Seidel [20], the height of the gap can be changed that result in a different LTF. The length of the gap is not explicitly a variable in this approach. In Figure 5.6, the LTFs for various gap heights are shown for this analytical approach for the reference model.

Figure 5.6: Non-linear LTF Seidel (2001) for various gap heights, obtained from Mathcad

In this figure, it can clearly be seen that increasing the gap height increases the forces in the bolt. When no gap is present, the first region of the LTF is an almost flat curve, where very little variation of bolt forces is obtained. When a gap is present, the slope of the first region becomes higher when the gap height increases, increasing the calculated bolt force significantly compared to no gap present at low external forces.

Polynomial LTF (Seidel, (2023))

The polynomial approach by Seidel is a less conservative approach compared to the abovementioned approaches, as it takes both gap height and gap length explicitly into account. Figure 5.7 shows the analytically obtained LTF with the polynomial approach for various gap lengths and heights for the reference model.

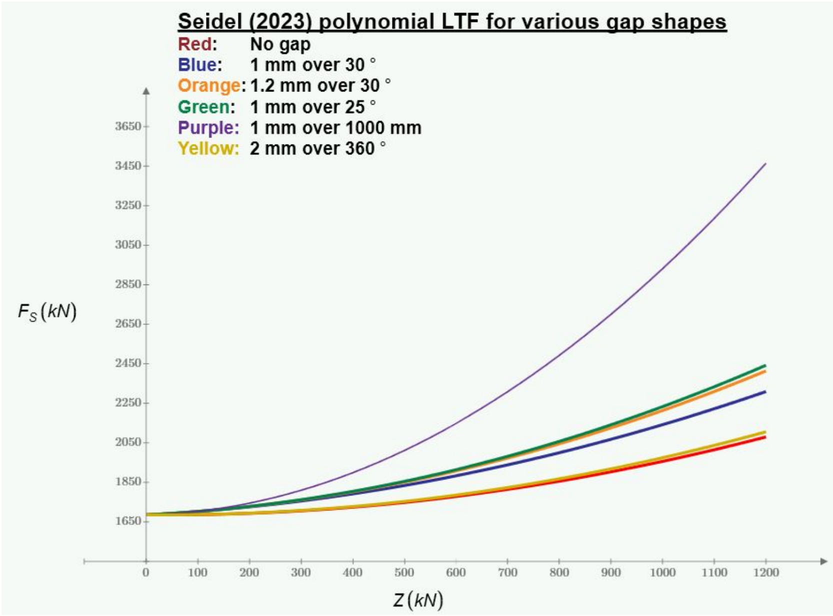

Figure 5.7: Polynomial LTF Seidel (2023) for various gap shapes, obtained from Mathcad

In this figure, an observation can be made that the bolt forces increase for a larger gap height or a smaller gap length. The LTF for a flange without gap shows a somewhat linear line without a large quadratic curve. The initial slope of the polynomial LTF without gap is larger than for the non-linear curve and closer to the LTFs with gaps.
A difference can be obtained for parameterizing a gap of 1 mm over 30° by decreasing the gap length or increasing the gap length with the same factor, see the orange and green line. With this polynomial approach, an increase in gap height (1.2 mm over 30°) gives a larger force in the bolt than a decrease in gap length (1 mm over 25°). This observation will be tested with FEA if numerical calculations show the same result. For a larger gap height of 2 mm over the entire circumference, the bolt force can be seen not to increase much compared to the model without gap. This observation will be checked with FEA results.

For a gap of 1 mm over 1000 mm, the approach shows much larger forces in the bolt compared to the abovementioned gaps. This is in line with the theory that a decrease in gap length results in larger forces in the most critical bolt.

Overview

The three approaches considered in this thesis differ in conservatism regarding geometric imperfections. The tri-linear LTF by Schmidt/Neuper [18] takes geometric imperfections implicitly into account, and therefore cannot be changed for different gaps. The non-linear LTF by Seidel (2001) [20] does have the gap height as a variable, where flanges with a higher gap result in larger bolt forces. The polynomial LTF by Seidel (2023) has both gap height and gap length as a variable, and therefore gives a different graph for each gap shape. With this approach, larger gap heights or shorter gap lengths result in a higher bolt force. Moreover, in the polynomial approach, LTFs for larger gap heights deviate more from the original gap than shorter gap lengths.
Numerical calculations will be done in Chapter 6 and these results are compared to the analytical approaches described in this section, to investigate which approach is more reliable for

each gap shape.

5.4. Parametrization connection dimensions

In this section, the connection is parameterized with the dimensions as discussed in Section 3.4. In Section 5.1, the LTF for a small gap and no gap present showed large differences. Therefore, the focus in this parametric study is on a connection with geometric imperfections, as a connection with geometric imperfections is more relevant to calculate. The gap height that is chosen for these analyses is a gap with a length of 1000 mm and a height of 1 mm per flange. In the following sections, the analytical results for the parameterized models and the influence of each dimension is discussed. Figures 5.8 to 5.12 show the LTFs for the tri-linear, the non-linear and the polynomial approach where in each figure one dimension is altered. In the figures, the blue graph represents the reference model, with the dimensions as explained in Section 3.2. The red graph represents the parameterized model, with the dimensions listed above the graph. The three approaches are distinguished by different line styles. In Section 3.4, the flange dimensions that are parameterized are listed and shown in a figure.

5.4.1. Bolt circle diameter

In Figure 5.8, the analytical approaches with a larger connection diameter are shown. As can be seen, for the tri-linear approach, the difference between the reference model and the larger connection diameter is negligibly small. For the non-linear approach, the difference is small as well. However, not as small as for the tri-linear approach. The non-linear approach gives a lower force in the bolt for the same external force. The polynomial approach gives a much larger difference for a larger connection diameter, where a larger connection diameter results analytically in a higher instead of a lower bolt force. For smaller gap heights and especially larger gap lengths, this difference becomes smaller.

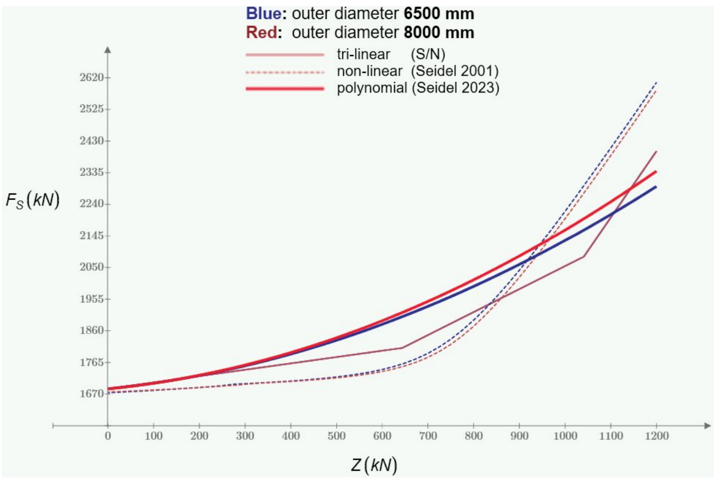

Figure 5.8: Analytical approaches reference model and BCD parameterized

As a conclusion, analytical calculations for a larger bolt circle diameter do not give the same results, as one approach shows no difference, another approach gives a lower bolt force for a larger diameter, and another gives a higher bolt force for a larger diameter. Numerical calculations have to be done to obtain what the actual influence is of this parameterization.

5.4.2. Distance bolt to inside flange

In this parameterization, the length of the flange is increased towards the inside of the turbine, resulting in a larger distance between the bolt and the inner part of the flange. The results for each of the three approaches show the same trend. Namely, a larger distance from the bolt to the inside of the flange results in a lower bolt force. In the first stage of the LTF, the difference is smaller or negligible. At high external forces, the difference becomes higher.

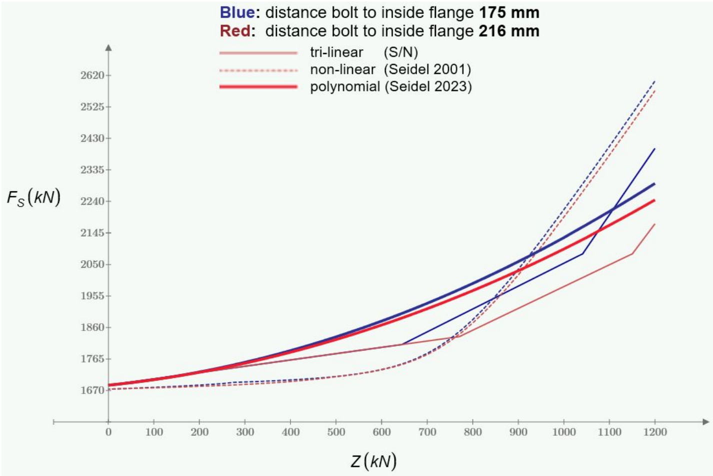

Figure 5.9: Analytical approaches reference model and DI parameterized

5.4.3. Distance bolt to outside flange

This section elaborates the difference between the reference model and an increased length between the center of the bolts and the outside of the tower wall. The results show very large differences between the reference model and the parameterized model. For all three approaches, the forces in the bolts increase drastically when this distance increases. It would therefore be more beneficial to reduce this distance.

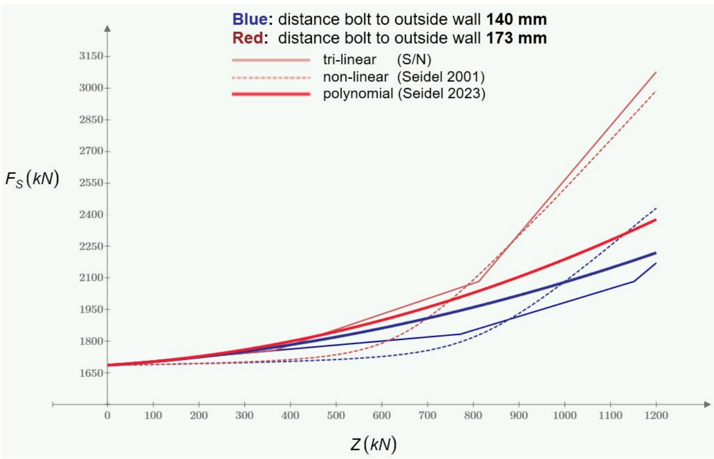

Figure 5.10: Analytical approaches reference model and DO parameterized

5.4.4. Tower wall thickness

A thicker tower wall results for the tri-linear approach identical slopes for all three regions. The difference lies in the tower shell force where the second region (successive flange opening) ends, where a thicker tower wall results in lower bolt forces from this region. Similarly for the non-linear approach, the LTF shifts to a line with a line where bolt forces are obtained at a slightly earlier external force, resulting in lower bolt forces. The polynomial approach, however, shows a higher bolt force for a larger tower wall thickness.

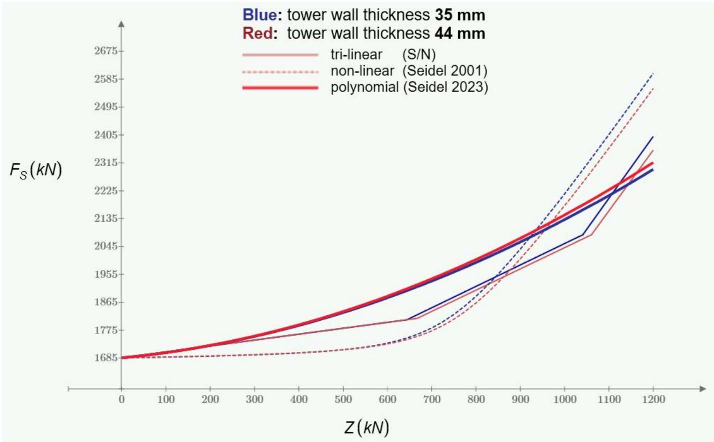

Figure 5.11: Analytical approaches reference model and TWT parameterized

As a conclusion, the analytical approaches show contradicting results, with lower bolt forces obtained by two approaches and higher bolt forces by the third. Numerical calculations will show which approach shows a correct trend.

5.4.5. Flange thickness

In the LTFs of the parameterized flange thickness, the following observations are made:
For the approach by Schmidt/Neuper, a difference can be found in the slope of the second region. The first region, representing the closed connection, is the same for both dimensions. The second region, which represents the successive opening of the flange, has a lower slope for the model with a larger flange thickness, ending at a lower external force and a lower bolt force. For the approach by Seidel, the function is similar for the first region and deviates especially at high shell forces, where a larger flange thickness results in a lower bolt force. The polynomial approach by Seidel shows a different result for short gaps or large gap heights. In Figure 5.12 can be seen that for a 1 mm over 1000 mm gap, the forces in the bolts are higher. For a smaller gap (0.5 mm per flange) and a longer gap (30°), which are more realistic scenarios (see the 95% fractile design gap Figure 3.4), the LTF for thicker flanges show similar results to the other two approaches, namely a lower bolt force.

As for one of the three approaches, a thicker flange results in a higher bolt force and for the other two a lower bolt force, numerical calculations need to be done to make a comparison. An extra numerical calculation will be done with a large gap height over a short length (1 mm over 1000 mm).

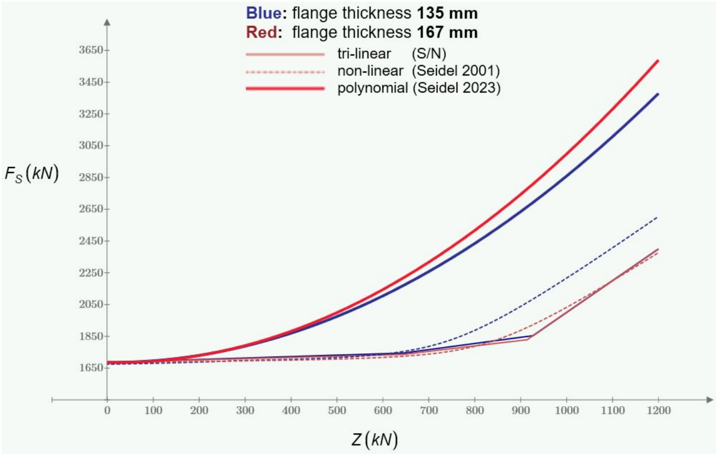

Figure 5.12: Analytical approaches reference model and FT parameterized

5.4.6. Overview

From this parametric study, it can be observed that increasing some dimensions as listed above give 'better' results, meaning a lower force in the bolt. For the dimensions DI (distance bolt to inside flange) and DO (distance bolt to outside wall), all three approaches show the same relation between the reference model and it's parameterized model. For DI, a larger distance results in a lower bolt force. For DO, a larger distance results in a significantly higher bolt force.

For the parameterization of BCD (bolt circle diameter), TWT (tower wall thickness) and FT (flange thickness), the polynomial approach by Seidel shows a different trend than the other two approaches. The tri-linear and non-linear approach give a lower bolt force for the increasing dimensions, and the polynomial approach gives a higher bolt force for the increasing dimensions (with a gap of 1 mm over 1000 mm). When the gap length increases or the gap height decreases to a more expected gap height, a thicker flange does result in lower bolt forces. An overview of all results for the dimension parameterization is shown in Table 5.5. In this table, the statement is shown if increasing the dimension results in higher (+), lower (−) or (nearly) equal (±) bolt forces for each approach.

Table 5.5: Overview parameterization (change in bolt force when increasing dimensions)

Approach	BCD	TWT	DO	DI	FT
Tri-linear (Schmidt/Neuper)	±	−	+	−	−
Non-linear (Seidel)	−	−	+	−	−
Polynomial (Seidel)	+	+	+	−	+

To make a proper comparison between the parameterization of these dimensions, in Chapter 6, calculations with FE models with the same dimensions are performed. These calculations will be done using the segment approach, as elaborated in Section 4.2. As parameterizing some of the analyzed dimensions show contradicting results for different gap shapes, extra FE calculations will be done for a full model with a gap of 1 mm over 1000 mm.

6 Numerical calculation

In this chapter, the results of the numerical calculations using ANSYS are elaborated. The results obtained with FEA are compared to the analytical approaches, and conclusions will be drawn from those comparisons.

6.1. Reading results

The results for the numerical calculation are obtained by reading out the bolt force F_S as a working load using the 'Bolt tool'. In this tool, the load is obtained from reading the forces in the nodes of the elements in the bolt shank. This option can read out the maximum and minimum load in the selected bolts. As the goal of this thesis is to obtain the force in the most relevant bolt, the highest force of all bolts is read and used for the LTF, see Figure 6.1.

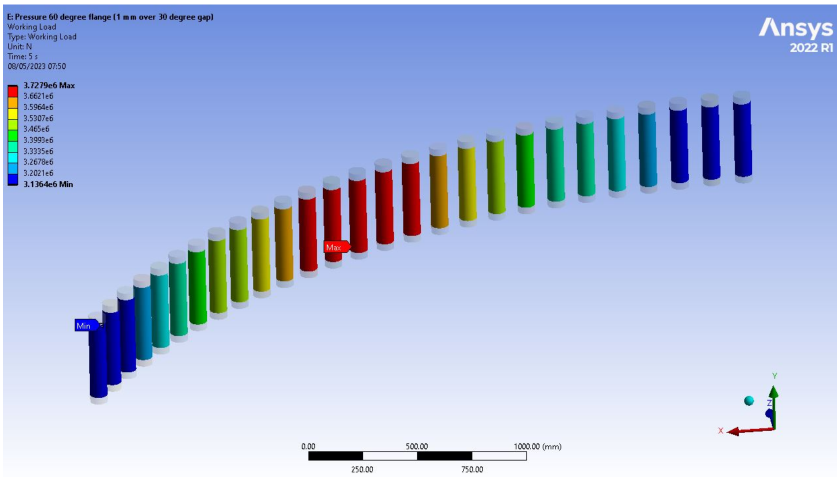

Figure 6.1: Force distribution in bolt shanks from ANSYS

6.2. Differences model size

As discussed in Chapter 4, it is desired to limit the computational effort of the FE model, by trying to reduce the size of the model. Therefore, firstly, analyses are performed to show the differences between segments of different lengths, to obtain what segment can be used for the analysis of geometric imperfections. The angle of the segment that is used as a 'check' is a full model of 360°, as that is the most realistic case. The segments that will be checked including this full model are:

- 360°
- 180°
- Smaller segment:
  - Gap present: Angle of imperfection (e.g. 60° for a gap of 1 mm over 30°)
  - No gap present: Segment of 1 bolt

On the models of 360° and 180°, a bending moment is applied at the largest gap height, as is the situation that will give the largest peak forces in the bolts. For the models with a smaller size, however, it is not possible to apply such a bending moment in ANSYS. Therefore, as stated in Section 4.4, the bending moment is converted to a pressure that is applied to the tower wall. In order to be able to use the results with these models, this approach must be verified. This will be done by comparing the numerically obtained LTFs of various models with different boundary conditions to the most realistic model of 360 ° with a bending moment applied.

All of the following checks are performed for the reference model (outer diameter: 6.5 m) with a perfect flange and a model with a gap of 1 mm over 30°($\approx 1700mm$):

- 360°
  - moment applied
  - pressure applied
- 180°
  - moment applied
  - pressure applied
- Segment
  - For no gap: segment of 1 bolt with pressure applied
  - For gap: segment of 60° with pressure applied

As stated in Section 3.5, when modelling a gap of '1 mm over 30°', the gap height per flange is equal to 1 mm, and therefore the total gap height is equal to 2 mm, and the total gap length is equal to 60°. The top view of a segment of 60° modelled in ANSYS is shown in Figure 6.2.

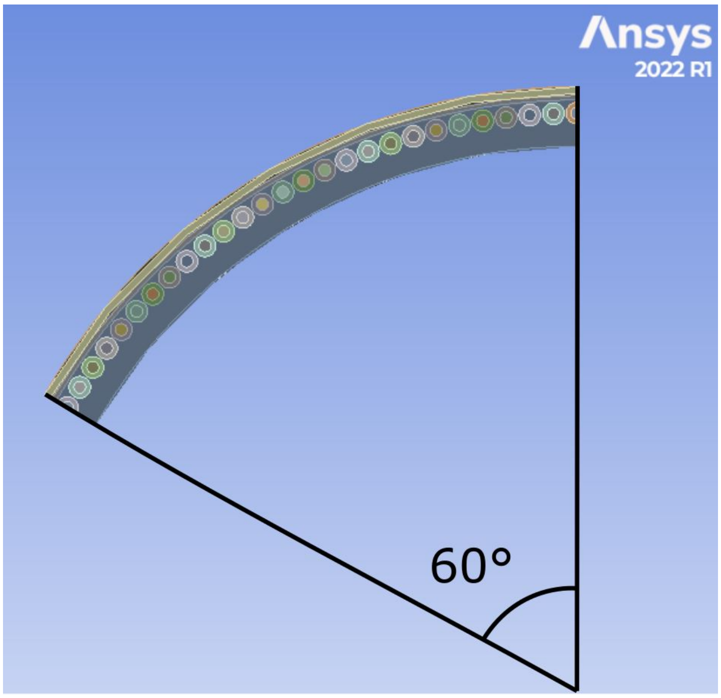

Figure 6.2: Top view of model of 60° as modeled in ANSYS

For models as listed above, the following LTFs are obtained. The black horizontal line in these figures is the design tensile resistance $F_{t.Rd}$ for the bolt used.

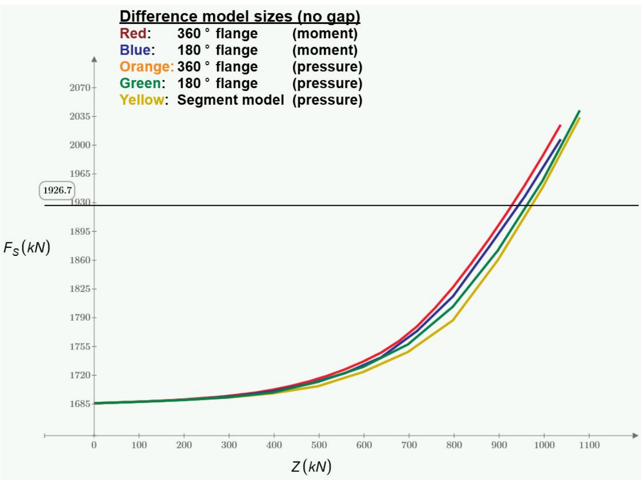

(a)

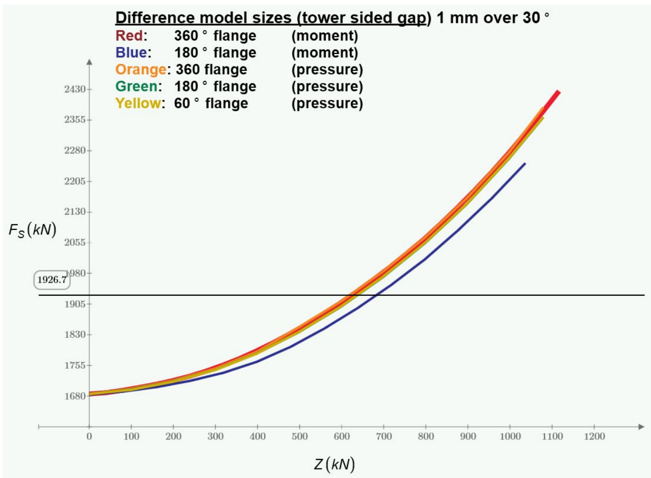

(b)

Figure 6.3: FE results for difference model sizes and load applied: (a) no gap (b) gap of 1 mm over 30 °

In the graph of the results for a connection with perfect flanges, so where no gaps are present, it can clearly be seen that all analyses give somewhat similar results. The flanges of 180° and 360° give the exact same results when a pressure is applied (the orange line in Figure 6.3(a) representing a 360° flange with a pressure applied is 'hidden' behind the green line). The segment of 1 bolt gives the largest difference, and is therefore less reliable than the other models. Even though the bolt forces for the models where a pressure is applied are not exactly equal to models where a bending moment is applied, its difference is very small. Therefore, it can be concluded that for flanges without geometric imperfections, a flange where a pressure is applied on a model of 360° or 180° can be used. The segment model is less reliable for absolute bolt force calculation, but will be used for dimension parameterization, as in those analyses, two (or more) segment models will be compared to each other.

For the analyses of the connection with a tower sided gap of 1 mm over an angle of 30°, similar differences can be seen between the models to the model without geometric imperfections. The red line, representing the most realistic loading scenario of a moment applied on a flange over the entire circumference, is slightly hidden behind the other lines. The biggest difference is between a model of 180° where a moment is applied, which is the dark blue thick line of Figure 6.3(b). This analysis shows a lower maximum bolt force compared to the other numerical results. The most presumable reason for this difference is that the model with a half flange was modeled such that both ends contain a half bolt. Even though these half bolts are modelled with symmetry conditions (including an applied preload of $\frac{1}{2} * F_V$, see Figure 6.4), the internal bolt forces were less than 0.5 times the forces in the adjacent bolts. Because the center of one of the half bolts is located at the largest gap height (the middle bolt in Figure 6.5), expected is that the force in this bolt is the highest, so it would be more than 0.5 times the force in the adjacent bolts. In the graph in Figure 6.3(b), the forces in the bolt that is located next to the center bolt in the gap is taken (bolt B in Figure 6.4), which obviously gives lower forces. Therefore, it can be concluded that the results of the moment applied on a segment of 180° cannot be used.

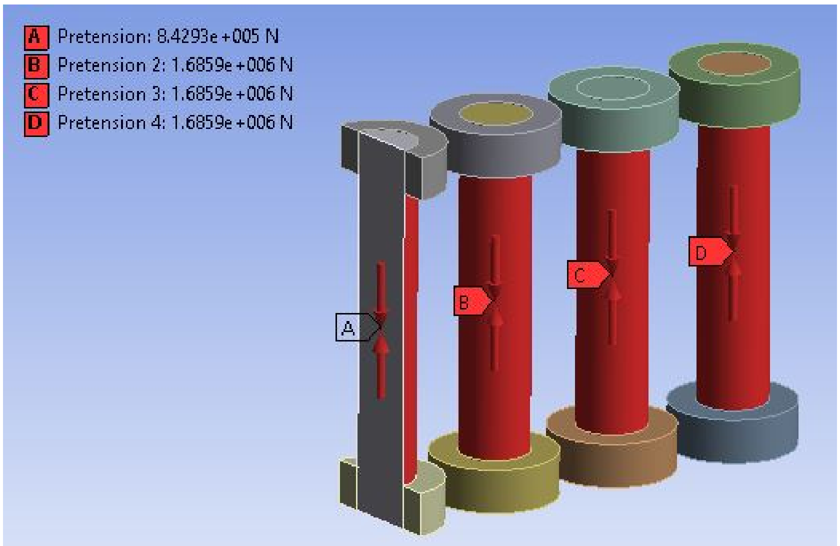

Figure 6.4: Pretension on whole bolts and half bolt as modeled in ANSYS

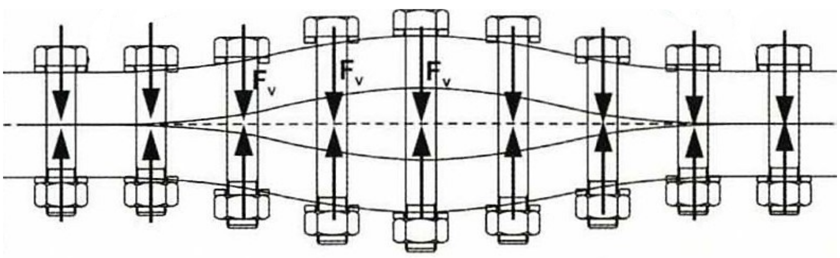

Figure 6.5: Forces in the bolt with presence gap [13]

The other analyses performed on the model with an initial gap show very similar results compared to the 'realistic' model of 360° with a bending moment applied. The differences in result are assumed to be negligible for all other models with geometric imperfections. The size of the data file that contains the solution is approximately proportionally smaller to the size of the model, meaning a half model (180°) has a three times as large data file as a model of 60°, used for the analysis of $u_{gap} = 1mm$ over $\alpha_{gap} = 30°$. For the models in this thesis, this difference is 7.9 GB for 180°. The computational time is proportionally reduced for these model sizes. An overview of some FEA with various gaps and model sizes with its data file size is shown in Table 6.1.

Table 6.1: Differences file size for various model sizes

Model size (° over circumference)	Used for analyzing gap of	Data file size
180°	$u_{gap} = 1.0mm$ over $l_{gap} = 1000mm$	7.9 GB
180°	$u_{gap} = 1.0mm$ over $\alpha_{gap} = 30°$	7.8 GB
60°	$u_{gap} = 1.0mm$ over $\alpha_{gap} = 30°$	2.4 GB
60°	$u_{gap} = 1.2mm$ over $\alpha_{gap} = 30°$	2.3 GB
50°	$u_{gap} = 1.0mm$ over $\alpha_{gap} = 25°$	2.2 GB

With these analyses, a conclusion can be made which model size with loading conditions can be used for further analyses. For all analyses with geometric imperfections, a model where a bending moment is applied on a fully modelled connection (360°) can be used. Moreover, models of 360° and the length/angle of the imperfection (e.g. 60° for a gap of 1 mm over 30°) can be used when a pressure is applied. This last model size will be used for further analyses with different gaps, as this model requires the least computational time and effort.

As shown above and obtained in the analytical results in Chapter 5, flanges with a gap present give much larger bolt forces at the same external load than flanges without initial gap. Moreover, from literature such as [1], it is obtained that flanges without gap seldom occur in practice and therefore are not relevant to investigate. Therefore, models without geometric imperfections are not considered hereafter.

6.3. Tower sided and parallel gaps

As stated in Chapter 2, three types of gaps are considered in this thesis. Flange-sided gaps are already determined to be irrelevant, as they are not expected to give much larger overall bolt forces after closing the gap. In this section, tower sided gaps and parallel gaps are analyzed to obtain differences in bolt forces and therefore which ones are more relevant for this thesis. In Figure 6.6(a), the LTFs for two gap shapes are shown for both tower sided and parallel gaps, with an illustration of tower sided and parallel gaps right of that. In this comparison, an observation can be made that parallel gaps give higher bolt forces. In the results from literature, including [1], it was found that parallel gaps are the most often occurring geometric imperfections in wind turbines.

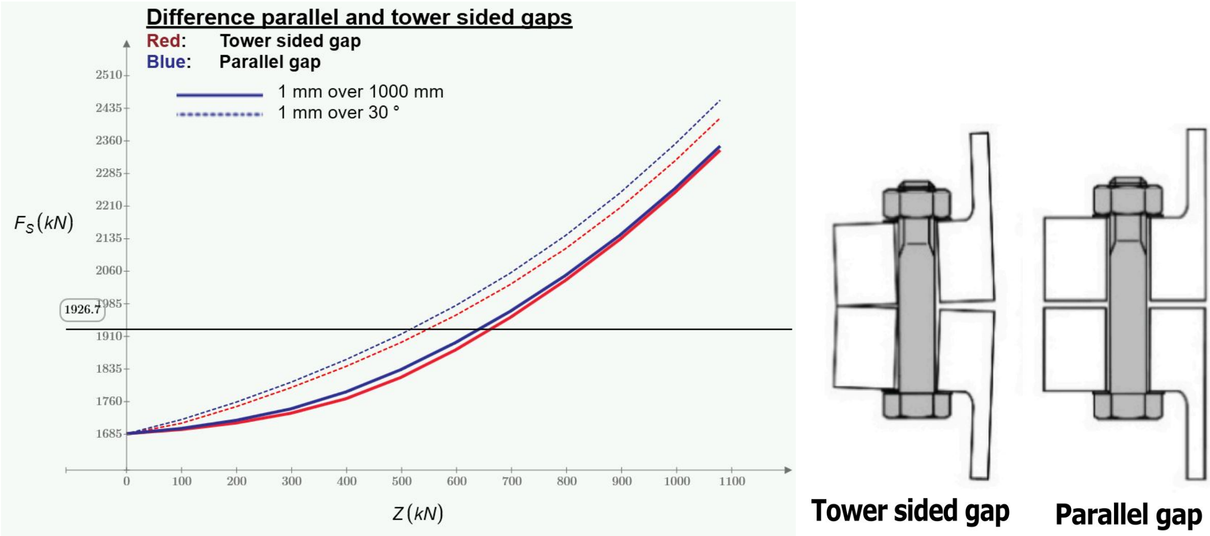

(a) (b)

Figure 6.6: (a) Difference tower sided and parallel gaps (a) LTFs for two gap shapes (b) illustration [22]

With this information, it can be concluded that parallel gaps are most relevant for this thesis and will only be considered in the following analyses.

6.4. Gap parameterization

In this section, various gap shapes are analyzed with numerical calculations. the gap that is applied to the model is parameterized to obtain the difference in bolt force for each gap numerically and a comparison is made between the numerical results and the analytically obtained results. The gaps that are considered are elaborated in Section 3.5 and are once more listed below:

- 1 mm over 30° (DNV verified)
- 1.2 mm over 30°
- 1 mm over 25°
- 2 mm over 360° (DNV verified)
- 2.4 mm over 360 °
- 1 mm over 1000 mm (≈ 17.63° for 6.5 m diameter)
- 0.5 mm over 1000 mm (≈ 14.32° for 8.0 m diameter)

As obtained in Section 6.2, for connections where initial gaps are present, the size of the model can be reduced to decrease the computational time, while obtaining similar results. Therefore, when, for example, analyzing gaps over an angle of 30°, the model used for the analyses is reduced to an angle of 60°.

6.4.1. Reference model

Firstly, the reference model is considered and a comparison is made between an increase in gap height and a decrease in gap length with the same factor of 1.2. A gap of 1 mm over 30°

will therefore be checked with a gap of 1.2 mm over 30° and with a gap of 1 mm over 25°. The differences are shown in Figure 6.7.

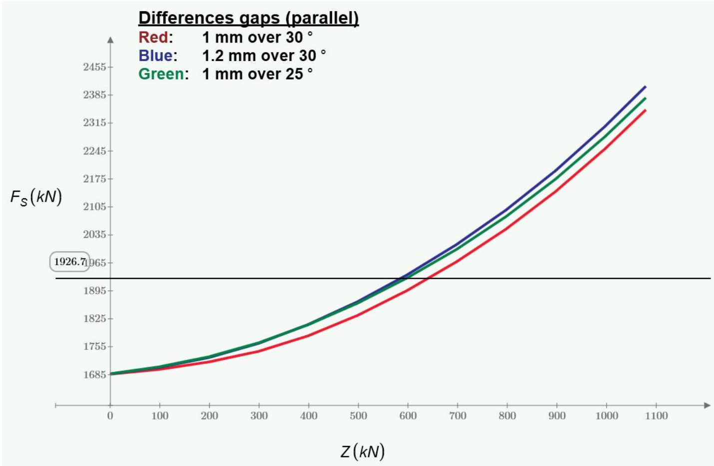

Figure 6.7: Difference between increasing gap height and decreasing gap length

A first conclusion can be made that an increase in gap height or a decrease in gap length result in a larger bolt force with FEA. This is in agreement with the theory in Chapter 2 and confirms the conclusions from the analytical calculations in Chapter 5. Moreover, it can be seen that the flange with a gap height of 1.2 mm results in larger forces in the bolt than the flange with a gap length of 25°. This observation confirms the result for the same gaps with analytical calculations using the polynomial approach. Therefore, a conclusion can be made that increasing the gap height has a larger influence on the LTF and therefore forces in the bolt than decreasing the gap length with the same factor. Moreover, geometric imperfections have an accurate influence on the polynomial approach. However, when increasing the gap length such that the gap spans the entire circumference (for gaps of 2 and 2.4 mm over 360°), the LTF for the largest force in the bolts becomes much closer to a connection without gap. This confirms the analytical results obtained with the polynomial approach, as can be found in Figure 5.7. The focus for further analyses therefore will be on gaps with shorter lengths that do not span the entire circumference.

Furthermore, various numerically obtained LTFs for the previously mentioned gap shapes are analyzed using the reference model and compared to the analytical results. In Figure 6.8 all three analytical approaches are compared to a gap of 1 mm over two different gap lengths. Again, the black horizontal line is the design tension resistance of the bolt ($F_{t.Rd}$), and the LTFs are shown for the external load of the first two ranges of the LTF of Schmidt/Neuper.

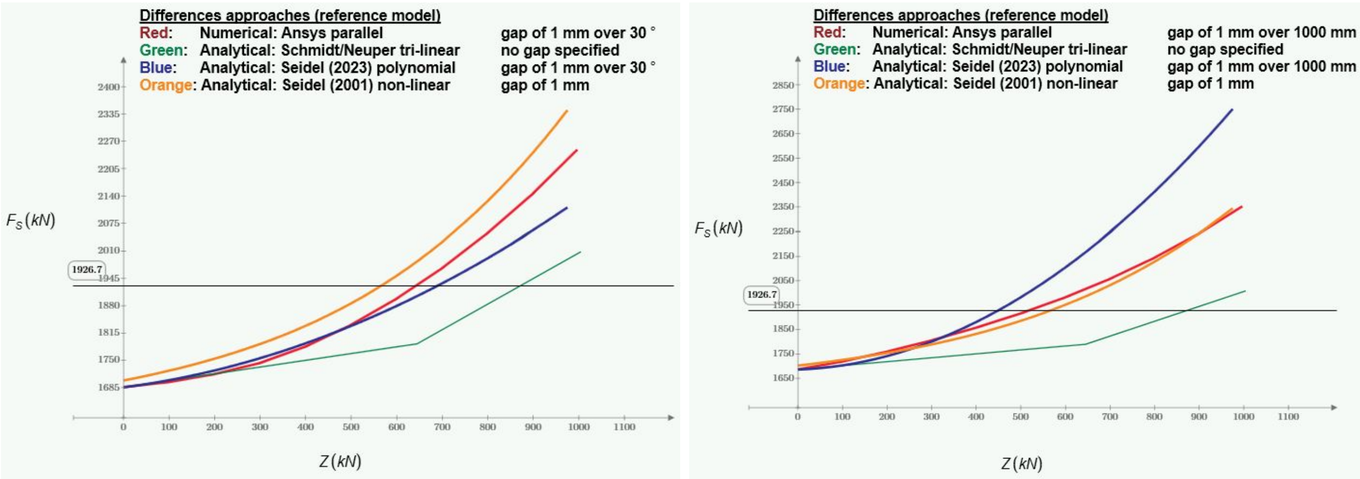

(a) (b)

Figure 6.8: LTFs for parallel gap of (a) 1 mm over 30° (b) 1 mm over 1000 mm (reference model)

A first conclusion can be made from these results that the tri-linear LTF by Schmidt/Neuper is too conservative for both gap lengths and highly underestimates the forces in the bolts. For comparisons for the reference model with other gap shapes, the tri-linear approach by Schmidt/Neuper will therefore not be used. In Figure 6.9, a comparison is made between the approaches and FE results separately for the same gaps as in Figure 6.7.

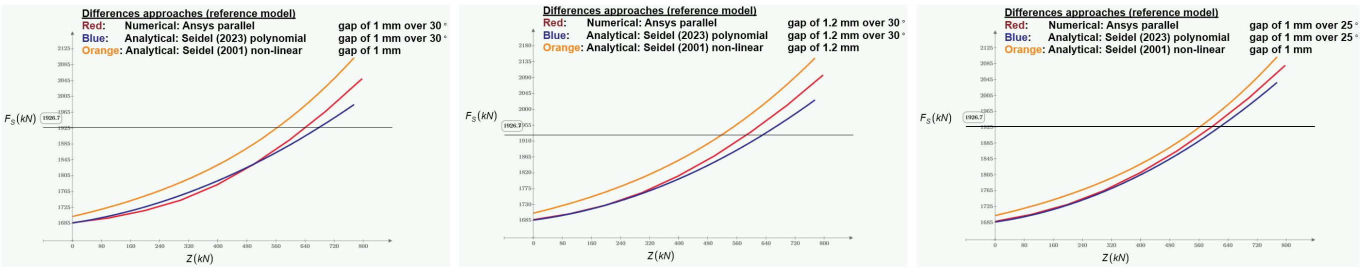

(a) (b) (c)

Figure 6.9: LTFs for parallel gap of (a) 1 mm over 30° (b) 1.2 mm over 30° (c) 1 mm over 25° (reference model)

The following observations are made for these gaps. Firstly, it can be obtained that the non-linear approach gives an LTF that has a very similar shape to the numerical LTFs, while still obtaining a higher bolt force than the FE calculated bolt force. Moreover, the slope of the non-linear approach is similar to the FE results, which is important for the cyclic loading.
The LTF of the polynomial approach is very similar in value and shape as the FE results. However, for all three gaps, this approach gives lower expected bolt forces than obtained with FEA after a certain external load, which is undesired for the design of a ring-flange connection. Especially for a larger gap height, namely 1.2 mm, the polynomial LTF underestimates the bolt forces at larger external forces.
For gaps that are close to the first DNV approved gap shape (1 mm over 30°) in a connection that is similar to the reference model, the non-linear approach by Seidel (2001) would therefore be recommended to use.

For a length of 1000 mm, a gap height of 1 mm per flange is analyzed, as proposed in [21], in addition to a gap height of 0.5 mm per flange, which is the 95% fractile gap height for this length. The LTF comparison between the numerical results and the non-linear and polynomial approaches are shown in Figure 6.10.

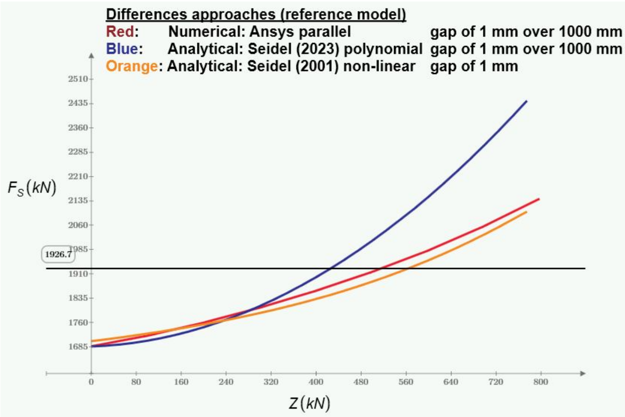

(a)

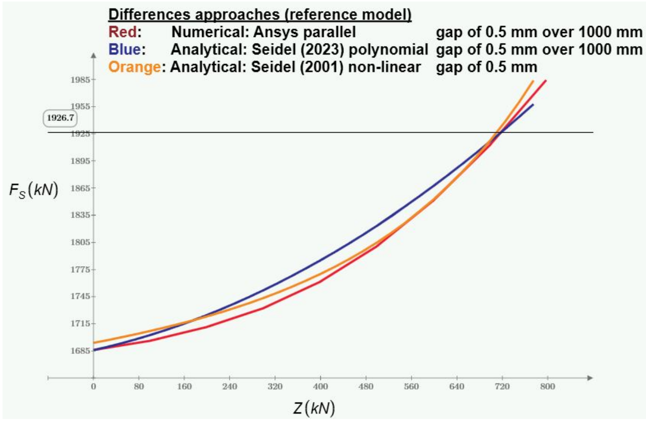

(b)

Figure 6.10: LTFs for parallel gap of (a) 1 mm over 1000 mm (b) 0.5 mm over 1000 mm (reference model)

Comparing the numerical results for these analyses, it can be seen that, unlike larger gap lengths, the polynomial approach calculates higher bolt forces than the FE results, which is desired.
For a gap height of 1 mm over 1000 mm, the calculated bolt force and slope of the polynomial LTF, however, is too large. With an expected bolt force F_S of 2148 kN with the polynomial approach and an FE obtained F_S of 1981 kN, and a load variation $\Delta F_S/\Delta Z$ of 0.53 for the polynomial versus 0.43 with FEA, an overestimation for both the bolt force and the load variation is obtained. For a gap height of 0.5 mm over the same length, the polynomial approach doesn't give a large overestimation in bolt forces. Before reaching the design tensile resistance of the bolt, however, crosses the polynomial approach the FE results, obtaining analytically lower bolt forces than expected. For these two gaps, the non-linear approach can be seen to give similar results in absolute bolt force. For a 0.5 mm gap height per flange, the non-linear approach slightly overestimates the bolt force. However, for a 1 mm gap, the non-linear approach slightly underestimates the FE results, which is undesired.

The results for all above analyzed gaps are shown in an overview in Table 6.2 for the analytical approaches and the results obtained with FEA. For each gap, the bolt force F_S is shown for a design damage external load of [redacted]. This external load value is the value until it is important to have an overestimation in the bolt force, as most damages are expected to occur until that external load. Moreover, the slope of the LTF, $\Delta F_S/\Delta Z$, which represents the load variation range that is relevant for FLS due to cyclic loading, is shown at a lower external force, with the largest frequency of occurring. When F_S at Z_D for an analytical approach gives larger bolt forces than obtained with FEA, and when $\Delta F_S/\Delta Z$ is larger than the FEA, which is desired, the value of the analytical approach is underlined.

Table 6.2: Overview result LTFs of gaps (reference model)

Gap	1 mm over 30 °		1.2 mm over 30 °		1 mm over 25 °	
	F_S at Z_D	$\Delta F_S/\Delta Z$	F_S at Z_D	$\Delta F_S/\Delta Z$	F_S at Z_D	$\Delta F_S/\Delta Z$
FEA	1896 kN	0.23	1935 kN	0.30	1927 kN	0.30
Tri-linear (S/N)	1762 kN	0.16	1762 kN	0.16	1762 kN	0.16
Non-linear (Sei)	1951 kN	0.32	1987 kN	0.36	1951 kN	0.32
Polynomial (Sei)	1895 kN	0.27	1915 kN	0.30	1921 kN	0.30
Gap	No gap		1 mm over 1000 mm		0.5 mm over 1000 mm	
FEA	1724 kN	0.03	1981 kN	0.43	1851 kN	0.18
Tri-linear (S/N)	1762 kN	0.16	1762 kN	0.16	1762 kN	0.16
Non-linear (Sei)	1733 kN	0.04	1951 kN	0.32	1852 kN	0.18
Polynomial (Sei)	1779 kN	0.10	2148 kN	0.53	1867 kN	0.25

6.4.2. Next generation

In this section, the connection that represents a next generation turbine is analyzed with numerical calculations. The dimensions of this next generation model are described in Section 3.3. Firstly, all three approaches are compared with the FE results for the same gaps as in Figure 6.8. The LTFs for these approaches are shown in Figure 6.11.

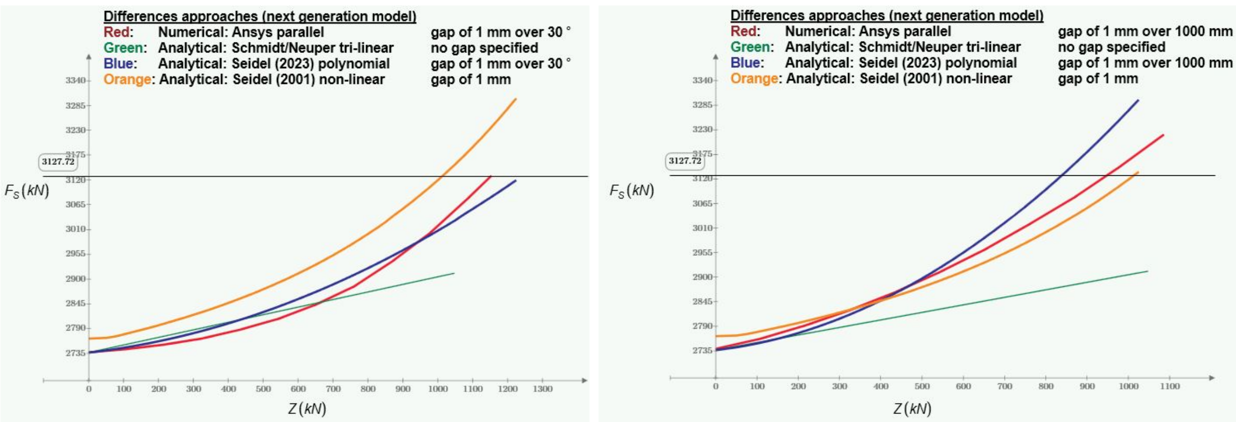

(a) (b)

Figure 6.11: LTFs for parallel gap of (a) 1 mm over 30° (b) 1 mm over 1000 mm (next generation model)

Similarly to the reference model, the tri-linear approach by Schmidt/Neuper can be seen to give too low forces in the bolts for both gaps. For the following gap analyses, the results will therefore not be compared to the tri-linear approach.

The first gaps that will be analyzed are gaps over an angle of 30°. For the next generation model, a gap length of an angle of 30° is larger than for the reference model, namely a total gap length of respectively 4.2 m compared to 3.4 m. Therefore, a larger gap height is expected for a gap with that angle, namely 1.12 mm per flange. The analyses that are performed for a gap with an angle of 30° are 1 mm, 1.2 mm and 1.45 mm, and are showed in Figure 6.12

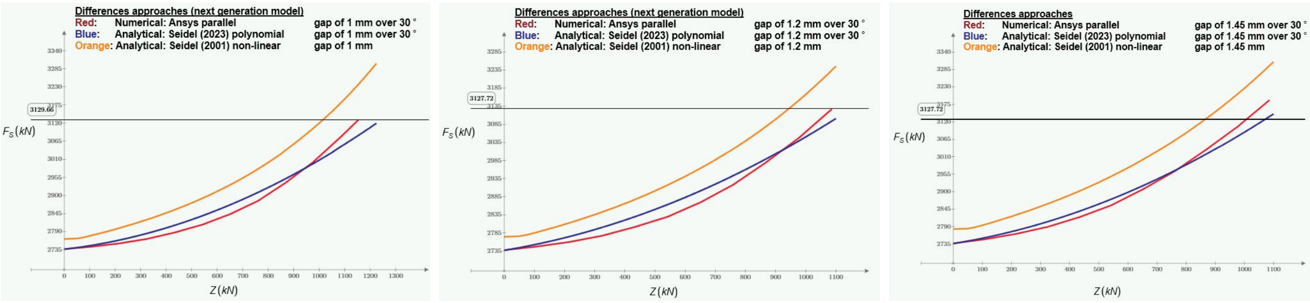

(a) (b) (c)

Figure 6.12: LTFs for parallel gap of (a) 1 mm over 30° (b) 1.2 mm over 30° (c) 1.45 mm over 30° (next generation model)

The following observations are made for these gaps. Similar to the reference model, the non-linear approach has a very similar shape to the LTF obtained with FEA, with somewhat larger bolt forces obtained. Therefore, the non-linear approach can be considered to be suitable for large gap lengths of approximately 30°, keeping in mind that the forces in the bolt are overestimated.

The LTF of the polynomial approach is in absolute value closer to the FE results than the non-linear approach. The slope in the first region of the polynomial is slightly higher than the FE results and from $Z \approx 600kN$ the slope of the FE results becomes larger. For each gap height, the two LTFs cross at a certain external load, where afterwards larger bolt forces are obtained with FEA than with the analytical polynomial approach, which is undesired. However, at the design damage external force of [redacted], the analytically obtained bolt forces remain larger than the FE results for a 1 mm and 1.2 mm gap. Before this load value, it is most important to overestimate the bolt forces, as most damages will take place before that value. For a 1.45 mm gap height per flange, the FE obtained bolt forces are slightly higher than the polynomial at this external force.

Concluding, for connections that have dimensions close to the next generation model, both approaches (non-linear and polynomial) are suitable to be used for the first DNV approved gap length (30°). However, for large gap heights of for example 1.45 mm per flange, the polynomial approach slightly underestimates the bolt force at Z_D.

For a length of 1000 mm, a gap height of 1 mm and 0.5 mm per flange are analyzed, similarly to the reference model. In Figure 6.13, the LTFs obtained with two analytical approaches and the FE results are shown for these gaps.

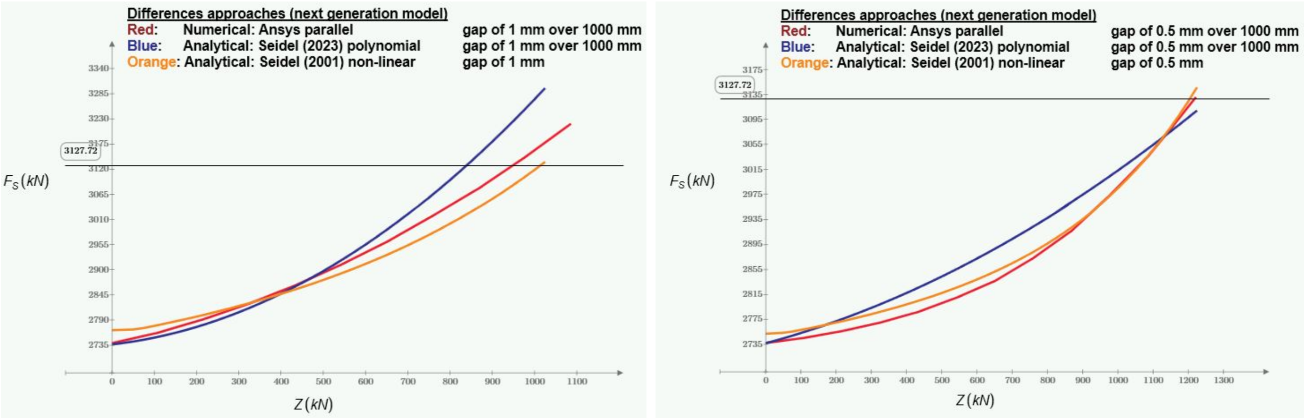

(a) (b)

Figure 6.13: LTFs for parallel gap of (a) 1 mm over 1000 mm (b) 0.5 mm over 1000 mm (next generation model)

What should be noted in Figure 6.13 is that the range on the x-axis with the external forces is larger than for the other next generation results. This range is increased to show the LTF until the design tension resistance of the bolt.
From these LTFs for short length gaps, it can be obtained that, similarly for the reference model, the polynomial approach gives larger forces than obtained with FEA. Likewise for the reference model, a gap height of 1 mm overestimates the forces in the bolt for the next generation model, but not as significantly. The difference in bolt force is small for the design external forces between FE- and polynomial results. Moreover, the slope of the LTFs are larger at the external forces with the largest frequency (see Table 6.3).
When analyzing the non-linear approach, the LTF for a 1 mm gap per flange gives lower bolt forces than the FE results, and therefore underestimates the forces in the bolts. For a gap of 0.5 mm, however, the non-linear approach gives very accurate results and a more similar slope than the polynomial approach.

An overview of the analytical and numerical results is shown in Table 6.3. For the next generation model, the design damage load is determined as [redacted], and the bolt force F_S at this external load and the slope of the graph $\Delta F_S/\Delta Z$ at the largest frequency design load is shown in this table.

Table 6.3: Overview result LTFs of gaps (next generation model)

Gap	1 mm over 30 °		1.2 mm over 30 °		1.45 mm over 30 °	
	F_S at Z_D	$\Delta F_S/\Delta Z$	F_S at Z_D	$\Delta F_S/\Delta Z$	F_S at Z_D	$\Delta F_S/\Delta Z$
FEA	2939 kN	0.14	2980 kN	0.18	3032 kN	0.22
Tri-linear (S/N)	2804 kN	0.17	2804 kN	0.17	2804 kN	0.17
Non-linear (Sei)	3041 kN	0.23	3083 kN	0.26	3135 kN	0.31
Polynomial (Sei)	2954 kN	0.17	2992 kN	0.22	3021 kN	0.24
Gap	No gap		1 mm over 1000 mm		0.5 mm over 1000 mm	
FEA			3079 kN	0.34	2917 kN	0.14
Tri-linear (S/N)	2804 kN	0.17	2804 kN	0.17	2804 kN	0.17
Non-linear (Sei)	2792 kN	0.03	3041 kN	0.23	2925 kN	0.13
Polynomial (Sei)	2859 kN	0.06	3159 kN	0.34	2965 kN	0.21

6.4.3. Overview

In the previous two sections, various gaps are analyzed that are relevant for the verification of bolted ring-flange connections. In Figure 3.4, an overview is shown for 95% fractile expected gap heights for certain gap lengths. Below, the proposed design gap heights are listed for certain gap lengths:

$\alpha_{gap} = 30°$
- Reference model (6.5 m diameter): $l_{gap} = 1.7m$, $u_{gap} = 0.91mm$
- Next generation model (8 m diameter): $l_{gap} = 2.1m$, $u_{gap} = 1.12mm$

$\alpha_{gap} = 180°$
- Reference model (6.5 m diameter): $l_{gap} = 5.1m$, $u_{gap} = 2.72mm$
- Next generation model (8 m diameter): $l_{gap} = 6.3m$, $u_{gap} = 3.35mm$

$l_{gap} = 1000mm$, $u_{gap} = 0.53mm$

The 95% fractile design gap height, obtained from [1], can be obtained with a linear relation to the gap length. The ratio of the gap height u_{gap} to the gap length l_{gap} that is expected, is equal to:

$$\frac{u_{gap}}{l_{gap}} = 0.533 * 10^{-3}$$

From the analyses performed in previous two sections, it can be obtained that gaps have a significant influence on the forces in the bolts. For short gaps (gaps over an angle smaller than or equal to 30°), increasing the gap height has a larger influence on the bolt force than decreasing the gap lenght with the same factor. For a very short gap length of 1000 mm, the expected gap height therefore gives a lower force in the bolt compared to a longer gap of 30° with its 95% fractile design gap height. However, as in the frequency distribution of many gap measurements (Figure 3.5) can be seen, either very short gaps or very long gaps are expected to occur, and a gap angle of 30° is not very likely to occur. Even though very long gaps that span the entire circumference are expected to occur often in these ring-flange connections, they are less relevant to calculate, because they show much lower peak bolt forces compared to smaller gaps. Therefore, it still needs to be investigated what gap height that corresponds to a gap length with this ratio of $0.533 * 10^{-3}$ gives the largest force in the bolts.

The polynomial approach was found to give the largest F_S and $\Delta F_S/\Delta Z$ for $l_{gap} = 1600mm$ with $u_{gap} = 0.85mm$. This could be a recommended gap to be analytically calculated to cover all possible expected gaps, under the condition that the results with FEA do not give a larger F_S and $\Delta F_S/\Delta Z$ and therefore larger damage.

When comparing the analytical approaches to the numerical results, a few conclusions can be made. Firstly, the tri-linear approach by Schmidt/Neuper is unreliable for connections of both 6.5 m and 8 m diameter with gaps, as it underestimates the forces in the bolt significantly. The region that is most relevant for the performance of the connection is the first region, and in some cases the second region too. A reason that the first region underestimates the bolt force for both considered connections, could be that the slope of that first region is only defined by the preload force (as a starting point), the length of the flange and the bolt- and flange stiffnesses. It doesn't take into account the gap closing behaviour, tower wall thickness and the preload force in the slope of this region. Most importantly, it does not explicitly consider geometric imperfections, which are shown to have a significant influence on the forces in the bolt. As the non-linear and polynomial approach by Seidel have respectively the gap height and the gap height and length as variables, they are less conservative.

For a connection with a diameter of 6.5 m, the non-linear approach is more reliable for larger gap lengths of approximately 30° than the polynomial approach. For smaller gap lengths, which are expected to occur frequently, the polynomial approach is very reliable, but overestimates the bolt forces too much for large gap heights at the design damage load. However, looking at Figure 3.4, this gap height of 1 mm over 1000 mm is a large overestimation, so is not expected to occur in practice.
For a connection with a diameter of 8 m, for both longer gaps and shorter gaps, the polynomial approach is more reliable than the non-linear approach in bolt force and bolt load variation. Only at large gap heights that are larger than the expected 95% fractile gap height, the bolt force at the design damage load is slightly underestimated. For the expected gap height for very short gaps (0.5 mm over 1000 mm), the load variation is overestimated in the polynomial approach, as the initial slope of the polynomial LTF is high.

When calculating the fatigue resistance, this load variation range is of high importance. With the Palmgreen-Miner rule as described in Section 3.5, an estimation can be given for the damage and therefore lifetime of the structure. An analytically calculated load variation range that is 0.01 lower than the actually obtained range can lead to a shortening in lifetime of multiple years. Therefore, similar to the design damage load, a lower load variation range that is lower when calculating analytically compared to FEA must be avoided.

Another important observation is made when comparing the polynomial approach and the FE results when increasing the gap length or decreasing the gap height with the same factor. For both models, the reference model and the next generation model, FEA show that increasing the gap height result in a larger bolt force than decreasing the gap length with the same factor. The polynomial approach, on the contrary, shows larger bolt forces when decreasing the gap length, see Figure 6.14.

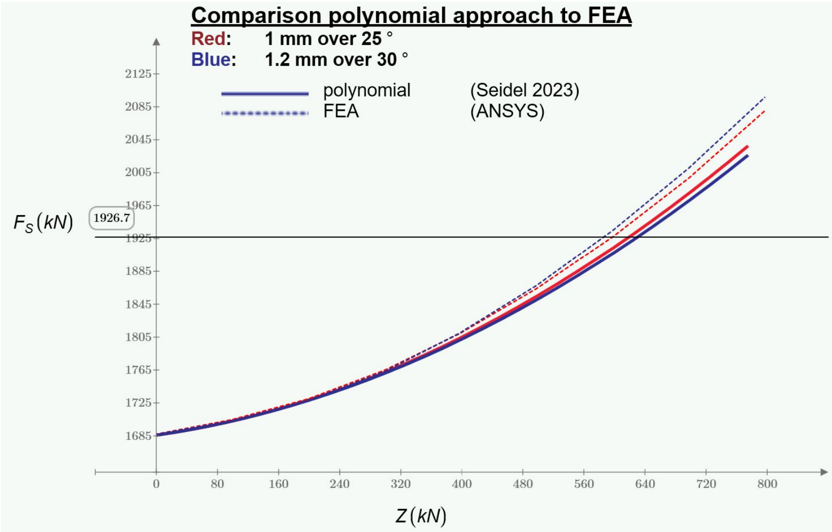

Figure 6.14: Comparison polynomial approach to FEA for 1 mm over 25° and 1.2 mm over 30°

From these observations, it can be concluded that the polynomial approach is more sensitive, meaning it overestimates the bolt forces more, for smaller gap lengths than for larger gap heights.

6.5. Dimension parametrization

In this section, the numerical calculations for the parameterization of certain dimensions of the connection are performed and results are discussed and compared to the analytical results obtained in Section 5.4. For the dimensions listed in Section 3.4, the first numerical calculations are performed on the reference model using the segment approach.

6.5.1. Reference model

The results of these abovementioned numerical calculations are shown in Figure 6.15. In these figures, the thick red line is the LTF for the reference model. The other lines are the parameterized models and are labeled with different colours. In Appendix D, extra figures are inserted where the parameterization of each dimension is shown with the corresponding analytical and numerical calculations.

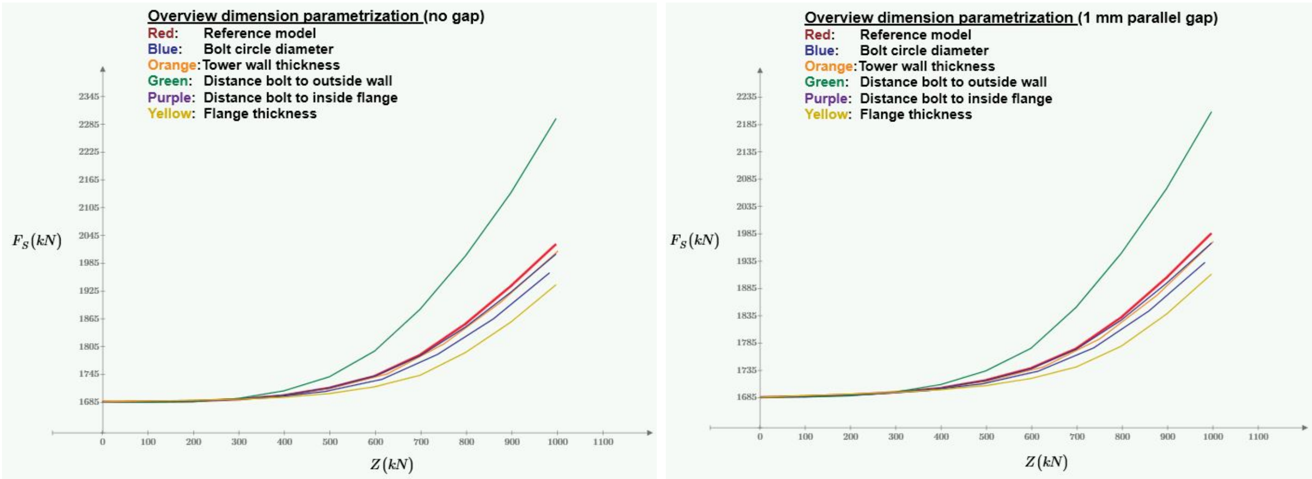

(a) (b)

Figure 6.15: LTFs of numerical results parameterization dimensions for (a) no gap (b) parallel gap of 1 mm

For both models, so without gap and with a gap of 1 mm per flange, similar differences can be seen for each parameterization. Some observations are made and summarized in the next sections.

Bolt circle diameter

In the LTF for a model with a larger bolt circle diameter, the results show lower forces in the bolt for a larger diameter. This is in line with the results for the non-linear approach. However, the polynomial approach showed a larger bolt force when increasing the bolt circle diameter. Therefore, the FE results of a full model with certain gaps need to be done to show how the analytical approaches relate to the next generation model.

Distance bolt to inside flange

In the segment model, the FEA show an increase in distance from the bolt to the inside of the flange results in lower forces in the bolt. This is in line with the analytical results for each approach, and will therefore not be analyzed with a full model.

Distance bolt to outside wall

FE calculations show that an increase in distance from the bolt to the outside of the wall results in a higher force in the bolt. This difference is, as the analytical approaches showed as well, large between the reference model and the parameterized model. It can therefore be concluded that decreasing the distance from the bolt to the outside of the wall results in a lower bolt force, and will not be further analyzed with a full model. However, a limitation exists in decreasing this distance, as the bolt nut needs to have a sufficient distance to the rounding of the weld.

Tower wall thickness

An increase in tower wall thickness can be seen not to have a very large difference in bolt force compared to the reference model. The numerical results are comparable to the non-linear and tri-linear analytical approaches, but gives contradicting results to the polynomial approach. Presumably a thicker tower wall gives a lower force in the bolts because the centroid of the external load shifts closer to the bolt. This results in the same effect as decreasing the distance from the bolt center to the tower wall, see previous section. Moreover, a limitation exists in increasing the tower wall thickness, due to the gap closing stress, see Section 5.1. Therefore, increasing the tower wall thickness would only be necessary for the resistance of the tower shell structure itself.

Flange thickness

The FE results of the segment model showed that an increase in flange thickness result in a decrease in forces in the bolt. This is in line with the tri-linear, non-linear approach and the polynomial approach for gaps around the 95% fractile design gap heights, but contradicting for the polynomial approach for a gap of 1 mm over 1000 mm. Therefore, an increase in flange thickness will be investigated for the next generation model using a full model with a gap shape of 1 mm over 1000 mm.

6.5.2. Next generation

For the connection with next generation dimensions, not all analyses as done in the reference model are done as well. As obtained in the previous section, parameterizing the distance from the bolts to the inside of the flange (DI) and the distance from the bolts to the outside of the wall (DO) show similar differences between the analytical approaches and the FE results.
The other three dimensions, bolt circle diameter (BCD), tower wall thickness (TWT) and flange thickness (FT), show contradicting results for certain analytical approaches and numerical results when parameterizing. Therefore, in this section, segments of larger sizes than one bolt are modeled with parameterized dimensions.

Flange thickness

Firstly, a flange with a gap of 1 mm over 1000 mm is parameterized with different flange thicknesses to obtain the influence of increasing the flange thickness on the LTF. Figure 6.16 shows the LTFs for the next generation model with it's flange thickness and an increased flange thickness by a factor 1.1 and a factor 1.2, making the flange thicknesses respectively 167 mm, 183.7 mm and 200.4 mm. What should be noted is that the second flange thickness might be a realistic designed flange thickness for larger turbines. A flange thickness of 200.4 mm, however, is very large and is unlikely to be realized in connections designed for a similar wind turbine as the next generation connection is approximated for (14-15MW, 8 m diameter). Moreover, the force required to close the gap for the very thick flange is larger than 50% of the desired preload, which results in a too high stiffness to close the gap.

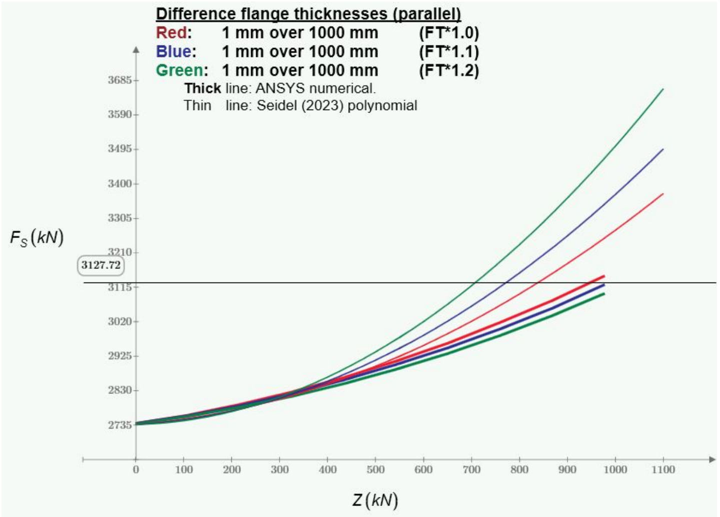

Figure 6.16: Parameterization FT for next generation model

From these results obtained with FEA, it can clearly be seen that a thicker flange results in lower bolt forces at the same external force. That is contradicting with the analytical results of the polynomial for a gap of 1 mm over 1000 mm. When decreasing the gap height or increasing the gap length to expected values (see Figure 3.4 and 3.5), thicker flanges with the polynomial approach show results that are in agreement with the numerical results. This parameterization would therefore give reliable results for expected gap shapes.

Tower wall thickness

Secondly, analyses are obtained by increasing the tower wall thickness (TWT) and transition piece wall thickness (TPWT). Calculations are done where both wall thicknesses are separately increased to obtain an insight in the difference per increasing thickness:

- TPWT *1.0, TWT *1.0
- TPWT *1.25, TWT *1.0
- TPWT *1.25, TWT *1.2

From this analyses, where the results can be seen in Figure 6.17, it can be seen that increasing each wall thickness increases the forces in the bolts. This is in line with the polynomial approach when parameterizing the wall thicknesses. An explanation for a slightly larger bolt force due to larger wall thicknesses, is that with a larger wall thickness, the stiffness of the flange increases, making it more difficult to close the gap and creating a higher initial slope of the LTF.

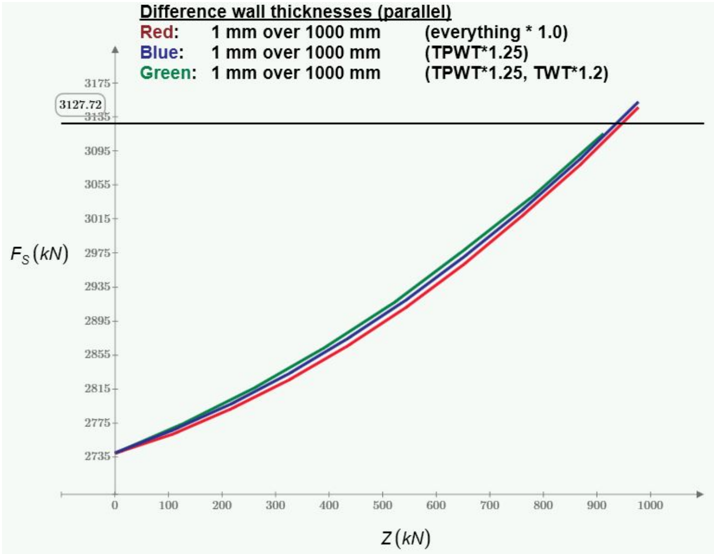

Figure 6.17: Parameterization TWT, TPWT for next generation model

7 Conclusions and recommendations

In this chapter, the most important findings within this thesis are summarized, that allows an answer to be given to the research question:

> "How do the increasing dimensions of offshore wind turbines influence the validity of the current used load transfer functions (LTFs) for bolted ring-flange connections?"

7.1. Conclusions

Based on the results obtained in the previous chapters, the following conclusions can be made:

- The widely used approach by Schmidt/Neuper [18] to obtain the LTF is found to be an unreliable approach for current and future bolted ring-flange connections. For both considered connections in this thesis (outer diameter of 6.5 m and 8 m), this tri-linear approach shows to highly underestimate the forces in the bolts, even when very small gaps of l_{gap}=1000 mm are present. Moreover, it underestimates the range in bolt forces at smaller external loads with large frequencies, which is of high importance for the large number of load cycles a wind turbine is subjected to. With such an underestimation of bolt forces, the lifetime of a structure can be overestimated compared to reality with multiple years.

- Two other approaches by Seidel to obtain the LTF show more reliable results than the tri-linear approach, meaning a better estimation of the forces in the bolts when the turbine is subjected to external loads. The very new approach, described by a polynomial, has been tested and showed accurate results for the gaps close to the 95% fractile design gaps (height to length ratio of $\frac{u_{gap}}{l_{gap}} = 0.53 * 10^{-3}$) of large connection diameters compared to FEA. This polynomial approach includes both gap height and gap length explicitly as variables and takes the stiffness to close the gap into account. Even though there are a number of contradicting results between this new method and FEA, it is obtained to be a reliable approach for connections with expected dimensions. For all considered gaps, the variation of bolt forces ΔF_S relevant for fatigue resistance is not underestimated. The expected lifetime of the structure is therefore not overestimated with this approach. The other approach [20], a non-linear function obtained iteratively, works well for a connection with a diameter of 6.5 m for current verified tolerances. This approach, however, is less accurate for smaller gap lengths than an angle of 30° or larger connection diameters, and is therefore not recommended to use.

- Current verified tolerances for gaps between flanges, namely a gap height of 1 mm per flange over an angle of 30° or 2 mm per flange over the entire circumference, are outdated. Either larger gap heights or smaller gap lengths are expected in practice, especially for connections with a diameter larger than 6.5 m. Increasing the height or decreasing the length of the gap with the same factor result in a larger force in the bolt that carries the biggest load. The shortest gap length with its 95% fractile design gap height (u_{gap}≈0.5 mm over l_{gap}=1000 mm), which has the largest measured frequency of occurring, however, gives lower bolt forces with finite element analyses (FEA) than the currently approved gap tolerance (u_{gap}=1 mm over α_{gap}=30°). Therefore, even though short gap lengths have a higher expected frequency, gap lengths ≥1000 mm should be considered in calculations for fatigue resistance (with its gap height over the ratio $\frac{u_{gap}}{l_{gap}} = 0.53 * 10^{-3}$) when designing a connection. If every gap with this ratio gives lower bolt forces with FEA than the polynomial approach with l_{gap}=1600 mm with u_{gap}=0.85 mm, this gap shape should be used for analytical calculations when designing a connection.

- When gaps with an irregular shape are present between the two flanges, a smaller model can be used than the full flange to calculate the forces in the bolts. The width of this segment, that is proven to be accurate with a fully modeled flange, is the complete size of the gap, meaning the length between the two contact points on both side of the gap, or larger. This significantly reduces the computational time and effort, while still obtaining very similar forces in the bolt compared to a full model. Decreasing the model size from $180°$ to $60°$, used for u_{gap}=1 mm over α_{gap}=30° is 2.4 GB against 7.9 GB, therefore requiring less than $\frac{1}{3}$ of the computational time and effort, saving multiple hours. Instead of applying a bending moment on the tower, which is a realistic loading scenario, a pressure can be applied that is converted from the bending moment.

7.2. Recommendations for further research

Based on the conclusions made in this chapter and the scope of this thesis, a number of recommendations are made for further research:

- In this thesis, the considered gaps are modeled as a sinusoidal wave, and are therefore perfectly symmetrical. In [1], it was obtained that (especially long) gaps deviate in shape from a perfect sinusoid, which could create extra contact points when closing the gap. This creates additional very short gaps that might be very difficult to close. As the analytical approaches do not consider these deviated shapes and a knowledge gap exists about gap shapes that deviate from a sinusoid, this should be investigated in further research.

- The parameterization of gaps and dimensions in this research are done for a connection diameter of 8 m, which is presumable for the currently announced wind turbines. However, offshore wind turbines developed from rotor diameters of 167 m to 236 m in a time span of 5 years. Therefore, we need to take into account that even larger wind turbines might be developed in the next years. The LTF of the polynomial approach with a very small gap length in a 8 m connection diameter is much closer to the FE results than for a 6.5 m connection diameter. Therefore, if even larger turbines are announced for production, FEA could be performed with the expected gap heights.

- In this thesis, a bolted ring-flange connection is considered, which is a connection type that has been researched by various institutions over the last decades. New connection types, such as the C1 Wedge Connection, are more recently developed, with a larger knowledge gap. Beforementioned analytical approaches for LTFs are designed for bolted-ring flange connections, and are therefore not applicable to these connection types. More research can be done to obtain an analytical LTF for the fatigue resistance of the C1 Wedge Connection.

- As the analytical polynomial approach is very new and is still under review, the calculation steps might be adjusted before publishing. Therefore, after approval of this approach, the worked out calculation in this thesis must be thoroughly checked with the approved polynomial approach in order for the conclusions to be valid.

References

[1] Buchholz, A., & Seidel, M. (2023, 1). Gap height prediction for bolted ring flange connections based on measurements. Steel Construction. Retrieved from https://doi.org/10.1002/stco.202200019 doi: 10.1002/stco.202200019

[2] DASt. (2013, 9). Richtlinie für Schraubenverbindungen [Guidelines for bolted connections] [Standard].

[3] DIBt. (2012, 10). Richtlinie für Windenergieanlagen [Guidelines for wind turbines] [Standard].

[4] DNV. (2018, 7). DNVGL-ST-0126: Support structures for wind turbines [Standard].

[5] DNV. (2019, 9). DNV-RP-C203: Fatigue design of offshore steel structures [Standard].

[6] EN 1993-1-8:2005. (2005, 5). Eurocode 3: Design of steel structures - Part 1-8: Design of joints (Standard No. EN 1993-1-8).

[7] EN 1993-1-9:2005. (2005, 5). Eurocode 3: Design of steel structures - Part 1-9: Fatigue (Standard No. EN 1993-1-9).

[8] Engineers Edge. (n.d.). Coefficient of Friction equation and table chart. Retrieved from https://www.engineersedge.com/coeffients_of_friction.html

[9] Faulhaber, A., & Thomala, W. (1978). Erläuterungen zur Richtlinie VDI 2230 Blatt 1 (1986): Der nichtlineare Berechnungsansatz. VDI-Z Zeitschrift des Vereins Deutscher Ingenieure, 129, 79-84.

[10] Frangoul, A. (2022, 9). Huge offshore wind farm Hornsea 2 is fully operational, Orsted says. Retrieved from https://www.cnbc.com/2022/09/01/huge-offshore-wind-farm-hornsea-2-is-fully-operational-orsted-says.html

[11] GWEC. (2023, 3). Global Wind Report 2023 [Document].

[12] Huges, O. (2020, 6). Wind farm with turbines taller than the Eiffel Tower could be built off North Wales coast. Retrieved from https://www.dailypost.co.uk/news/north-wales-news/wind-farm-turbines-taller-eiffel-18363294

[13] Jakubowski, A., & Schmidt, H. (2003). Experimentelle Untersuchen an vorgespannten RingflanschstöSSen mit Imperfektionen [Experimental investigations on preloaded bolted ring flange connections with imperfections]. Stahlbau.

[14] Jalbi, S., & Bhattacharya, S. (2020, 12). Concept design of jacket foundations for offshore wind turbines in 10 steps. Soil Dynamics and Earthquake Engineering, 139, 106357. Retrieved from https://doi.org/10.1016/j.soildyn.2020.106357 doi: 10.1016/j.soildyn.2020.106357

[15] Natarajan, A. (2022, 6). Damage equivalent load synthesis and stochastic extrapolation for fatigue life validation. Wind Energy Science, 7(3), 1171–1181. Retrieved from https://doi.org/10.5194/wes-7-1171-2022 doi: 10.5194/wes-7-1171-2022

[16] Petersen, C. (1997). Stahlbau: Grundlagen der Berechnung und baulichen Ausbildung von Stahlbauten [Steel construction: Fundamentals of calculation and structural design of steel structures] [Book].

[17] Schaumann, P., Eichstädt, R., Oechsner, M., & Simonsen, F. (2015, 12). Fatigue Assessment of High-Strength Bolts with Very Large Diameters in Substructures for Offshore Wind Turbines. Stahlbau, 84(12), 1010–1015. Retrieved from https://doi.org/10.1002/stab.201510343 doi: 10.1002/stab.201510343

[18] Schmidt, H., & Neuper, M. (1997). Zum elastostatischen Tragverhalten exzentrisch gezogener L-StöSSe mit vorgespannten Schrauben. Stahlbau.

[19] Seidel, M. (2001a). Measuring fatigue loads of bolts in ring flange connections. Stahlbau.

[20] Seidel, M. (2001b, 7). Zur Bemessung geschraubter Ringflanschverbindungen von Windenergieanlagen (M. Seidel) (Vol. 70) (No. 7). Ernst Sohn. Retrieved from https://doi.org/10.1002/stab.200101770 doi: 10.1002/stab.200101770

[21] Seidel, M. (2018, 9). Tolerance requirements for flange connections in wind turbine support structures. Stahlbau, 87(9), 880–887. Retrieved from https://doi.org/10.1002/stab.201810050 doi: 10.1002/stab.201810050

[22] Seidel, M., Stang, A., Wegener, F., Schierl, C., & Schaumann, P. (2021, 12). Full-scale validation of FE models for geometrically imperfect flange connections. Journal of Constructional Steel Research, 187, 106955. Retrieved from https://doi.org/10.1016/j.jcsr.2021.106955 doi: 10.1016/j.jcsr.2021.106955

[23] Shahan, Z. (2014, 3). History of Wind Turbines. Retrieved from https://www.renewableenergyworld.com/storage/history-of-wind-turbines/

[24] Siemens Gamesa. (n.d.). Offshore Wind Turbines. Retrieved from https://www.siemensgamesa.com/products-and-services/offshore

[25] Tran, T.-T., & Lee, D. (2022, 12). Understanding the behavior of l-type flange joint in wind turbine towers: Proposed mechanisms. Engineering Failure Analysis, 142, 106750. Retrieved from https://doi.org/10.1016/j.engfailanal.2022.106750 doi: 10.1016/j.engfailanal.2022.106750

[26] VDI 2230. (2014, 12). Blatt 2: Systematic calculation of highly stressed bolted joints: Multi bolted joints [Standard].

[27] VDI 2230. (2015, 11). Blatt 1: Systematic calculation of highly stressed bolted joints: Joints with one cylindrical bolt [Guideline].

[28] Veljkovic, M., Feldmann, M., Naumes, J., Pak, D. T., Simões, L., Silva, D., & Rebelo, C. (2011, 1). Wind turbine tower design, erection and maintenance. Retrieved from https://doi.org/10.1533/9780857090638.2.274 doi: 10.1533/9780857090638.2.274

[29] Vestas. (n.d.). Offshore Wind Turbines. Retrieved from https://www.3dcadworld.com/shell-or-solid-elements-for-thin-walled-parts/

[30] Weijtjens, W., Stang, A., Devriendt, C., & Schaumann, P. (2021, 1). Bolted ring flanges in offshore-wind support structures - in-situ validation of load-transfer behaviour. Journal of Constructional Steel Research, 176, 106361. Retrieved from https://doi.org/10.1016/j.jcsr.2020.106361 doi: 10.1016/j.jcsr.2020.106361

Appendices

A

Appendix A: Summary dimensions connection

MSc. Thesis
Ruth Korthals Altes
26-05-2023

Dimensions Summary
Reference model

Geometry according to drawing:
The following approximations are made for the calculation of the flange

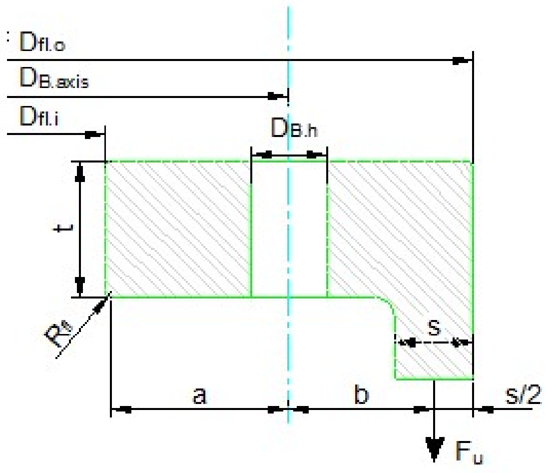

Outer diameter: $D_{fl.o} = 6500\ mm$

Inner diameter: $D_{fl.i} = 5870\ mm$

Diameter to bolt axis: $D_{B.axis} = 6220\ mm$

No. of bolts in whole flange: $n_{bolt} = 156$

Diameter of the bolt: $d_{B.nom} = 64\ mm$

Diameter of the bolt hole: $d_{B.h} = 70\ mm$

Distance from the inner edge of flange to the bolt axis: $a = 175\ mm$

Distance from the bolt axis to the load axis: $b = 122.5\ mm$

Thickness of the TP wall: $s_{low} = 60\ mm$

Thickness of the tower wall: $s_{up} = 35\ mm$

Thickness of the flange: $t = 135\ mm$

Preload force per bolt: $F_V = 1686\ kN$

MSc. Thesis
Ruth Korthals Altes
26-05-2023

Dimensions Summary
Next generation model

Geometry according to drawing:
The following approximations are made for the calculation of the flange

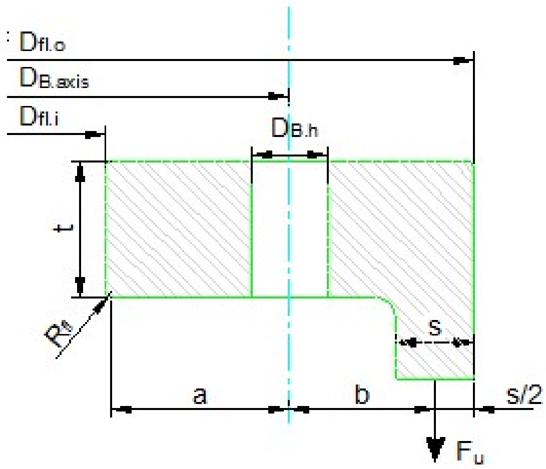

Outer diameter:	$D_{fl.o} = 8000$ ***mm***
Inner diameter:	$D_{fl.i} = 7222$ ***mm***
Diameter to bolt axis:	$D_{B.axis} = 7654$ ***mm***
No. of bolts in whole flange:	$n_{bolt} = 162$
Diameter of the bolt:	$d_{B.nom} = 80$ ***mm***
Diameter of the bolt hole:	$d_{B.h} = 86$ ***mm***
Distance from the inner edge of flange to the bolt axis:	$a = 216$ ***mm***
Distance from the bolt axis to the load axis:	$b = 151$ ***mm***
Thickness of the TP wall:	$s_{low} = 60$ ***mm***
Thickness of the tower wall:	$s_{up} = 44$ ***mm***
Thickness of the flange:	$t = 167$ ***mm***
Preload force per bolt:	$F_V = 2737$ ***kN***